Protein Repair Strategies for the Functional Restoration of CARASIL-relevant HTRA1 Mutants

Inaugural-Dissertation

zur

Erlangung des Doktorgrades

Dr. rer. nat.

der Fakultät für

Biologie

an der

Universität Duisburg-Essen

vorgelegt von

Linda Ingendahl

geb. in Mönchengladbach

Oktober 2018

Die der vorliegenden Arbeit zugrunde liegenden Experimente wurden am Zentrum für medizinische Biotechnologie (ZMB) in der Arbeitsgruppe Mikrobiologie II, Prof. Dr. Michael Ehrmann, an der Universität Duisburg-Essen durchgeführt.

1. Gutachter: Prof. Dr. Michael Ehrmann

2. Gutachter: Prof. Dr. Markus Kaiser

Vorsitzender des Prüfungsausschusses: Prof. Dr. Peter Bayer

Tag der mündlichen Prüfung: 06.12.2018

DOI: 10.17185/duepublico/47773
URN: urn:nbn:de:hbz:465-20230508-124701-5

Content

List of Figures

List of Tables

Abbreviations

°C	degree Celsius
aa	amino acid
AD	Alzheimer's Disease
AMD	age related macular degeneration
AP	alkaline phosphatase
APS	ammonium persulfate
ATP	adenosintriphosphate
BCiP	5-Bromo-4-chloro-3-indolyl phosphate
bp	base pairs
BSA	bovine serum albumin
CAPN2	calpain 2
CADASIL	Cerebral Autosomal Dominant Arteriopathy with Subcortical Infarcts and Leukoencophalopathy
CARASIL	Cerebral Autosomal Recessive Arteriopathy with Subcortical Infarcts and Leukoencophalopathy
CD	circular dichroism
CFD	complement factor D
cm	centimeter
CRV	cerebroretinal vasculopathy
CV	column volume
DMEM	Dulbecco's modified Eagle's medium
DMF	dimethylformamide
DMSO	dimethyl sulfoxide
DNA	desoxyribonucleic acid
DNase	desoxyribonuclease
dNTP	2'-desoxynucleotide-5'-triphosphate
DOSY	diffusion ordered spectroscopy
DTT	dithiothreitol
E. coli	*Escherichia coli*
ECM	extracellular matrix
EDTA	ethylenediaminetetraacetic acid
EGF	epidermal growth factor

EMT	epithelial-mesenchymal-transition
ER	endoplasmatic reticulum
ESS	embolic stroke syndrome
EtOH	ethanol
FPLC	fast protein liquid chromatography
GCP	guadinium carbonyle pyrrole
GOM	granular osmiophilic material
GST	gluthathione-S-transferase
h	hours
HAP	hydroxyl apatite
HAX-1	HS1-associated protein X1
HCl	hydrogen chloride
HEPES	4-(2-hydroxyethyl)-1-piperazineethanesulfonic acid
HHT	Hereditary Haemorrhagic Telangiectasia
HEK	human embryonic kidney
HRP	horseradish peroxidase
HTRA	high-temperature requirement A
HVR	hereditary vascular retinopathy
IGFBP	insulin-like growth factor-binding protein
IM	inner membrane
IPTG	isopropyl-β-D-thiogalactoside
ITC	isothermal titration
kDa	kilo dalton
LAD	large artery disease
LC-MS	liquid chromatography-mass spectrometry
LTBP	latent TGF-β-binding protein
M	molar (mol/l)
MeOH	methanol
min	minutes
MMP	matrix metallo protease
MRI	magnetic resonance imaging
MW	molecular weight
MWCO	molecular weight cut off
NBT	nitro blue tetrazolium chloride

NEB	New England Biolabs
Ni-NTA	nickel-nitrilotriacetic acid
Ni-TED	nickel-tris(carboxymethyl)ethylene diamine
nm	nanometer
NMR	nucleomagnetic resonance
nt	nucleotide
NZA	NZ-amine
OD	optical density
OM	outer membrane
OMM	outer mitochondrial membrane
OMP	outer membrane proteins
o.n.	over night
PAGE	polyacrylamide gel electrophoresis
PBS	phosphate buffered saline
PCR	polymerase chain reaction
PDZ	postsynaptic density of 95 kDa, discs large, zonula occludens-1
pNA	para-nitroaniline
PINK1	PTEN-induced putative kinase 1
ppm	parts per million
RANKL	receptor activator of nuclear factor-κB ligand
RNA	ribonucleic acid
rpm	revolutions per minute
PRR	proline-rich region
RT	room temperature
RVCL	Retinal Vasculopathy with Cerebral Leukodystrophy
s	seconds
SAM	sorting and assembly machinery
SDS	sodium dodecyl sulfate
SEC	size-exclusion chromatography
SMC	smooth muscle cell
SNIP	single nucleotide polymorphism
SS	signal sequence
SVD	small vessel disease

TAE	tris-acetate-EDTA buffer
TBS	tris-buffered saline
TBS-T	TBS with 0.05 % Tween
TCEP	tris(2-carboxyethyl)phosphine
TCEP-HCl	hydrochloride salt of TCEP
TEMED	N,N,N’,N’-tetramethylethylendiamine
TGF	transforming growth factor
TIMP	tissue inhibitor of metalloprotease
Tm	melting temperature
TOM	translocase of the outer mitochondrial membrane
TRIS	tris(hydroxymethyl)aminomethane β-ME β-mercaptoethanol
UV	ultraviolet
V	volt
VSMC	vascular smooth muscle cell
v/v	volume per volume
w/v	weight per volume
W	Watt
wt	wildtype
XIAP	X-linked inhibitor of apoptosis protein

1 Introduction

1.1 HtrA proteins: Structure-function relationships in a conserved family of oligomeric serine proteases

Oligomeric protein complexes comprising two or more subunits play a pivotal role in a number of cellular processes requiring complex interactions and finely-tuned regulation. Comprising on average one third of the proteome oligomeric components constitute a large fraction of cellular proteins (Goodsell and Olson 2000). The oligomeric composition of these complexes offers a plethora of advantages to the cell, since it allows for structural plasticity and tight allosteric regulation thus providing a new level of functional control.

Most oligomeric complexes are homo-oligomers displaying a symmetric structure that can be mirror-inverted, cyclic, dihedral or cubic. They are interconnected by extensive protein-protein contacts often comprising both hydrophobic and ionic interactions. Most often the residues involved in these interactions are highly conserved, especially at so called 'oligomerization hot spots', which are typically found at the center of an interface and constitute a major fraction of the binding energy of an oligomeric interaction. Substitution of these hot spot residues is often found to result in a loss of oligomerization (Harbury *et al.* 1993). Depending on the affinities of these protein-protein interactions the association between subunits can vary in strength and duration. Thus some proteins form highly stable complexes with dissociation constants in the nanomolar range, whereas for others complex formation is a transient event depending on a number of environmental conditions (e.g. concentration, temperature, pH). Yet for some protein complexes the affinities between subunits can change in response to external stimuli such as substrate- or ligand-binding thus allowing for the regulation of cellular processes via dynamic oligomerization events (Nooren and Thornton 2003). Despite the extensive conservation of oligomeric interfaces even closely related proteins may display variations regarding their oligomeric forms. For example variations in the lengths of inter-domain linkers might render deviations in the relative orientations of domains constituting the interface hence enabling different oligomer combinations (Albright *et al.* 1996; MacBeath *et al.* 1998; Pei *et al.* 1997).

A highly conserved family of oligomeric proteins are the HtrA (High Temperature Requirement A) serine proteases. HtrA proteins are found in both pro- and eukaryotic organisms, where they are implicated in protein quality control and a variety of regulatory mechanisms (Page and Di Cera 2008). One feature, that distinguishes the HtrA family from other serine proteases is their conserved domain architecture consisting of a chymotrypsin-like protease domain - containing the catalytic triad, the oxyanion hole and the substrate specificity pocket - and at least one C-terminal PDZ (Postsynaptic density of 95 kDa, Discs large and Zonula occludens 1) domain (figure 1.1) (Pallen and Ponting 1997).

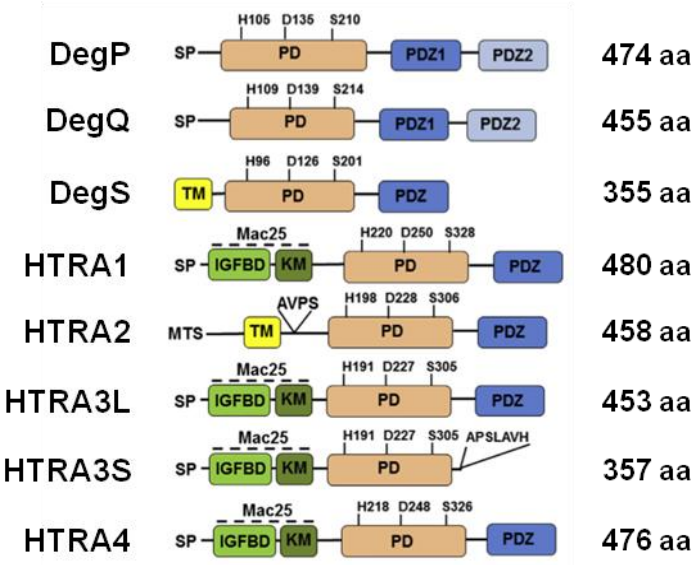

Figure 1.1 Conserved domain organization of HtrA proteases
SP (signal peptide), IGFBD (insulin-like growth factor-binding domain), KM (Kazal-type module), TM (transmembrane domain), PD (chymotrypsin-like protease domain), L (long isoform), S (short isoform), aa (amino acids). Residues of the catalytic triad are marked. (Zurawa-Janicka *et al.* 2017, modified)

The basic building block of all HtrA proteases is a funnel-shaped trimer, in which the protease domains form the central core, whereas the PDZ domains protrude to the outside. This homooligomeric assembly is stabilized by an elaborate network of interactions between the three protease domains involving both hydrophobic ringstacking interactions between highly conserved aromatic residues at the far tip of the trimer as well as ionic interactions within the larger interface area. However, some HtrA proteases were found to form higher oligomeric complexes involving interactions between adjacent PDZ domains. Dynamic rearrangements from lower to higher oligomeric forms upon substrate recognition have been described for DegP, DegQ and

HTRA1, but might also apply to other less studied HtrA proteases (Krojer *et al.* 2008; Li *et al.* 2002; Wilken *et al.* 2004; Truebestein *et al.* 2011).

Whereas the composition of the N-terminal region varies between different homologues containing either localization signals, transmembrane anchors or regulatory elements of unknown function, the protease and PDZ domains are highly conserved. The protease domain in HtrA proteases adopts the canonical chymotrypsin fold consisting of two perpendicularly arranged six-stranded β-barrel lobes connected by flexible loops that are termed according to the chymotrypsin nomenclature. The catalytic triad is located in a crevice between the two lobes with the catalytic serine residue being situated in loop L1 within the C-terminal lobe (β7-β12) and the histidine and aspartate residues in loop LB and LC respectively of the N-terminal lobe (β1-β6) (figure 1.2). The oxyanion hole is situated immediately before the active site serine so as to stabilize the negatively charged carbonyle oxygen intermediate occurring during cleavage (Hansen and Hilgenfeld 2013; Clausen *et al.* 2011).

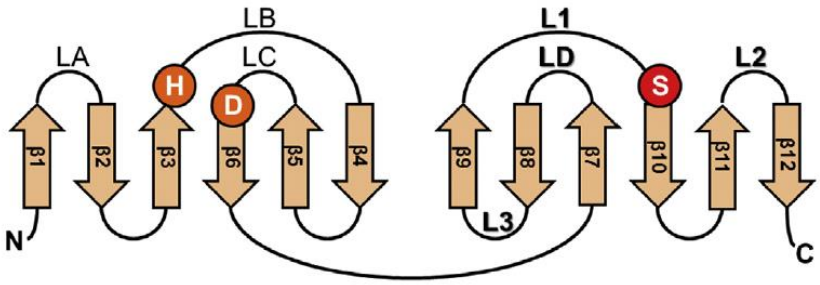

Figure 1.2 Arrangement of secondary structure elements of the protease domain
β-strands are shown as arrows and residues of the catalytic triad (histidine, aspartate and serine) are depicted in circles.The α-helices are omitted. Loops of the protease domain are named according to chymotrypsin nomenclature. The regulatory loops: LD, L1, L2 and L3 are marked in bold. (Zurawa-Janicka *et al.* 2017)

The catalytic triad conducts the cleavage of peptide bonds in an ATP-independent manner via an addition-elimination-mechanism. Upon binding of a protein substrate to the active site one proton is transferred from the catalytic serine residue located in loop L1 to the active site histidine positioned in loop LB, which functions as a reversible proton reservoir in the reaction mechanism. This proton transfer is stabilized by the active site aspartate in loop LC via ionic interactions thereby facilitating a nucleophilic attack on the scissile peptide bond by the catalytic serine residue in order to form the tetrahedral intermediate. Upon donation of a proton to the peptide nitrogen by the active site histidine the peptide bond is cleaved and the first product is released.

Subsequently a hydroxyl group is transferred to the substrate from a nearby water molecule and the remaining proton is transferred to the active site histidine. Following the release of the second product the proton is transferred to the catalytic serine residue thus regenerating the enzyme and completing the catalytic cycle.

Connected to the protease domain via a flexible linker there is at least one C-terminal PDZ domain. PDZ domains are conserved globular protein-protein interaction modules of 80 to 90 residues, which are rarely found in unicellular organisms, but occur frequently in metazoans (Letunic *et al.* 2012). The HtrA PDZ domains display remarkable functional diversity, since they are implicated in a variety of processes including substrate- and effector-binding, activity regulation, oligomerization as well as the determination of cellular localization. This functional plasticity is reflected in the overall architecture of the domain comprising multiple binding and interaction motives (Clausen *et al.* 2011) (figure 1.3). The PDZ domains in HtrA proteases are composed of five β-strands forming two separate β-sheets and two α-helices capping the edges of the sheets. In contrast to the canonical PDZ domains found in other proteins the HtrA PDZ domain is circularly permutated resulting in an exchange of the N- and C-terminal strands. Thus the canonical peptide-binding cleft is located at the immediate N-terminus in close proximity to the proteolytic domain. The cleft is constituted of the carboxylate-binding loop (GLGF loop) and the first β-strand and α-helix. This fold allows for the recognition of both peptidic ligands and exposed C-termini of substrate molecules via binding of hydrophobic residues to the carboxylate-binding loop and incorporation of the adjacent peptide stretch into the β-sheet in a β-augmentation process. Typically this binding event induces specific conformational changes within the PDZ domain, which thereupon propagates the signal to the sensor loop L3 thereby passing it to a neighbouring protease domain (Lee and Zheng 2010). Additionally, substrate-binding to the canonical peptide-binding cleft can directly contribute to proteolysis via a 'hold-and-bite' mechanism. Since both the PDZ's peptide-binding site and that of the proteolytic domain display a pronounced similarity in peptide specificities, the PDZ might prevent the premature release of cleavage intermediates by capturing them and re-presenting them to the active site (Meltzer *et al.* 2009).

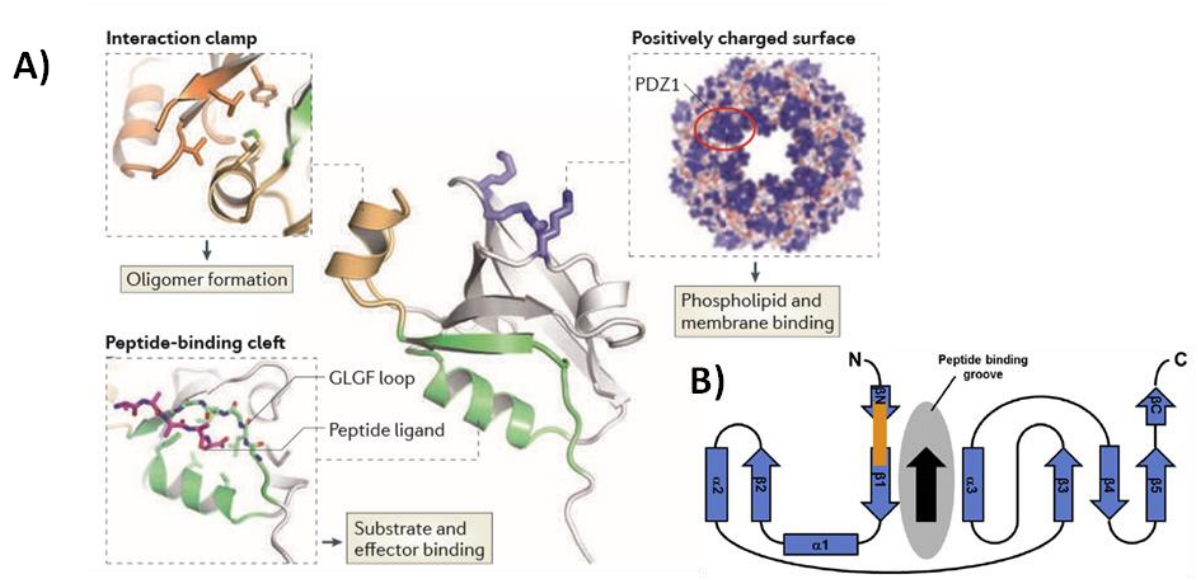

Figure 1.3 Architecture of HTRA PDZ domains
A) Structural representation of the HtrA PDZ domain. Functionally relevant interaction sites are highlighted. (Clausen *et al.* 2011) B) Schematic representation of the HtrA PDZ domain. α-helices are depicted as rectangles, β-strands as arrows and the peptide-binding site is marked with a grey ellipse. The carboxylate-binding loop is indicated by an orange rectangle and a peptide ligand by a black arrow. (Zurawa-Janicka *et al.* 2017)

Furthermore, PDZ domains are thought to mediate subcellular localization by interacting with membrane phospholipids. This interaction most likely occurs via association of a positively charged surface patch located opposite the peptide-binding cleft with the negatively charged phospholipid headgroups. Indeed, mutations within the predicted binding area were found to significantly reduce or even abolish membrane-binding. Membrane association of HtrA proteases functioning as a chaperone is thought to contribute to the proper folding of secreted proteins (Shen *et al.* 2009). Moreover, the PDZ domains of some HtrA proteases that are capable of higher oligomer formation exhibit an additional feature, the so called interaction clamp. This motive is situated immediately C-terminal of the peptide-binding cleft after the first β-strand and constitutes a major fraction of the mainly hydrophobic interaction surface and binding energies in higher order HtrA oligomers.

The proteolytic activity of HtrA proteases needs to be tightly regulated to prevent uncontrolled, eventually deleterious proteolysis. Thus their function is based on the presence of activating stimuli such as peptide-binding to the PDZ domain, induced-fit substrate-binding or substrate induced oligomer conversion. Remarkably, for all HtrA proteins proteolytic activity depends on a highly conserved activation cascade requiring interactions between adjacent protomers, which allows their activity to be

finely tuned in a reversible fashion. In the inactive state the active site loops are severely disordered thereby impeding the function of the catalytic triad, the substrate specificity pocket and the oxyanion hole. Upon an allosteric activation stimulus the sensor loop L3 undergoes a conformational change facilitating its interaction with the activation loop LD* of the neighbouring protomer via a conserved arginine residue and inducing the proper positioning of the activation domain in a disorder-to-order transition. Since propagation of the activation signal proceeds from one protomer receiving the signal to a neighbouring subunit via a highly conserved activation cascade ([PDZ] → L3 → LD* →L1/L2), trimerization appears indispensable for proteolytic activity (Hasselblatt *et al.* 2007; Krojer *et al.* 2002).

The following sections will provide an overview on both pro- and eukaryotic HtrAs focusing on their diversity in oligomeric structure and its implications for activity regulation.

1.1.1 Bacterial HtrA proteases

For the bacterial cell protein quality control within the envelope displays a major challenge, since this compartment is exposed to a multitude of environmental stresses and ATP, which is required in many repair and degradation processes, is not available (Duguay and Silhavy 2004). Thus HtrA proteases play an important role in bacterial integrity, as they perform a number of protective and regulatory functions within this compartment. In this respect, they can act either as sensory proteases, which initiate stress response pathways upon detection of unfolded proteins, or perform a dual task as bifunctional protease-chaperones in order to directly counteract folding stress. Furthermore, HtrAs are implicated in bacterial virulence due to their role in the folding of secreted virulence factors and their contribution to the tolerance of harsh conditions encountered during host infection.

The *E. coli* HtrAs DegP, DegQ and DegS reside inside the periplasm or inner membrane, where they participate in protein quality control thereby contributing to periplasmic homeostasis. DegP is a bifunctional enzyme acting as both a protease and

a chaperone, whose activity is tightly regulated on two levels: On the DNA level it is upregulated in response to folding stress via both the Cpx- and the σ^E- pathways, while on the protein level its activation requires an elaborate allosteric mechanism involving the transfer of the activation signal within the trimer as well as conversion to higher oligomeric species (Krojer *et al.* 2008).

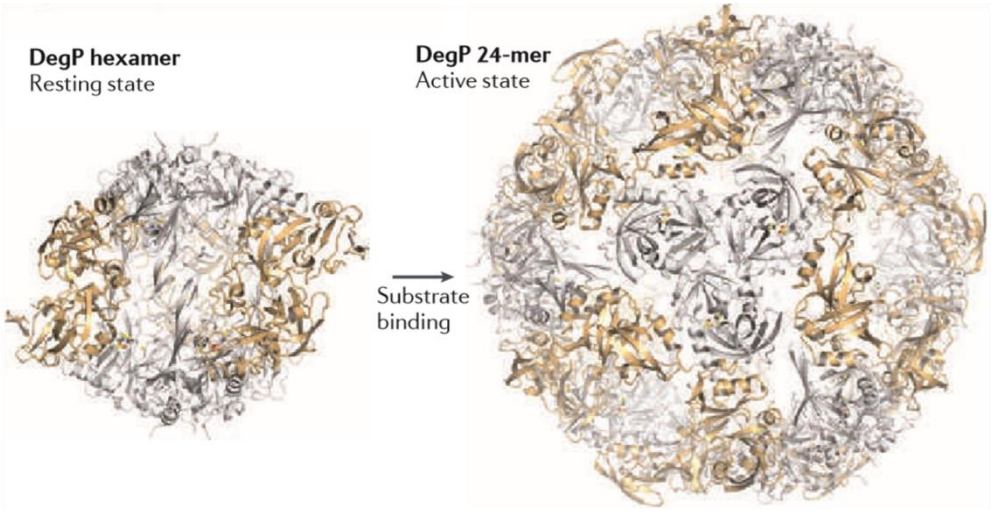

Figure 1.4 Substrate-induced oligomeric switch in DegP
Crystal structures of the DegP hexamer (left panel) which undergoes a conformational transiton to the 24-meric form (right panel) upon substrate-binding. Protease domains are shown in grey, PDZ domains are displayed in orange. (Clausen *et al.* 2011)

The reversible switch from the inactive to the active conformation is based on substrate-induced oligomer conversion from resting hexamers to spherical, proteolytically active 12- and 24-mers. The resting hexamer is formed by two opposing DegP trimers. In this conformation the LA loops, which in DegP contain a unique 48 residue extension, protrude into the active sites of the opposite subunits, where they interact with loops L1* and L2* thus locking the activation domain in a distorted conformation and restricting substrate entrance to the catalytic cavity. However, upon substrate-binding to the first PDZ domain conformational rearrangements are induced resulting in the formation of cage-like 12- and 24-meric structures (figure 1.4). Within these structures the LA loops are extracted from the active sites and the PDZ domains, which had formed flexible protrusions in the resting hexamer, interact with each other to build fixed spherical scaffolds. Notably, the PDZ1 becomes locked in a conformation, that allows it to directly interact with the sensor loop L3 thereby stabilizing its interaction with the activation loop LD* of the neighbouring protomer and inducing the conserved activation cascade (Krojer *et al.* 2010; Merdanovic *et al.* 2010). Thus in DegP substrate

recognition, oligomerization as well as transfer of the activation signal to the active site are mediated by the PDZ domains hence highlighting their versatile function.

Similar to DegP DegQ is a bifunctional enzyme harbouring both protease and chaperone activities (Malet *et al.* 2012). Despite its profound sequence homology to DegP, DegQ does not contain an elongated LA loop indicating that in contrast to DegP the hexamer does not represent the resting state. Instead the trimer appears to constitute the inactive conformation (Wrase *et al.* 2011). In presence of unfolded substrates DegQ was found to form cage-like 12- and 24-meric structures similar to DegP. However, characterization of these structures via cryo-electron microscopy of *E. coli* DegQ followed by a comparison with higher order DegP oligomers revealed profound structural perturbations within the L2 and L3 loops that are not compatible with proteolytic function suggesting that substrate induced oligomer conversion alone may not suffice to induce proteolytic activity in DegQ. These findings might indicate that either further stimuli are necessary to properly position the DegQ active site loops or that the cage-like structures formed by DegQ might serve as a molecular reaction chamber enabling the proper folding of periplasmic substrate proteins rather than their proteolytic degradation. Indeed, intact OmpA was found in many of the cage-like particles indicating that similar to DegP DegQ contributes to the proper folding and trafficking of outer membrane proteins (Bai *et al.* 2011).

In contrast to DegP and DegQ, which as general chaperones and proteases display limited substrate specificity, the proteolytic activity of DegS is confined to only a single substrate – the anti-σ factor RseA. RseA is a negative regulator of the σ^E unfolded protein response pathway, that resides in the inner membrane of *E. coli*. Under stress conditions outer membrane proteins mislocalize to the periplasm, where their C-termini, which are deeply buried within the β-barrel structure of the pores, become accessible to interact with the DegS PDZ domain thus promoting its switch to the active conformation. The membrane-associated DegS thereupon performs the first and rate-limiting cut in RseA hence facilitating its further processing by other membrane-bound and cytosolic proteases and the release of the RseA-bound sigma factor σ^E finally resulting in the expression of stress-induced periplasmic chaperones and regulatory proteases such as DegP (Hasenbein *et al.* 2010).

Unlike DegP and DegQ DegS contains only one PDZ domain and its switch to the active state is not associated with a conversion to higher oligomeric species. Remarkably, in DegS the PDZ domain is closely associated with the protease domain in a fixed orientation, that is stabilized by a number of polar interactions. Structural data obtained from X-ray crystallography of DegS in presence of different OMP-derived C-terminal peptides displaying the conserved consensus motive Φ-x-F indicate that the peptides bind to the PDZ domain as an additional β-sheet via a β-augmentation process (Hasselblatt *et al.* 2007). In this conformation the conserved residues at position 0 and -2 bind directly to the PDZ domain with the C-terminal phenylalanine being deeply buried within the carboxylate-binding pocket, whereas the side-chain at position -1 forms close contacts with loop L3 thereby triggering conformational changes that result in the remodelling of the active site loops within the adjacent protomer. Notably, the central segment of loop L3 displays remarkable flexibility, which allows for variable interactions with different -1 residues thus catering to the lack of sequence conservation at this position and enabling it to integrate signals from different C-terminal sequences. Thus the ability of the DegS PDZ domain to act as a binding site for activating C-terminal sequences as well as the inherent flexibility of the L3 loop allow DegS to function as an efficient sensor for periplasmic folding stress, that is able to integrate signals from various misfolded outer membrane proteins into a single response pathway (Wilken *et al.* 2004; Hasselblatt *et al.* 2007).

1.1.2 Human HTRA proteases

To date there are four HTRA proteases identified in humans. Similar to their bacterial counterparts the human HTRAs share the characteristic domain architecture consisting of a PDZ and a chymotrypsin-like protease domain. However, the human HTRAs except HTRA2 differ from the bacterial HTRAs in the presence of an N-terminal domain consisting of a signal sequence for secretion, an IGFBP (insulin-like growth factor-binding protein)-like and a Kazal-type module. So far, the role of these modules is not fully understood. Structural analysis of the HTRA1 N-domain showed that polar interactions within the domain cause the Kazal-type to pack against the IGFBP-like module making a function similar to that of their eponymous homologues highly

unlikely. Furthermore, a functional characterization of the N-domain revealed that the Kazal-type module did not show any inhibitory effects against a vast panel of different serine proteases and that unlike other IGFBP proteins the IGFBP-like module of HTRA1 was found to bind neither IGF-I, nor IGF-II (Eigenbrot *et al.* 2012). These results indicate the IGFBP-like and the Kazal-type module in human HTRAs presumably exhibit a function that differs from that of their closest homologues.

In contrast to other human HTRAs the N-terminal domain of HTRA2 (*Omi*) consists of an inhibitor of apoptosis protein (IAP)-binding motive, a transmembrane segment and a mitochondrial localization signal, which targets it to the mitochondrial intermembrane space, where it is anchored to the inner membrane (Hegde *et al.* 2002). Upon proteolytic maturation a 133 amino acid fragment is cleaved from the N-terminus and HTRA2 is released into the intermembrane space, where it is assumed to be involved in protein quality control thereby contributing to mitochondrial homeostasis (Gray *et al.* 2000). Cleavage of the transmembrane anchor during proteolytic maturation reveals the IAP-binding motive suggesting a role of HTRA2 in promoting apoptosis (Martins *et al.* 2002; Yang *et al.* 2003). In line with this observation, it has been demonstrated, that apoptotic stimuli lead to the release of HTRA2 into the cytoplasm, where it is implicated in both caspase-dependent and caspase-independent apoptotic pathways via the degradation of antiapoptotic proteins (Hegde *et al.* 2002; Srinivasula *et al.* 2003).

Like other HtrAs HTRA2 was found to form a funnel-shaped trimer, whose stability is ensured via an elaborate network of both ionic and van der Waals interactions in the protease interface and a conserved aromatic cluster formed by tyrosine 147, phenylalanine 149 and phenylalanine 256 within the N-terminal segment of the protease domain. Disruption of this aromatic cluster via conversion of phenylalanine 149 to aspartate was shown to render the protein monomeric hence abolishing its proteolytic activity (Nam *et al.* 2006). Structure determination of an inactive HTRA2 variant lacking the active site serine 306 revealed that in the resting state the PDZ domain is tightly packed against the proteolytic domain thereby restricting substrate access to the inner catalytic cavity and trapping the active site in a nonfunctional conformation. Upon peptide-binding to the hydrophobic groove of the PDZ domain it is thought to be removed from the protease domain resulting in the release of the flexible L3 loop, which thereupon initiates transduction of the activation signal to the adjacent

protomer via LD* and L1* (Li *et al.* 2002). However, in the resting state the PDZ's peptide recognition motive ^{361}YIGV^{364} is partially blocked by proline 225 and valine 226 of the protease domain's LC loop indicating that additional mechanisms such as XIAP-binding to the N-terminal IAP-binding motive (Bejugam *et al.* 2013; Singh *et al.* 2014) or binding of peptides to a predicted selective binding pocked located in the flexible linker region between the PDZ- and the protease domain (Bejugam *et al.* 2013) might contribute to propagation of allosteric signals and the establishment of the active conformation.

HTRA3 (*PRSP*) was first identified as a protease associated with pregnancy that is involved in embryo implantation and placenta development (Nie *et al.* 2003a; Nie *et al.* 2003b). In this regard, aberrant expression of HTRA3 beyond the first trimester has been associated with preeclampsia, a pathological condition involving abnormal formation of blood vessels within the placenta (Dynon *et al.* 2012; Li *et al.* 2011). Moreover, HTRA3 was found to be downregulated in several cancer cell lines and tumor types suggesting a potential tumor suppressor function (Bowden *et al.* 2006; Narkiewicz *et al.* 2008; Narkiewicz *et al.* 2009; Singh *et al.* 2013). Consistent with its role in cancer progression and similar to its homologue HTRA1 HTRA3 was found to be involved in TGF-β signalling and the reorganization of the extracellular matrix (ECM) via cleavage of extracellular proteins (Tocharus *et al.* 2004).

Due to alternative mRNA splicing HTRA3 can exist in two isoforms: a long one (HTRA3L) comprising a C-terminal PDZ domain and a short one (HTRA3S), in which the PDZ domain is replaced by a sequence of seven amino acids (A-P-S-L-A-V-H) encoded by a separate exon (Nie *et al.* 2003a). Interestingly trimer formation in HTRA3 appears to require unique interactions between the loop LB and the PDZ* domain of an adjacent subunit. Thus the short isoform does not form trimers in solution, which is in striking contrast to all other HTRA proteases, in which trimer formation is independent of the PDZ domain. Nevertheless, the short and long isoforms display similar proteolytic activities making HTRA3 the only HTRA protease found to form active monomers.

Another pregnancy associated HTRA protease is HTRA4. However, information regarding its physiologic relevance is scarce. There has been evidence that HTRA4

mediates trophoblast invasion (Wang *et al.* 2012) during the early stages of pregnancy and that its role might be antagonistic to that of its homologues HTRA1 and 3 within this process (Inagaki *et al.* 2012; Singh *et al.* 2015). Furthermore, HTRA4 was found to cleave ECM proteins such as fibronectin (Wang *et al.* 2012) and might play a role in the development of several cancer types (Chien *et al.* 2009a).

1.1.3 HTRA1

Similar to its homologues HTRA3 and HTRA4 HTRA1 (*PRSS1*) shares the characteristic domain architecture of human HTRA family members consisting of a PDZ domain, a chymotrypsin-like protease domain and an N-terminal domain of unknown function with a signal sequence for secretion located at the far N-terminus. Previous studies indicate that in line with its bacterial counterparts DegP and DegQ HTRA1 is a bifunctional enzyme harbouring both protease and chaperone activities allowing it to fulfil a diverse repertoire of functions. Among other features, HTRA1 is implicated in the degradation of misfolded proteins as well as the disintegration of potentially toxic protein aggregates thereby contributing to protein homeostasis (Poepsel *et al.* 2015). Furthermore, it participates in the regulation of signaling pathways associated with cell growth, proliferation and ECM remodeling (Beaufort *et al.* 2014; Schillinger *et al.* 2018).

Of the overall HTRA1 the major fraction is secreted to the extracellular matrix (ECM), where it contributes to protein turnover via the degradation of various ECM components including decorin, aggrecan, fibronectin (Grau *et al.* 2006), type II collagen (Hosseini-Farahabadi *et al.* 2013), fibromodulin, vitromodulin (An *et al.* 2010), clusterin, biglycan and the amyloid precursor protein Aβ (Grau *et al.* 2005) thereby regulating ECM integrity and homeostasis. Within the cell HTRA1 was found to be located to the cytoplasm and nucleus (Chien *et al.* 2009c; Clawson *et al.* 2008). Whereas the role of HTRA1 within the nucleus is still under discussion, the cytosolic form was found to be associated to microtubules, where it is implicated in the proteolytic degradation of tuberin (Campioni *et al.* 2010), the microtubule-associated protein Tau (Tennstaedt *et*

al. 2012) and tubulins (Chien *et al.* 2009c; Chien *et al.* 2009b) hence affecting cell growth and migration.

HTRA1 is ubiquitously expressed, yet its expression levels vary depending on tissue types and developmental stages. This ubiquitous expression pattern as well as its functional ambiguity raise the need for tight regulation on both the transcriptional and the protein level. Whereas the mechanisms underlying its transcriptional regulation are not yet fully understood, activity regulation on the protein level is known to follow an elaborate mechanism based on intra-trimer communication. The trimer is stabilized by a complex interaction network, that includes both hydrophobic ringstacking interactions between highly conserved aromatic residues at the far tip of
the protease domain (Y169, F171 and F278) and ionic interactions within the larger interface area including salt bridges formed between arginine 274 and aspartate 174* and glutamate 177* as well as between glutamate 277 and arginine 166*. An oligomeric switch to higher oligomeric species upon interaction with unfolded substrates has been suggested due to the observation of a ~600 kD multimer in presence of unfolded citrate synthase (Truebestein *et al.* 2011). Yet the formation of higher-order oligomers is still a matter of controversy.

Despite maintaining the basic structural features of HtrA proteases HTRA1 has evolved unique mechanisms of activity regulation. Similar to its human and bacterial homologues the inactive state is characterized by severely disordered active site loops hindering the proper positioning of the catalytic triad as well as the formation of the S1 specificity pocket and the oxyanion hole, whereas in the active conformation these structural features are properly positioned and poised for catalysis. Remarkably this conformational transition appears to proceed independent of the PDZ domain, since the active conformation was also observed in PDZ-less HTRA1 constructs. Furthermore, the finding that the PDZ domain was not resolved in a crystal structure of HTRA1 suggests an inherent *en bloc* mobility and thus a lack of stable contacts to the proteolytic domain. In line with these findings, proteolytic activities measured against a panel of model substrates in constructs lacking the PDZ domain were similar to that of the wildtype enzyme. However, the PDZ domain was found to impact the average length of proteolytic products indicating its contribution to a hold-and-bite cleavage mechanism analogous to that observed in DegP (Truebestein *et al.* 2011;

Meltzer *et al.* 2009). Additionally, several peptides derived from C-terminal protein sequences were found to influence HTRA1 activity in a PDZ dependent manner (Rey 2018). Thus the PDZ domain might be required for the delicate adjustment of proteolytic functions as well as the integration of external signals, while being dispensable for overall proteolytic activity.

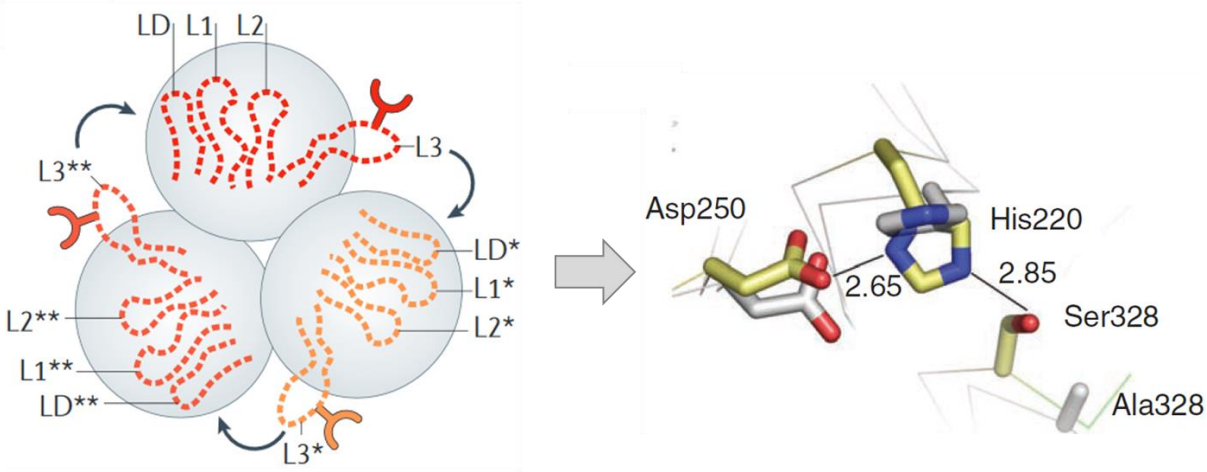

Figure 1.5 Substrate-induced disorder-order-transition in HTRA1
Upon substrate-binding HTRA1 undergoes a disorder to order transition involving interactions between adjacent protomers. The left panel shows a schematic representation of the conserved HTRA activation cascade highlighting the need for inter-protomer interactions. The right panel presents the repositioning of the catalytic triad upon substrate-induced active site remodelling as an overlay of the inactive (grey) and active (yellow) conformation. Compilation based on Clausen *et al.* 2011 and Truebestein *et al.* 2011.

Instead structural data derived from an HTRA1 construct bound to the substrate-mimicking inhibitor DPMFKLboroV indicate that substrate-binding itself is the immediate stimulus triggering active site rearrangement. Within the stably folded active conformation the inhibitor appeared deeply buried within the activation domain forming close contacts to several structural features determining the active conformation of HTRA1 thereby arranging them in a catalytically competent position. Hydrophobic interactions were observed between the inhibitor's P2-leucine and P4-phenylalanine with leucine 307, leucine 309 and tyrosine 316 of the sensor loop L3. The L3 loop thereupon transduces the activation signal to the adjacent protomer via interactions between its arginine 302 with the backbones of glutamine 289* and threonine 291* in loop LD* thus initiating the conserved activation cascade (figure 1.5). Transition to the active state is accompanied by a conformational rearrangement of the lysine 325 - histidine 326 peptide bond in loop L1, which facilitates the formation of the oxyanion hole to accommodate the tetrahedral intermediate (Truebestein *et al.* 2011). Furthermore, the inhibitor's P1-valine was inserted into the S1 specificity pocket formed

by isoleucine 323 of loop L1 and lysine 346 of loop L2, which occludes access to the active site in the inactive state (Cabrera *et al.* 2017). Thus induced-fit substrate-binding appears to be sufficient to trigger the proper positioning of the active site, since the substrate itself constitutes an integral part of the hydrophobic core of the activation domain hence stabilizing the active conformation. Furthermore, it contributes to the induction of the conserved activation cascade thereby conveying the signal to the adjacent subunits (Truebestein *et al.* 2011).

The model of substrate-induced active site remodelling has been challenged in a recent study by Eigenbrot *et al.* (2012) which reports a structure displaying the catalytically competent conformation in the absence of substrate. Based on this finding the group suggested a "conformational selection" model, in which HTRA1 exists at an equilibrium between different conformational states and the substrate merely samples the active conformer out of the equilibrium. These contradictory findings show that our current understanding of HTRA1 activity regulation is still insufficient and that further research needs to be done to fully elucidate the events determining its catalytic function.

Due to its implication in protein homeostasis as well as cellular signalling pathways associated with growth and proliferation defects in HTRA1 regulation can lead to serious physiological malfunctions often culminating in pathologic processes. In line with its involvement in protein homeostasis and the removal of misfolded proteins HTRA1 has been implicated in the aetiology of Alzheimer’s disease (AD), a protein folding disorder depending largely on the formation of extracellular Aβ- and intracellular Tau-aggregates. Both Tau and Aβ are confirmed HTRA1 substrates (Grau *et al.* 2005; Tennstaedt *et al.* 2012) suggesting an involvement of HTRA1 in the prevention of aggregate formation. Further evidence linking HTRA1 to Alzheimer's disease is the observation that HTRA1 catalyzes the disintegration of Tau fibrils as well as their subsequent degradation thus contributing to the clearance of existing aggregates (Poepsel *et al.* 2015). Additionally, HTRA1 was found to colocalize to Tau aggregates within the cytoskeletal network and an inverse correlation has been observed between HTRA1 and Tau levels in brain tissues taken from AD patients (Tennstaedt *et al.* 2012). It has also been shown that HTRA1 is involved in the amyloid β-pathway and that

downregulation of its activity via chemical inhibitors causes increased aggregation of Aβ (Grau *et al.* 2005).

There are several lines of evidence suggesting an involvement of HTRA1 in cancer development. However, findings regarding its exact implications can be contradicting depending on the type of cancer cell and its stage in the progression of the disease. In general, HTRA1 appears to be differentially regulated in several types of cancer and its expression levels can be correlated to a number of disease markers such as cell proliferation, probability of metastasis, disease prognosis and responsiveness to chemotherapeutic treatment (Baldi *et al.* 2002; Chien *et al.* 2006). Several findings suggest, that HTRA1 functions as a tumor suppressor. For example, it is down-regulated in several types of cancer including leukaemia, Burkitt's lymphoma and ovarian cancer (Chien *et al.* 2004; Shridhar *et al.* 2002) and its upregulation was demonstrated to cause a negative effect on tumor metastasis due to increased degradation of the cytoskeletal component tubulin (Chien *et al.* 2009b; Chien *et al.* 2009a).

Upregulation of HTRA1 has also been proposed to contribute to the development of arthritic disease - a chronic inflammatory condition characterized by progressive ECM degradation within cartilage tissues. HTRA1 catalyzes the degradation of various cartilaginous ECM proteins including aggrecan, fibronectin, decorin and fibromodulin (Hosseini-Farahabadi *et al.* 2013) hence driving disease progression in a direct manner. Additionally, degradation products of fibronectin and other HTRA1 substrates induce the expression of matrix metallo-proteases thus further enhancing cartilage degradation.

Finally, loss of function mutations within the HTRA1 locus have been directly linked to CARASIL (Cerebral Autosomal Recessive Arteriopathy with Subcortical Infarcts and Leucoencephalopathy) (Hara *et al.* 2009), a rare hereditary disease affecting the small vessels of the brain, which will be described in the following sections.

1.2 Hereditary Small Vessel Disease of the Brain

With approximately 7 million deaths per year stroke ranks as the second most frequent cause of death worldwide (Sörös and Hachinski 2012) and with circa 700 000 cases annually it is regarded the leading cause of disability among the North American population (Donnan *et al.* 2008). It is described as a medical condition resulting in cerebral malperfusion associated with extensive tissue loss commonly attributed to a combination of both genetic and environmental risk factors, rather than a single cause (Yan *et al.* 2017). Among the environmental risk factors hypertension and smoking are the most prevalent. Yet obesity, diabetes and high blood cholesterol also contribute to neuronal malperfusion and thus an increased likelihood of stroke. Additionally, a number of single nucleotide polymorphisms (SNPs) causing a familial predisposition for stroke have been identified. However, a small portion of strokes (approximately 5 %) can be attributed to genetic disorders based on mutations within a single DNA locus. Lately a number of genes associated with these hereditary stroke syndromes has been discovered. Reflecting the variety of causative genes several subtypes including Small Vessel Disease (SVD), Large Artery Disease (LAD) and Embolic Stroke Syndromes (ESS) can be distinguished.

Familial Small Vessel Disease is defined as a variety of syndromes predisposing to ischaemic and haemorrhagic strokes within the capillaries, arterioles and small arteries or veins of the brain (Pantoni 2010). Common features distinguishing the hereditary form from sporadic SVD are its early age of onset, a familial history occurring in a Mendelian pattern and often an absence of conventional risk factors predisposing for stroke. Among the characteristic features there are microbleeds, lacunar infarcts and diffuse white matter lesions (leukoencephalopathy) identified upon Magnetic Resonance Imaging (MRI), which result from progressive degenerative changes within the intracerebral vessels and a dysregulation of vascular permeability leading to chronic tissue malperfusion and cell death. Together these vascular malfunctions contribute to a variety of clinical symptoms including early-onset stroke, psychiatric disturbances, cognitive impairment and dementia. However, the phenotype depends not only on the causative gene, but also on a number of environmental factors including age, gender and lifestyle often resulting in variable penetrance even within the same family (Yamamoto *et al.* 2011).

Thus far four major causes of familial SVD have been identified resulting in distinct clinical syndromes, which will be described in the following sections. The unifying feature of these syndromes is that they result from a single defective gene, whose loss or toxic gain of function induces progressive intracerebral malperfusion. Yet, despite differences in the causative genes all syndromes converge to produce overlapping symptomatic phenotypes displaying the characteristic features of familial SVD.

1.2.1 Cerebral Autosomal Dominant Arteriopathy with Subcortical Infarcts and Leucoencephalopathy (CADASIL)

CADASIL is the most prevalent form of familial SVD with approximately 400 cases identified worldwide, although actual numbers might be substantially higher, as the syndrome often remains undiagnosed due to its resemblance to sporadic SVD (Leyhe *et al.* 2005; Razvi *et al.* 2005). Yet the distinctive feature separating CADASIL from other SVDs is the presence of granular osmiophilic material (GOM) accumulating in the vicinity of vascular smooth muscle cells (VSMC).

CADASIL causing mutations are located within the *NOTCH3* gene, which encodes a dimeric transmembrane receptor typically expressed in cerebral pericytes and VSMCs, where it is implicated in cell fate specification and differentiation during vasculogenesis (Artavanis-Tsakonas *et al.* 1999; Shawber and Kitajewski 2004). During its maturation the NOTCH3 receptor undergoes proteolytic cleavage by the protease furin generating an N-terminal extracellular fragment containing 34 epidermal growth factor (EGF)-like repeats and a C-terminal fragment comprising the transmembrane and intracellular domains. Remarkably all CADASIL-relevant mutations are located in the extracellular domain and result in an odd number of cysteine residues in the EGF-like repeats suggesting that aberrant disulfide bond formation might be involved in the pathogenic processes underlying CADASIL (Kotorii *et al.* 2006). However, the exact mechanism connecting defects in the NOTCH3 receptor to CADASIL pathology remains unknown. Due to its involvement in the upregulation of matrix metallo-protease (MMP) expression aberrant NOTCH3 signaling might lead to defects in VSMC migration

(Yamamoto *et al.* 2017). Furthermore, the NOTCH3 receptor is implicated in suppression of apoptosis via the Akt pathway indicating that an imbalance in VSMC death and survival might contribute to CADASIL (Wang *et al.* 2003; Downward 2004; Wang *et al.* 2007). Yet, recent findings suggest, that loss of NOTCH3 signalling is not the mechanism underlying CADASIL pathology, since NOTCH3-deficient transgenic mice showed neither accumulations of GOM, nor other symptoms indicative of CADASIL (Ruchoux *et al.* 2003) presumably due to the circumstance that a lack of NOTCH3 signalling can partially be compensated by NOTCH1 (Domenga *et al.* 2004; Kitamoto *et al.* 2005; Li *et al.* 2009; Sweeney *et al.* 2004). Rather the CADASIL phenotype is thought to be caused by a toxic accumulation of NOTCH3-ectodomain containing aggregates in the tunica media of small vessels (Joutel *et al.* 2000), which might serve as a seed for the prion-like propagation of protein aggregation, as has been described in a number of neurodegenerative diseases including Alzheimer's and Parkinson's syndrome (Choi and Gandhi 2018). Remarkably such protein aggregates have been found in close proximity to GOM accumulations in the vicinity of VSMCs (Joutel *et al.* 2000).

1.2.2 Retinal Vasculopathy with Cerebral Leukodystrophy (RVCL)

Retinal Vasculopathy with Cerebral Leukodystrophy (RVCL) is characterized by progressive retinal vasculopahy, retinal haemorrhages and neovascularization of the optic disc, which lead to continuous visual impairment during the fourth or fifth decade of life. Yet the distinctive feature of RVCL is the occurrence of so called pseudotumors – large areas of coagulative necrosis resulting from obliterative vessel damage, that are surrounded by vasogenic oedema and are typically found in the white matter of the cerebrum and cerebellum (Kavanagh *et al.* 2008).

RVCL is caused by mutations in the *TREX1* gene. *TREX1* codes for DNase III - a highly abundant 3'-5'-exonuclease implicated in DNA repair. In the absence of cell stress DNase III localizes to the perinuclear endoplasmatic reticulum (ER) via its C-terminal transmembrane helix, from where it is translocated to the nucleus upon oxidative stress stimuli. Remarkably, *TREX1* mutations found in RVCL patients did not alter the

enzyme's activity, but its cellular localization due to C-terminal truncations in the predicted transmembrane domain causing it to diffuse freely through the cytoplasm (Richards *et al.* 2007).

1.2.3 *COL4A1/A2*-related Arteriopathies

The spectrum of *COL4A1/A2*-related Arteriopathies comprises a number of separate phenotypes displaying both cerebral and systemic features. Whereas the juvenile form manifests with infantile hemiparesis, mental retardation, intracerebral haemaorrhages and porencephaly (Lanfranconi and Markus 2010), the adult form is distinguished into a cecebral variant displaying mainly neurological symptoms and a systemic phenotype involving defects in a number of organs (Alamowitch *et al.* 2009). Yet upon neuroimaging the three separate phenotypes display a distinct pattern of vascular defects typical for SVD with white matter lesions, subcortical infarcts and microbleeds being the most prominent features (Lanfranconi and Markus 2010). However, there are also common SNPS within the *COL4A1* and *COL4A2* genes that are associated with an increased risk for sporadic SVD thus linking *COL4A*-related arteriopathies to sporadic age- and environment-related disorders (Rannikmäe *et al.* 2015).

The *COL4A1* and *COL4A2* genes encode the collagen type IV α1 and α2 chains respectively. Type IV collagen is an integral component of the vascular basal membrane and contributes to tensile strength and endothelial cell integrity (Gould *et al.* 2006). Almost all mutations associated with *COL4*-related disorders are missense mutations affecting the highly conserved glycine residues within the glycine-proline-hydroxyproline motives, which are essential for α1/α2-triple helix formation, thus causing loss of the protein’s three dimensional structure (Gunda *et al.* 2014). As a result of the structural changes within the collagen type IV molecule the vascular basal membrane displays an elevated susceptibility to rupture, when exposed to environmental stresses, causing an increased fragility of the vessel walls (Gould *et al.* 2006).

1.2.4 Cerebral Autosomal Recessive Arteriopathy with Subcortical Infarcts and Leucoencephalopathy (CARASIL)

Cerebral Autosomal Recessive Arteriopathy with Subcortical Infarcts and Leucoencephalopathy (CARASIL) is an inherited small vessel disease caused by loss of function mutations in the *HTRA1* locus (Hara *et al.* 2009). Among the clinical characteristics of CARASIL there are both neuronal and extraneuronal manifestations (figure 1.6). The neuronal manifestations include recurrent lacunar strokes mainly located in the basal ganglia and thalamus or progressive deterioration in brain function with accumulating deficits in motor ability, cognitive decline and a final progression to dementia by the 40th decade of life (Fukutake 2011).

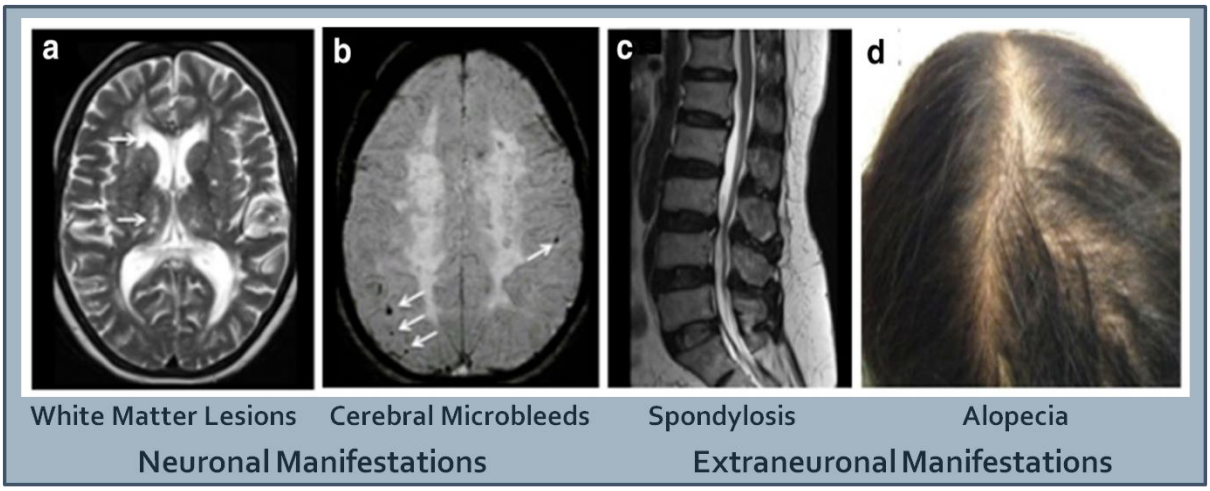

Figure 1.6 Neuronal and extraneuronal manifestations of CARASIL
Own compilation based on Khaleeli *et al.* 2015.

These symptoms are accompanied by a plethora of MRI findings matching the coherent pattern of SVD pathogenesis, which comprises cerebral microbleeds and diffuse white matter lesions. MRI abnormalities are usually found in the periventricular and deep white matter at the onset of symptoms, but subsequently extend to the basal ganglia, brain stem and cerebellum as the disease progresses (Fukutake and Hirayama 1995). Histologic examination of the cerebral small vessels reveals extensive arteriosclerotic changes associated with fibrous intimal thickening, loss of vascular smooth muscle cells, hyaline degeneration of the tunica media and fragmentation of the internal elastic membrane, but no deposition of GOM, as is regularly found in CADASIL patients (Arima *et al.* 2003). Notable these findings are

highly reminiscent of those observed in sporadic SVD. Yet in contrast to sporadic arteriopathies CARASIL pathology is associated with distinct extraneuronal manifestations including diffuse alopecia and spondylosis deformans in the cervical and thoracolumbar spine. Typically, the onset of these precedes that of the cerebral symptoms with spondylosis deformans beginning in the 30th decade of life and alopecia occurring already in the teenage years (Hara *et al.* 2009).

Approximately 50 verified cases of CARASIL have been reported to date with the first cases identified exclusively among the Japanese population (Hara *et al.* 2009). However, the syndrome's exact prevalence remains unknown, since it is thought to be substantially underdiagnosed due to its close resemblance to sporadic SVD. Recently a growing number of publications reported cases of CARASIL also among Chinese (Chen *et al.* 2013; Cai *et al.* 2015), Caucasian (Mendioroz *et al.* 2010), Gypsie (Menezes Cordeiro *et al.* 2015), Turkish (Bayrakli *et al.* 2014) and Pakistani (Khaleeli *et al.* 2015) families. Furthermore, the large number of different mutations identified and the absence of a founder haplotype indicate that the increased incidence of reported cases within Japanese pedigrees is rather due to a heightened awareness among scientists and physicians in Japan, where the condition was first described (Maeda *et al.* 1965), than due to an increased prevalence among its population. Taken together these findings suggest, that CARASIL is much more widespread than it was initially believed.

The association of CARASIL with mutations in *HTRA1* was first described by Hara *et al.* in 2009, who reported two missense (A252T and V297M) and two nonsense (R302X and R370X) mutations present homozygously in four independent consanguineous pedigrees in Japan. Both missense mutations are located in the protease domain affecting highly conserved residues and resulting in a profound decrease in proteolytic activity compared to the wildtype enzyme. As expected the truncated protein $HTRA1_{R302X}$ lacking the active site serine at position 328 appeared proteolytically inactive, whereas the R370X mutation displayed no apparent effect on proteolytic activity. Instead the mutation was reported to result in nonsense-mediated mRNA decay thus causing a reduction in overall HTRA1 levels.

The first reported case of CARASIL within the Caucasian population was described by Mendioroz *et al.* in 2010 in a patient displaying the novel mutation G295R in both his HTRA1 alleles. Remarkably symptoms of nonhypertensive arteriopathy were also found in heterozygous carriers within his family. Since the first cases of CARASIL were reported in individuals from consanguineous families, whose parents appeared unaffected, the disease was initially believed to follow a strictly recessive inheritance pattern. However, a growing number of reports on heterozygous mutation carriers displaying a CARASIL-like syndrome is emerging recently. The first of these was a study by Verdura *et al.* in 2015 presenting results from a genetic screening of 201 unrelated familial SVD cases of unknown aetiology, in which mutations in *NOTCH3* had been excluded prior to the investigation. Remarkably, 5 % of the screened individuals displayed heterozygous mutations in the *HTRA1* locus leading to the identification of 11 novel *HTRA1* mutations causing an SVD-like phenotype in an autosomal dominant manner. To some respect clinical and MRI findings in the affected individuals resembled those previously described in homozygously affected CARASIL patients. Yet the disease clearly differed from the classic CARASIL syndrome by a later age of onset, milder progression and a lack of extraneuronal manifestations thus impeding its distinction from sporadic SVD. All identified mutations were absent from both a control group containing sequences from 192 healthy individuals and commonly used databases (Exome Variant Server and 1000 Genomes Database). Furthermore, the mutations were located in residues conserved among HTRA1 family members and predicted to be detrimental by at least two of three *in silico* tools (SIFT, PolyPhen2 and Mutation Taster). Assessment of the mutants' proteolytic activities revealed a deleterious effect for all but two mutations (S284G and D450H) indicating that the pathogenic phenotype conferred by these two mutations might not result from changes in basic proteolytic activity. Notably, two of the investigated mutations (R166H and A173T) were detected in residues recently found to be mutated in homozygously affected CARASIL patients (Khaleeli *et al.* 2015; Menezes Cordeiro *et al.* 2015) and one (Y325-L335del) was found to cause a deletion of the catalytic serine 328 residue, as was previously described by Hara *et al.* (2009) for the R302X variant – one of the first mutations demonstrated to cause CARASIL in a homozygous manner – suggesting an overlap in the pathomechanisms conveyed by both homo- and heterozygous mutations.

Thus far it remains unknown whether the occurrence of a mild, late-onset phenotype in heterozygously affected individuals is a common feature in CARASIL pathogenesis or whether it is restricted to a certain subset of mutations causing the mutant allele to interfere with the physiological function of the remaining wildtype allele. Yet, symptoms in heterozygous carriers might have been overlooked in previous studies due to the disease's late age of onset and phenotypic resemblance to sporadic SVD. Furthermore, in a number of cases the occurrence of symptomatic disease was coupled to a history of smoking or hypertension indicating that heterozygous mutations in the *HTRA1* gene might rather be considered a genetic risk factor for the development of sporadic SVD than an independent syndrome.

Table 1.1 HTRA1 mutations associated with CARASIL or CARASIL-like phenotypes

Mutation	Effect	Reported Genotypes	Ethnicity	References
E42fs	frameshift resulting in premature stop-codon	homo- and heterozygous	Chinese	(Cai *et al.* 2015)
		compound heterozygous		(Bianchi *et al.* 2014)
S121R	aa substitution in the Kazal-like domain	heterozygous	Caucasian	(Verdura *et al.* 2015)
A123S	aa substitution in the Kazal-like domain	heterozygous	Caucasian	(Verdura *et al.* 2015)
R133G	aa substitution in the Kazal-like domain	heterozygous	Caucasian	(Verdura *et al.* 2015)
S136G	aa substitution in the Kazal-like domain	heterozygous	Caucasian	(Di Donato *et al.* 2017)
Q151K	aa substitution in the Kazal-like domain	homo- and heterozygous	Caucasian	(Di Donato *et al.* 2017)
Q151X	premature stop-codon	heterozygous	Caucasian	(Thaler *et al.* 2018)
R166C	aa substitution in the protease domain	homozygous	Gypsie	(Menezes Cordeiro *et al.* 2015)
R166H	aa substitution in the protease domain	heterozygous	Caucasian	(Verdura *et al.* 2015)
K168X	premature stop-codon	homozygous	Indian	(Preethish-Kumar *et al.* 2017)
A173P	aa substitution in the protease domain	heterozygous	Caucasian	(Verdura *et al.* 2015)
A173T	aa substitution in the protease domain	homo- and heterozygous	Pakistani	(Khaleeli *et al.* 2015)
V175M	aa substitution in the protease domain	homo- and heterozygous	Caucasian	(Di Donato *et al.* 2017)
V176A	aa substitution in the protease domain	heterozygous	Chinese	(Xie and Zhang 2018)
R197X	premature stop-codon	heterozygous	Chinese	(Xie and Zhang 2018)
G206E	aa substitution in the protease domain	heterozygous	Caucasian	(Di Donato *et al.* 2017)
G206R	aa substitution in the protease domain	homozygous	Caucasian	(Ibrahimi *et al.* 2017)
V216M	aa substitution in the protease domain	heterozygous	Japanese	(Kono *et al.* 2018)
A252T	aa substitution in the protease domain	homozygous	Japanese	(Hara *et al.* 2009) (Nozaki *et al.* 2016; Ito *et al.* 2016)
R274Q	aa substitution in the protease domain	homozygous	Japanese	(Nishimoto *et al.* 2011)
E277V	aa substitution in the protease domain	homo- and heterozygous	Indian	(Preethish-Kumar *et al.* 2017)
G283E	aa substitution in the protease domain	heterozygous	Japanese	(Nozaki *et al.* 2016)
S284G	aa substitution in the protease domain	heterozygous	Caucasian	(Verdura *et al.* 2015)
S284R	aa substitution in the protease domain	heterozygous	Caucasian	(Verdura *et al.* 2015)
P285L	aa substitution in the protease domain	homo- and heterozygous	Chinese	(Chen *et al.* 2013)
			Japanese	(Nozaki *et al.* 2016)
P285Q	aa substitution in the protease domain	heterozygous	Caucasian	(Verdura *et al.* 2015)
F286V	aa substitution in the protease domain	heterozygous	Caucasian	(Verdura *et al.* 2015)
G295R	aa substitution in the protease domain	homo- and heterozygous	Caucasian	(Mendioroz *et al.* 2010)
V297M	aa substitution in the protease domain	homozygous	Japanese	(Hara *et al.* 2009)
R302Q	aa substitution in the protease domain	heterozygous	Japanese	(Nozaki *et al.* 2016)
R302X	truncation due to premature stop-codon	homo- and heterozygous	Japanese	(Hara *et al.* 2009)
				(Tateoka *et al.* 2016)
				(Ito *et al.* 2016)
T319I	aa substitution in the protease domain	heterozygous	Japanese	(Nozaki *et al.* 2016)
A321T	aa substitution in the protease domain	compound heterozygous	Chinese	(Bianchi *et al.* 2014)
Y325_L335del	deletion due to abnormal splicing	heterozygous	Caucasian	(Verdura *et al.* 2015)
E347R	aa substitution in the protease domain	homozygous	Indian	(Preethish-Kumar *et al.* 2017)
L364P	aa substitution in the protease domain	homozygous	Chinese	(Chen *et al.* 2013)
R370X	nonsense-mediated mRNA decay	homozygous	Japanese	(Hara *et al.* 2009)
			Turkish	(Bayrakli *et al.* 2014)
D450H	aa substitution in the PDZ domain	heterozygous	Caucasian	(Verdura *et al.* 2015)

Table 1.1 gives an overview on all *HTRA1* mutations reported in both homo- and heterozygously affected individuals. The great majority of disease causing mutations is located within the protease domain indicating that the observed phenotype is most likely based on a loss of proteolytic activity. Yet, the exact mechanism underlying the deleterious effect of *HTRA1* mutations on vascular homeostasis is not yet fully understood. Since most CARASIL-relevant mutations were found to cause a loss of HTRA1 activity, defects in substrate processing appear as a plausible disease mechanism.

Previous studies revealed that HTRA1 activity is implicated in Transforming Growth Factor-β (TGF-β) signalling, a key pathway in the regulation of vascular remodelling and homeostasis, whose dysregulation might be a critical event in CARASIL pathogenesis (Beaufort *et al.* 2014). TGF-β belongs to a group of evolutionary conserved cytokines and is associated with a variety of physiological processes including smooth muscle cell (SMC) differentiation and the recruitment of SMCs both during vasculogenesis and in response to tissue damage (Dijke and Arthur 2007). Yet, its effects can be diverse due to the pathway's tight regulation and marked dependence on cellular context, differentiation state and the presence of other cytokines.

TGF-β is synthesized as a homodimeric proprotein (proTGF-β) subsequently undergoing proteolytic maturation. During maturation within the trans-Golgi network it is cleaved by the pro-protein convertase furin thus generating an N-terminal latency-associated peptide and mature TGF-β, which associate to form the small latent TGF-β complex (Liu *et al.* 2001). Following its assembly, the complex is bound to the latent TGF-β binding protein (LTBP) thereby forming the large latent TGF-β complex. Upon secretion, the complex is anchored to the ECM via interactions between the N-terminal domain of LTBP and components of the ECM network such as fibrillin-1 and fibronectin (Hynes 2009). Thus the ECM serves as a physiological reservoir for TGF-β, from which it can be released upon chemical or proteolytic stimuli – a process that is thought to be the rate-limiting step in TGF-β signalling. Following its release the TGF-β dimer can bind to TGF-β receptors which then transduce the signal to the nucleus via the Smad pathway (Scharpfenecker *et al.* 2007).

Due to its role in vascular homeostasis dysregulation of TGF-β signalling is associated with a number of cardiovascular disorders. These include (i) Hereditary Haemorrhagic Telangiectasia (HHT), a condition correlated with mutations within the TGF-β receptor or Smad genes (Goumans 81), (ii) Marfan syndrome, which is based on mutations in fibrillin, an ECM component controlling TGF-β bioavailability via its interaction with LTBP (Robinson *et al.* 2006), (iii) Loeys-Dietz syndrome, which is caused by mutations within the TGF-β receptors (Loeys *et al.* 2006) as well as (iiii) age-related sporadic SVD (Thompson and Hakim 2009).

Previous studies assumed that the clinical picture observed in CARASIL patients resulted from a pathologic upregulation of TGF-β signalling caused by insufficient proteolysis of either mature TGF-β (Launay *et al.* 2008; Oka *et al.* 2004), TGF-β receptors (Graham *et al.* 2013) or proTGF-β (Shiga *et al.* 2011) due to defects in HTRA1. However, this notion has been challenged in a recent report by Beaufort *et al.* (2014) demonstrating that reduced proteolytic processing of LTBP-1, which anchors the large latent TGF-β complex to the ECM thus regulating TGF-β bioavailability, is the key process driving CARASIL pathogenesis. In contrast to earlier studies the group observed a consistent down-regulation of TGF-β signalling in both HTRA1 knockout mice and skin fibroblasts isolated from a CARASIL patient, who carried the previously reported A173T mutation, suggesting a facilitating, rather than an inhibitory function of HTRA1 in TGF-β signalling. Processing of LTBP-1 appeared to be restricted to the N-terminal domain thus preventing its interaction with fibronectin and hindering its adhesion to the ECM. HTRA1 mutations found in CARASIL patients consistently abolished proteolytic cleavage. Remarkably, limited proteolysis of LTBP-1 was observed at HTRA1 concentrations as low as 1 nM, which corresponds to a thousandth of the amount required to observe efficient processing of previously reported substrates such as mature TGF-β itself (Launay *et al.* 2008; Oka *et al.* 2004). These findings strongly suggest that HTRA1 regulates TGF-β bioavailability via limited proteolysis of LTBP-1 and that abolishment of LTBP-1 processing due to CARASIL-relevant mutations results in a pathologic upregulation of TGF-β signalling thus driving disease progression.

1.2.5 Unifying Pathways in Familiar and Sporadic SVD

Despite differences in aetiology hereditary and sporadic SVD display a common pattern of histological, macroscopical and symptomatical findings indicating potential mechanistic similarities in disease progression. Especially in CARASIL histologic findings display a substantial resemblance to those detected in non-hereditary SVD. Furthermore, phenotypes observed in heterozygous carriers of disease causing *HTRA1* alleles are highly reminiscent of sporadic SVD except for their familial recurrence suggesting that an imbalance in HTRA1 activity might also be implicated in mechanisms underlying the non-familial form. Shared molecular mechanisms underlying hereditary and sporadic SVD have previously been reported in the context of both CADASIL and *COL4A1/A2*-related arteriopathies, since common polymorphisms in the *NOTCH 3* and *COL4A1/A2* genes were found to correlate with an enhanced risk for age- and hypertension-related white matter lesions and stroke (Rannikmäe *et al.* 2015; Schmidt *et al.* 2011).

A possible unifying disease pathway might also be considered on the molecular level based on the observation that CADASIL-relevant mutations in *NOTCH3* lead to toxic accumulation of the NOTCH3 ectodomain serving as seeds for the prion-like propagation of protein aggregates via a mechanism similar to that observed in neurodegenerative disease (Joutel *et al.* 2000). Within these aggregate deposits a number of other proteins involved in cerebral vessel integrity have been identified. These include LTBP-1 (Kast *et al.* 2014), which anchors TGF-β to the ECM thus regulating its bioavailability, suggesting that disruption of TGF-β signalling might not only contribute to CARASIL, but also to CADASIL pathology. Additionally, a variety of proteins implicated in ECM maintenance, such as vitronectin and tissue inhibitor of metalloprotease-3 (TIMP-3), were found within the NOTCH3 ectodomain aggregates. Abnormal activity of these proteins has been linked to vessel fibrosis (Monet-Leprêtre *et al.* 2013) thus providing a mechanistic explanation for the fibrotic changes detected in the small vessels of CADASIL patients, which are reminiscent of fibrosis observed in *COL4A1/A2*-related pathology. In line with these findings chronic upregulation of TGF-β signalling, as has been reported in cells lacking HTRA1 activity (Beaufort *et al.* 2014), has been shown to contribute to microvascular fibrosis via its impact on ECM remodelling as well as its facilitating role in epithelial-mesenchymal-transition (EMT) –

a process promoting the formation of fibroblasts upon destructive stimuli. Under physiological conditions this conversion from resident epithelial cells to collagen secreting fibroblasts enables rapid ECM turnover in response to injury thereby facilitating wound healing. However, dysregulation of these processes either due to mutations in components of the TGF-β pathway or due to permanent exposure to the mechanic stresses imposed by elevated blood pressure can result in chronic fibrosis finally leading to microvascular degeneration and SVD (Kalluri and Neilson 2003).

Previous studies demonstrated that HTRA1 facilitates the disintegration of amyloid Tau and Aβ aggregates frequently occurring in Alzheimer's disease thus promoting their subsequent proteolysis (Tennstaedt *et al.* 2012). The implication of prion-like protein aggregation in CADASIL aetiology might provide a link between the pathologic mechanisms underlying CARASIL and CADASIL hence yielding an explanation for their phenotypic similarities. Furthermore, HTRA1 was found to contribute to the regulatory processes underlying angiogenesis in a NOTCH-dependent manner by cleaving the physiological NOTCH interactor JAG1 (Klose *et al.* 2018). Thus, HTRA1 appears to be a key player in the maintenance of small vessel integrity, since it combines ECM turnover, the removal of aggregated proteins and regulation of both NOTCH and TGF-β signalling in one enzyme activity.

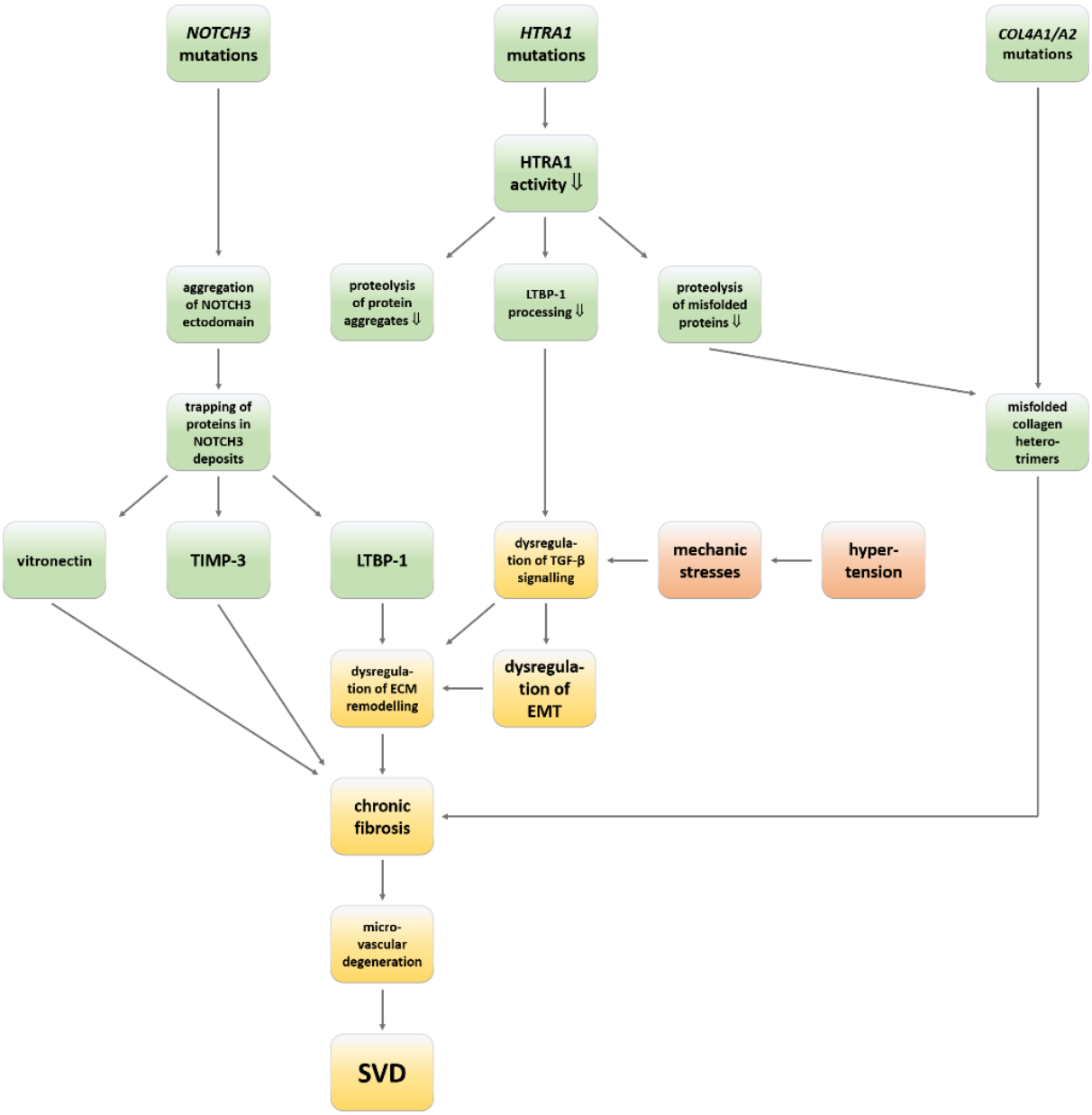

Figure 1.7 Pathway intersections linking various forms of SVD
Pathways linked to familial SVD are shown in green, mechanisms contributing to sporadic SVD are displayed in red and shared pathways are depicted in yellow.

Taken together the discovery of pathway intersections linking different types of SVD (figure 1.7) suggests that despite their distinct aetiology both familial and non-familial SVD might culminate in a common disease mechanism finally resulting in the disruption of small vessel integrity and cerebral malperfusion. Hence the investigation of pathogenic mechanisms underlying monogenic SVDs such as CARASIL might not only provide perspectives for future treatment of a single disease, but also contribute to our general understanding of sporadic SVD.

2 Aims

Dysregulation of HTRA1 activity is implicated in a number of pathologic processes including CARASIL, a monogenetic disorder based on loss of function mutations within the *HTRA1* locus. The loss of function phenotype is typically associated with mutations causing either premature stop codons or deleterious changes within the active site. Yet a small subset of mutations was found to be located at the trimer interface suggesting an effect on trimer stability rather than direct implications on active site integrity. The aim of this study was to biochemically characterize the CARASIL-relevant interface mutants regarding their proteolytic activity and oligomeric state in order to elucidate the molecular mechanisms underlying their functional impairment and gain deeper insights into the pathologic processes determining CARASIL progression.

On the basis of this characterization a diverse repertoire of protein repair strategies to achieve a functional restoration of the mutants' proteolytic activities was developed. These strategies include the reconstitution of trimer formation via molecular clamps that bridge the gap between two monomers thus shifting the monomer-trimer equilibrium back towards the trimeric state. Based on the observation that HTRA1 activity can be modulated allosterically via small peptides a second approach focuses on the application of peptidic activators chosen from an internal library. Both approaches will be evaluated regarding their impact on the proteolytic activity as well as oligomeric state of wildtype HTRA1 and constructs carrying CARASIL-relevant mutations. Whereas these two strategies are widely applicable to a broad range of HTRA1 interface mutants, an additional approach developed by the group of Martin Dichgans (Institute for Stroke and Dementia Research, University Clinic Munich, unpublished) focuses on the allele specific reconstitution of the disease-relevant mutant $HTRA1_{R274Q}$ via a compensatory mutation. Herein the determination of a crystal structure for HTRA1 comprising both the disease-relevant and the compensatory mutation is reported, which gives deeper insights into the structural implications underlying the rescue of oligomer formation as well as proteolytic activity.

The overall objective of this work is to generate a diverse portfolio of different proof of concept approaches aiming at the functional restoration of a catalytically defective

enzyme. On a conceptual level these approaches should be widely applicable to a vast number of biological problems involving the modulation of protein-protein interactions.

3 Materials and Methods

3.1 Materials

3.1.1 Equipment

Agarose Gel Chambers	Peqlab, Erlangen, Germany
Äkta FPLC	GE Healthcare, Little Chalfont, UK
Avance Ultrashield NMR Spectrometer	Bruker, Billerica, MA, USA
Buffer Exchange Columns (PD-10)	GE Healthcare, Little Chalfont, UK
Concentrators (Vivaspin)	Thermo Fisher Scientific, Rockford, IL, USA
Benchtop Shakers	Eppendorf, Hamburg, Germany
Benchtop Centrifuges	Eppendorf, Hamburg, Germany
French Pressure Cell	SLM Instruments Inc., Rochester, NY, USA
Glutathione Sepharose Column	GE Healthcare, Little Chalfont, UK
Incubator Shaker (Innova44)	Edison, NJ, USA (now Eppendorf Group)
J-710 CD spectrometer	Jasco, Easton, MD, USA
Microplates	Greiner Bio-One, Frickenhausen, Germany
Nanodrop Spectrophotometer	PeqLab, Erlangen, Germany
Ni-NTA Superflow Resin	GE Healthcare, Little Chalfont, UK
Power Supply (PowerPac 200)	Bio-Rad Laboratories, Hercules, CA, USA
Rotor (JA-25.50)	Beckman Coulter, Brea, CA, USA
Rotor (JLA-9.1000)	Beckman Coulter, Brea, CA, USA
Rotor (TLA-55)	Beckman Coulter, Brea, CA, USA
Semi-Dry Electrophoretic Transfer Cell	Bio-Rad Laboratories, Hercules, CA, USA
Size Exclusion Columns	GE Healthcare, Little Chalfont, UK
Sonication Water Bath (Bioruptor)	Diagenode, Seraing, Belgium
Spectrophotometer (Spectra Max M5)	Molecular Devices, San Jose, CA, USA
Tabletop ultracentrifuge	Beckman Coulter, Brea, CA, USA
Thermocycler	Biometra, Göttingen, Germany
Ultacentrifgue (Avanti J-E)	Beckman Coulter, Brea, CA, USA
UV/Vis Spectrophotometer	Molecular Devices, Sunnyvale, CA, USA
700 MHz NMR spectrometer	Bruker, Bremen, Germany

3.1.2 Bacterial strains

Table 3.1 shows the list of *E. coli* strains utilized in the course of this thesis.

Table 3.1 E. coli strains

Strain	Genotype
BL21 (DE3) Rosetta	F- ompT hsdSB(rB- mB-) gal dcm (DE3) pRARE (CamR)
BL21 (DE3) Rosetta II	F- ompT hsdSB(rB- mB-) gal dcm (DE3) pRARE2 (CamR)
DH5α	F-, supE44, ΔlacU169, [Φ80lacZΔM15], hsdR17, recA1, endA1, gyrA96, thi-1, (res-, mod+), deoR
TOP10	F– mcrA Δ(mrr-hsdRMS-mcrBC) φ80lacZΔM15 ΔlacX74, recA1 araD139 Δ(ara-leu)7697 galU galK rpsL (StrR) endA1, nupG λ-

3.1.3 Commercial vectors

Table 3.2 displays the commercial vectors utilized in the course of this thesis.

Table 3.2 Commercial vectors

Vector	Description
pET3d	vector for protein expression in bacteria, no tag, ampicillin resistance
pET21d	vector for protein expression in bacteria, C-terminal 6 x His tag
pET28a	vector for protein expression in bacteria, N-terminal 6x His-tag and thrombin cleavage site
$pET41b_{mod}$	vector for protein expression in bacteria, N-terminal 6 GST-tag and PreScission cleavage site, kanamycin resistance

All commercial vectors were obtained from Novagen, Darmstadt.

3.1.4 Plasmids utilized for protein expression

Table 3.3 displays the plasmids utilized for protein expression during this thesis.

Table 3.3 Plasmids utilized for protein expression
Amino acid residues are given in brackets and refer to the sequence of HTRA1 including the N-terminal signal peptide. HTRA1 lacking the N-terminal IGFBP (insulin-like growth factor-binding protein)-like and the Kazal-type modules is denoted as HTRA1dmac. HTRA1 lacking both the N-terminal IGFBP (insulin-like growth factor-binding protein)-like and the Kazal-type modules and the PDZ domain is denoted as HTRA1prot.

#	Description	Constructed by
945	pET21d HTRA1dmac (158-480)	Linda Truebestein
946	pET21d HTRA1dmacSA (158-480)	Linda Truebestein
1346	pET3d Tau 2N4R	Simon Poepsel
1426	pET21d HTRA1dmac R166H (158-480)	Till van Oepen
1437	pET21d HTRA1dmac R274Q (158-480)	Till van Oepen
1511	pET41b(mod) HtrA1dmacSA (158-480)	Linda Ingendahl
1512	pET41b(mod)HTRA1protSA (158-375)	Linda Ingendahl
1513	pET41b(mod)HTRA1protSA R166H (158-375)	Linda Ingendahl
1514	pET41b(mod)HTRA1protSA R274Q (158-375)	Linda Ingendahl
1517	pET41b(mod)HTRA1prot R274Q (158-375)	Linda Ingendahl
1520	pET21d HTRA1dmac A173T (158-480)	Linda Ingendahl
1522	pET21d HTRA1dmac G295R (158-480)	Linda Ingendahl
1551	pET41b(mod) HTRA1dmac (158-480)	Linda Ingendahl
1557	pET21d HTRA1dmac A252T (158-480)	Linda Ingendahl
1562	pET41b(mod) HTRA1dmacSA R274Q (158-480)	Linda Ingendahl
1615	pET28a HTRA1protSA R274Q D174R (161-375)	Linda Ingendahl
1679	pET41b(mod)HTRA1protSA A173T (158-375)	Linda Ingendahl

3.1.5 Oligonucleotides

Tables 3.4 and 3.5 display the oligonucleotides utilized for cloning and site-directed mutagenesis, respectively.

Table 3.4 Oligonucleotides used for cloning

#	Name	Sequence	Application
857	PreScission BamH1 for	GATCCCTGGAAGTTCTG TTCCAGGGGCCCG	Insertion of PreScission cleavage site
858	PreScission BamH1 rev	GATCCGGGCCCCTGGAA CAGAACTTCCAGG	
880	*HTRA1*prot pET41b for	TATATAGGGCCCGGGCA GGAAGATCCC	Cloning of *HTRA1*prot into pET41b
881	*HTRA1*prot pET41b rev	TTATTAGGCGCGCCTTAT TTTCCTTTGGCCTG	
882	*HTRA1*dmac pET41b for	TATATAGGGCCCGGGCA GGAAGATCCCAACAG	Cloning of *HTRA1*dmac into pET41b
883	*HTRA1*dmac pET41b rev	TTATTAGGCGCGCCCTAT GGGTCAATTTCTTCGGG	
1005	*HTRA1* pET28a for	TATATACATATGGATCCC AACAGTTTGCGC	Cloning of *HTRA1*dmac into pET28a
1006	*HTRA1*dmac pET28a rev	TTATTAGAGCTCCTATGG GTCAATTTCTTCGG	
1005	*HTRA1* pET28a for	TATATACATATGGATCCC AACAGTTTGCGC	Cloning of *HTRA1*prot into pET28a
1007	*HTRA1*prot pET28a rev	TTATTAGAGCTCTTATTTT CCTTTGGCCTGTC	

Table 3.5 Oligonucleotides used for site-directed mutagenesis

#	Name	Sequence	Application
497	*HTRA1* R274Q for	CGTTGGCCGCTCCTCAGAGCTGCAGCCGGGAGAGTTCGTGGTCGC	*HTRA1* R274Q
498	*HTRA1* R274Q rev	GCGACCACGAACTCTCCCGGCTGCAGCTCTGAGGAGCGGCCAACG	
859	*HTRA1* R166H for	GCAGGAAGATCCCAACAGTTTGCACCATAAATATAACTTTATCGC	*HTRA1* R166H
860	*HTRA1* R166H rev	GCGATAAAGTTATATTTATGGTGCAAACTGTTGGGATCTTCCTGC	
898	*HTRA1* D174R for	CTTTATCGCGCGCGTGGTGGAG	*HTRA1* D174R
899	*HTRA1* D174R rev	TTATATTTATGGCGCAAACTG	
992	*HTRA1* A328S for	CTATGGAAACTCGGGAGGCCCGTTAG	*HTRA1* A328S
993	*HTRA1* A328S rev	TTGATGATGGCGTCGGTC	
1242	*HTRA1* A173T for	TAACTTTATCACGGACGTGGTG	*HTRA1* A173T
1243	*HTRA1* A173T rev	TATTTATGGCGCAAACTG	
1244	*HTRA1* A252T for	AGCAGACATCACACTCATCAAAATTG	*HTRA1* A252T
1245	*HTRA1* A252T rev	TTCTCATCCACATCCTTG	
1246	*HTRA1* G295R for	AGTCACCACCCGGATCGTGAG	*HTRA1* G295R
1247	*HTRA1* G295R rev	GTGTTTTGAAGGGAAAACG	

All oligonucleotides were obtained from Sigma Aldrich, Munich, Germany and dissolved to a concentration of 100 µM in ddH_2O.

3.1.6 Peptides

Peptide sequences (table 3.6) were derived from the C-termini of various human proteins. In order to simplify the nomenclature peptides were named after the proteins they originate from. All synthetic peptides were provided by Intavis, Tübingen, Germany.

Table 3.6 Peptides

Number	Name	Sequence
18	CCNH (Cyclin H)	EWTDDDLVESL
76	CAPN2.1	LISWLSFSDL
93	CCNH-CFD.1	EWTDDDLSVDA
95	CCNH.2	EWTDDDLELEA
96	CCNH-VDAC2AL	EWTDDDLELEL
372	VDAC1	KLGLGLEFQA
373	VDAC2	KVGLALELEA
374	VDAC3	KVGLGFELEA
433	VDAC2.1	KVGLALFLKA
434	VDAC2.2	KVGLYLWLKV
435	VDAC2.3	ALFLKA
436	VDAC2.4	YLWLKV

3.1.7 Commercially obtained proteins and enzymes

Commercially obtained enzymes utilized in the course of this thesis are given in table 3.7.

Table 3.7 Commercially obtained proteins and enzymes

Protein/Enzyme	Manufacturer
α-casein	Sigma-Aldrich, Munich, Germany
β-casein	Sigma-Aldrich, Munich, Germany
BSA (bovine serum albumin)	Sigma-Aldrich, Munich, Germany
DNaseI	Sigma-Aldrich, Munich, Germany
T4 ligase	Roche, Mannheim, Germany
Phusion High Fidelity Polymerase	NEB, Ipswich MA, USA
Restriction enzymes	NEB, Ipswich MA, USA

3.1.8 Protein- and nucleic acid standards

Commercially obtained standards utilized for the determination of protein molecular weights and nucleic acid lenghts are enlisted in table 3.8.

Table 3.8 Protein- and nucleic acis standards

Standard	Company
FPLC Gelfiltration LMW&HMW Standard	Bio-Rad, Munich, Germany
Prestained SDS-PAGE Standard	Bio-Rad, Munich, Germany
Unstained SDS-PAGE Standard	Bio-Rad, Munich, Germany
HiMark Prestained HMW Standard	Invitrogen, Waltham MA, USA
Quick-Load 2-Log DNA Ladder	NEB, Ipswich MA, USA

3.1.9 Compounds, chemicals and kits

Compounds were provided by Michael Kuszner and Alexander Zimmermann, Department of Supramolecular Chemistry, University of Duisburg-Essen. Chemicals were obtained from Sigma Aldrich, AppliChem, Roth, Invitrogen, Fisher Scientific, New England Biolabs and Merck. Kits and purification systems utilized in the course of this thesis and their manufacturers are enlisted in table 3.9. Antibiotics were obtained from Roth and are shown in table 3.10.

Table 3.9 Kits and purification systems

Kit	Manufacturer
NucleoBond Xtra Maxi	Macherey-Nagel, Düren, Germany
NucleoBond Xtra Midi	Macherey-Nagel, Düren, Germany
NucleoSpin PCR Clean-up	Macherey-Nagel, Düren, Germany
Q5 Site directed mutagenesis	NEB, Ipswich MA, USA
QIAprep Spin Miniprep Kit	Qiagen, Hilden, Germany
QIAquick Gel Extraction Kit	Qiagen, Hilden, Germany
Roti-Nanoquant	Roth, Karlsruhe, Germany

Table 3.10 Antibiotics

Antibiotic	Concentration
Ampicillin	200 µg/ml
Kanamycin	100 µg/ml
Chloramphenicol	30 µg/ml

3.1.10 Software

Software used for experiment design and data analysis is displayed in table 3.11.

Table 3.11 Software

Software	Company
Photoshop Elements	Adobe Systems Inc., San Francisco, USA
Citavi 6	Swiss Academic Software GmbH, Wädenswil, Switzerland
CodonCode Aligner	CodonCode Corporation, Centerville, USA
Endnote X8	Clarivate Analytics, Stamford, USA
Fiji	Open Source (Schindelin *et al.* 2012)
GraphPad Prism 5	GraphPad Software Inc, LaJolla, USA
Microsoft Office	Microsoft Corporation, Redmond, USA
PyMOL 1.1	Schrödinger, LLC., New York, USA
Serial Cloner 2.6	Open Source (Serial Basics)
UMSAP	Open Source (Bravo-Rodriguez *et al.* 2018)
Unicorn 6	GE Healthcare, Little Chalfont, UK

3.2 Microbiological methods

3.2.1 Sterilization

Media and solutions were sterilized by autoclaving. In the course of this, they were heated to 120 °C for 20 minutes. Heat sensitive solutions were sterile filtered with a 0.22 µm filter (Millipore).

3.2.2 Growth and cultivation of *E. coli*

Liquid cultures of *E. coli* were grown in Erlenmeyer flasks of appropriate size at 37 °C unless stated otherwise. Flasks were shaken at 180 rpm. Streak-outs were done on media plates using wooden applicators.

NZA media	10 g NZ amine A
	5 g yeast extract
	5 g NaCl
	1 l H_2O
M9 media	50 mM Na_2HPO_4
	25 mM KH_2PO_4
	10 mM NaCl
	0.1 % NH_4Cl
	5 mM $MgSO_4$
	0.2 mM $CaCl_2$
	0.25 mM trace metals
	1 % BME vitamins
	1 % glucose

3.2.3 Glycerol stocks of *E. coli* strains

Glycerol stocks of *E. coli* strains were made from stationary phase cultures grown overnight. 500 µl of culture were mixed with the same volume of 50 % (v/v) glycerol and subsequently stored at -80 °C in appropriate cryo vials.

3.2.4 Determination of cell densities in liquid cultures

The cell density of liquid cultures was determined by measurement of the optical density in a photometer at a wavelength of 600 nm. NZA media or M9 minimal media was used as a blank.

3.2.5 Preparation of chemically competent *E. coli* cells

Cells from overnight cultures were diluted at a ratio of 1:100 in 200 ml NZA media containing 0.2 % arabinose and subsequently grown to an OD_{600} between 0.8 and 1.0. All following steps were carried out at 4 °C or on ice. After centrifugation at 6000 x g for 10 minutes the bacterial pellet was resuspended in 100 ml 0.1 M $CaCl_2$ followed by a second centrifugation step (6000 x g, 10 minutes). Cells were thereupon resuspended in 10 ml 0.1 M $CaCl_2$ followed by a third centrifugation step (6000 x g, 10 minutes). After resuspension of the bacterial pellet in 2 ml of 15 % cold glycerol, 0.1 M $CaCl_2$ samples were stored at -80 °C.

3.2.6 Transformation of chemically competent *E. coli* cells

Aliquots of cells (50 µl) were transformed with 100 ng of plasmid DNA and incubated on ice for 30 minutes before exposure to 42 °C for 1 minute. After incubation for 2 minutes on ice 500 µl NZA medium were added and the cells were incubated at 37 °C for 1 hour on a shaker (400 rpm). Afterwards, they were plated on NZA selective media containing the appropriate antibiotic and grown overnight at 37 °C.

3.2.7 Preparation of electrocompetent *E. coli* cells

Cells from overnight cultures were diluted at a ratio of 1:100 in 200 ml NZA media containing 0.2 % arabinose and subsequently grown to an OD_{600} between 0.5 and 0.6. All following steps were carried out at 4 °C or on ice. Cells were harvested by centrifugation at 5000 x g for 10 minutes and the bacterial pellet was thereupon resuspended in 1 ml of cold ddH_2O followed by centrifugation at 13000 x g for 2 minutes. These washing steps were repeated four times. After resuspension of the final pellet in 1 ml of 10 % cold glycerol in ddH_2O samples were stored at -80 °C.

3.2.8 Transformation of electrocompetent *E. coli* cells

40 µl of electrocompetent *E. coli* cells were thawed on ice for 5 minutes, mixed with 200 ng of plasmid DNA and transferred to an ice cold 2 mm gap electroporation cuvette. Cells were subsequently pulsed for 4.7 to 5.5 milliseconds at 2.5 kV, 25 µF and 200 Ω. Following the pulse cells were diluted in 500 µl NZA medium and grown at 37 °C, shaking at 180 rpm, for 1 hour. Afterwards cells were spread on appropriate agar plates containing the suitable selective antibiotic and incubated over night at 37 °C.

3.3 DNA analytical methods

3.3.1 Plasmid DNA isolation

Plasmid DNA was isolated from 5 ml late stationary phase *E. coli* cultures using the QIAprep Spin Miniprep Kit.

3.3.2 Polymerase Chain Reaction

Polymerase Chain Reaction (PCR) was used to amplify DNA fragments from a given DNA template. Reactions were assembled on ice according to table 3.12. Cycling parameters of a typical PCR reaction are depicted in table 3.13 as an example.

Table 3.12 Reaction mixture for PCR

Component	Amount per reaction
5x reaction buffer	10 µl
DNA template (20 ng/µl)	1 µl
forward primer (100 ng/µl)	1 µl
reverse primer (100 ng/µl)	1 µl
dNTPs	1 µl
DNA template (20 ng/µl)	1 µl
phusion polymerase	1 µl
water	34 µl

Table 3.13 Cycling parameters for PCR

Segment	Number of cycles	Temperature	Duration
1	1	95 °C	1 minute
2	25	95 °C	30 seconds
		62 °C	30 seconds
		72 °C	1 minute
3	1	72 °C	10 minutes

3.3.3 Restriction digests

Restriction digests were performed using restriction enzymes provided by New England Biolabs in the recommended buffers or in the case of two enzymes used simultaneously in the buffer in which both enzymes retain most of their activity. Both PCR products and vectors were digested over night at 37 °C. Following the restriction reaction the digested PCR products were cleaned up with PCR DNA clean-up kits (Macherey-Nagel), whereas the digested vector was separated from the insert via agarose gel electrophoresis and subsequent gel extraction (QIAquick Gel Extraction Kit, Qiagen), followed by an analytical agarose gel electrophoresis in order to estimate the relative amounts of DNA to be used in the ligation reactions.

3.3.4 DNA ligation

Following restriction digests ligation of the insert into the vector was performed using the Rapid DNA Ligation kit (Roche) which allows ligation at room temperature within 5 minutes. Typically several ratios between 2:1 and 10:1 were tested for each pair of insert and target vector. Ligation products were transformed into competent *E. coli* cells immediately after the reaction.

3.3.5 Agarose gelelectrophoresis

Agarose gelelectrophoresis was used for the analytical and preparative separation of DNA fragments. The appropriate amount of agarose powder (1 % if not stated otherwise) was dissolved in TAE-buffer. The mixture was heated and subsequently cast into a gel chamber to solidify. Samples were mixed with an appropriate volume of 5x loading dye and 50x Midori Green Nucleic Acid Gel Stain. Separation was subsequently performed at 100 V until the dye front had migrated two-thirds of the gel's length. Bands were visualized using UV light at a wavelength of 300 nm.

TAE buffer:	20 mM TRIS
	10 mM Sodium acetate
	0.5 mM EDTA
	pH 7.8

3.3.6 Extraction of DNA fragments from agarose gels

DNA fragments were purified from cut out agarose gel bands using the QIAquick Gel Extraction Kit (Qiagen).

3.3.7 DNA sequencing

Sequencing was performed by Seqlab Microsynth. All samples were prepared according to the company's specifications.

3.3.8 PCR mutagenesis

PCR mutagenesis was applied to generate site directed point mutations on a template vector using synthetic oligonucleotide primers containing the desired mutation. The primers, which are complementary to opposite strands of the vector DNA, bind to the template and are subsequently extended by Phusion High Fidelity DNA polymerase during temperature cycling thus generating a mutant plasmid containing staggered nicks. The reaction mixture and cycling parameters are depicted in tables 3.14 and 3.15.

Table 3.14 Reaction mixture for PCR mutagenesis

Component	Amount per reaction
water	40.5 µl
10x cloned Pfu reaction buffer AD	5.0 µl
dNTP mix (25 µM each dNTP)	1.0 µl
DNA template (100 ng/µl)	0.5 µl
Primer 1 (100 ng/µl)	1.0 µl
Primer 2 (100 ng/µl)	1.0 µl
Phusion High Fidelity DNA Polymerase (2.5 U/µl)	1.0 µl

Table 3.15 Cycling parameters for PCR mutagenesis

Segment	Number of cycles	Temperature	Duration
1	1	95 °C	1 minute
2	28	95 °C	30 seconds
		Primer Tm -5 °C	30 seconds
		72 °C	1 minute per kb
3	1	72 °C	10 minutes

Following temperature cycling PCR products were incubated with the endonuclease *Dpn*-I, which degrades methylated and hemimethylated DNA, for 4 hours in order to digest the parental DNA template. The enzyme was subsequently inactivated by incubating samples at 60 °C for 10 minutes.

3.4 Biochemical Methods

3.4.1 Purification of His-tagged HTRA1

Human recombinant HTRA1 was purified as described by Truebestein *et al.* (2011). For expression of His-tagged HTRA1, BL21 (DE3) Rosetta 2 cells were transformed with pET vectors containing the respective HTRA1 sequences and grown over night in 250 ml NZA medium containing the appropriate antibiotic. The preculture was used to inoculate larger volume expression cultures (2 l per flask) starting at an OD_{600} of 0.05. After growing the cultures to an OD_{600} of 0.6-0.8 protein expression was induced with 0.5 mM IPTG. 1 hour before induction, the cultures were transferred to 25 °C. Expression was carried out for 5 hours, 25 °C, 180 rpm.

Following expression, cells were harvested by centrifugation (15 minutes, 8000 x g, 4 °C) and resuspended in 100 ml of buffer A. DNAse I was added to reduce the viscosity of the suspension. Subsequently cells were disrupted using a French Press (SLM Inc.). The lysate was centrifuged at 50000 x g for 1 hour. Purification was performed using an Äkta FPLC system. The cleared supernatant was loaded on a Ni-NTA column (GE Healthcare) equilibrated with buffer A. The column was washed with 6 column volumes buffer A and subsequently with 6 column volumes buffer B and 6 column volumes 12 % buffer C (30 mM imidazole) to remove unspecific bound proteins. HTRA1 was eluted via a gradient containing increasing amounts of buffer C (12-100 %). Eluted fractions were analyzed by SDS-PAGE. After Ni-NTA purification, the protein was concentrated to 1 ml and loaded on a Superdex-200 preparation grade column (GE Healthcare) equilibrated with buffer D. Fractions containing HTRA1 were combined, concentrated to approx. 20 mg/ml, flash-frozen in liquid nitrogen and stored at -80 °C.

Buffers

Buffer A: 100 mM TRIS
150 mM NaCl
pH 7.5

Buffer B: 100 mM TRIS
1 M NaCl
pH 7.5

Buffer C: 100 mM TRIS
150 mM NaCl
250 mM imidazole
pH 7.5

Buffer D: 50 mM NaPi
100 mM NaCl
pH 8

3.4.2 Purification of tag-less HTRA1

In order to obtain tag-less HTRA1 for the implementation of NMR experiments a three step purification procedure consisting of a glutathione-sepharose column, a reverse glutathione-sepharose column and a final gel filtration step was established in the course of this thesis. For expression of HTRA1, BL21 (DE3) Rosetta cells were transformed with a modified pET41b vector containing the respective HTRA1 sequences. In the modified vector the thrombin cleavage site situated between the glutathione-S-transferase (GST)-tag and the multiple cloning site was exchanged for a PreScission cleavage site thus generating an HTRA1 construct with only two additional amino acid residues (glycine and proline) remaining at the N-terminus after cleavage.

After expression, harvesting and lysis as described above for 6x His-tagged HTRA1 the lysate was applied to a glutathione sepharose 4 Fast Flow column (GE Healthcare) connected to an Äkta FPLC system. The column was washed with 4 column volumes buffer A and subsequently with 3 column volumes buffer B to remove unspecifically bound proteins. In the next step 100 U of GST-tagged PreScission protease diluted in 80 ml of buffer A were loaded onto the column to facilitate cleavage of the immobilized protein at the PreScission cleavage site. The buffer containing the PreScission protease was cycled through the column at 1 ml/min over night. Thereafter cleaved HTRA1 was eluted from the column with 3 column volumes of buffer A and the eluted fractions were collected and concentrated using a Vivaspin centrifugal device. To ensure the removal of residual unspecifically bound proteins as well as uncleaved GST-HTRA1 and the GST-tagged PreScission protease a reverse glutathione-sepharose purification step was carried out. The column was washed with 5 column volumes buffer A and HTRA1 was collected in the flowthrough, whereas unspecific binders and proteins containing a GST-tag were retained on the column. Fractions from the flowthrough were analyzed by SDS-PAGE and samples containing HTRA1 were subjected to size exclusion chromatography (SEC) on a Superdex 75 preparation grade gel filtration column (GE Healthcare) equilibrated with buffer C. Fractions containing HTRA1 were combined, concentrated, flash-frozen in liquid nitrogen and stored at -80 °C

Buffers

Buffer A	50 mM NaPi
	300 mM NaCl
	pH 7
Buffer B	50 mM NaPi
	100 mM KPi
	10 mM $MgCl_2$
	5 % glycerol
	5 mM DTT
	250 µM ATP
	pH 7

Buffer C	50 mM KPi
	pH 6.7

3.4.3 Purification of Tau-2N4R

Tau-2N4R was purified by boiling of cleared bacterial lysates followed by hydroxylapatite (HAP) chromatography and size-exclusion chromatography (SEC). BL21 (DE3) Rosetta II cells were transformed with pET3d vectors containing the respective Tau sequence and grown as 250 ml over night cultures that were used to inoculate expression cultures of 2 l each starting at an OD_{600} of 0.05. The expression cultures were grown to an OD_{600} of 0.6-0.8 and induced with 0.1 mM IPTG for expression. After 5 hours at 37 °C, the cells were harvested at 8.000 x g, 4 °C for 15 minutes. Lysis was performed with a French pressure cell in buffer A. The lysate was cleared by centrifugation (50,000 x g, 4 °C, 1 hour), and the supernatant was transferred to 2 ml tubes (ca. 1.5 ml per tube) for boiling in a water bath for 20 minutes. The boiling step was followed by centrifugation (35.000 x g, 4 °C, 40 minutes) and recovery of the supernatant containing Tau and little amounts of contaminating proteins. The supernatant was further purified by HAP chromatography, where Tau was loaded onto the column in buffer A, washed with 4 column volumes of the same buffer, followed by Tau elution via an NaCl gradient (0-100 % buffer B). Typically, Tau eluted at an NaCl concentration of ca. 240 mM. The flowthrough from HAP chromatography purification was re-applied to the column after the first purification step to increase the total yield of protein, since large amounts of Tau appeared in the flowthrough after the first round of HAP chromatography. Pooled fractions were concentrated in centrifugal concentration devices. The concentrated sample was ultracentrifuged at 150000 x g for 1 hour at 4 °C in order to remove potential aggregates. The supernatant was further purified by SEC using a Superdex 200 preparation grade size exclusion chromatography column equilibrated with buffer C. Following SEC, the sample was concentrated to approximately 10-25 mg/ml storage concentration, flash-frozen in liquid nitrogen and stored at -80 °C until usage. Due to its low staining by Bradford reagent, the concentration of Tau was determined by

comparison of Coomassie Brilliant Blue stained bands after SDS-PAGE with bands of a serial dilution standard of BSA.

Buffers

Buffer A	100 mM HEPES
	10 mM KPO_4
	2 mM DTT
	pH 7.6
Buffer B	100 mM HEPES
	10 mM KPO_4
	1 M NaCl
	2 mM DTT
	pH 7.6
Buffer C	10 mM HEPES
	50 mM $(NH_4)_2SO_4$
	2 mM TCEP
	pH 7.5

3.4.4 Protein ultrafiltration

Protein concentration was achieved by application to a centrifugal device containing a porous membrane, which allows for the passage of molecules below a given molecular weight, and centrifugation at 3000 x g, 4 °C until the desired volume of concentrated sample was reached.

3.4.5 Determination of protein concentrations

Protein concentrations were measured using the Bradford method (Bradford 1976). Upon binding of the Bradford reagent to the protein the absorption maximum of the sample shifts from 465 nm to 595 nm. Absorptions were acquired using a Spectra Max M5 spectrometer (Molecular Devices). The $Quotient_{465/595}$ derived from these measurements was proportional to the protein concentration of the solution. All assays were performed according to the Roti Nanoquant (Roth) manual.

Alternatively, determination of protein concentrations was achieved by subjecting different dilutions of the protein to SDS-PAGE analysis and subsequent comparison to a BSA concentration standard.

3.4.6 SDS-Polyacrylamide Gel Electrophoresis (SDS-PAGE)

Sodium dodecyl sulfate – polyacrylamide gel electrophoresis (SDS-PAGE) is an analytical method that allows for the separation of proteins according to their molecular weight. The chemical compound sodium dodecyl sulfate denatures protein structures and evenly covers the polypeptide chain with portions of negative charge. As a consequence, proteins move through the polyacrylamide matrix towards the anode with a speed that corresponds to their molecular weight and that is independent of their folding state. Proteins are visualized in the gel by staining methods such as Coomassie Brilliant Blue staining. Identification is carried out via protein size or, alternatively, with immunological methods such as Western blotting. The polyacrylamide concentration determines the size of the pores in the resulting gel matrix. Therefore, different concentrations are recommended for various ranges of protein size. In this study gels containing 12-15 % polyacrylamide were utilized.

Buffers:

SDS-Loading Dye 5 x	0.3 M TRIS 10 % SDS 40 % glycerol 0.001 % bromophenol blue 30 mM DTT (added just before usage) pH 6.8
10 x SDS running buffer	1.92 M glycine 333 mM TRIS, 1 % SDS pH 8.3

3.4.7 Coomassie Brilliant Blue staining

Proteins separated in SDS-PAGE gels were visualized by staining the gels according to Wong *et al.* (2000). A major advantage of this method is the very low processing time of about 10 minutes per gel. Gels were successively heated in buffers A and B in the microwave at 600 W for 1 minute. Used buffers were discarded after each heating step. Heating with buffer A was followed by gentle shaking for 5 minutes. After heating in buffer B the gels were destained in buffer B for several hours.

Buffers:

Buffer A	20 % 2-propanol 10 % acetic acid 0.05 % Coomassie Brilliant Blue
Buffer B	10 % acetic acid

3.4.8 Silver staining

To visualize proteins in TRIS-acetate gels silver staining was performed according to Merril *et al.* (1981). This method is very sensitive and allows for the visualization of proteins down to the low nanogram level. Following electrophoresis gels were transfered to a staining basin and incubated in fixing solution at room temperature for 30 minutes. Subsequently the gels were washed for 10 minutes in washing solution. This step was repeated 2 times followed by an additional 1 hour washing step in ddH_2O. Gels were then incubated in thiosulfate solution for exactly 1 minute and washed 3 x 20 seconds with ddH_2O. Following a 20 minute incubation in silver nitrate solution and an additional 3 x 20 seconds washing step in ddH_2O the gels were incubated in developing solution until desired staining was gained. To stop the staining reaction gels were rinsed with ddH_2O and incubated in stopping solution for 10 minutes.

Buffers:

Fixing solution	40 % EtOH 10 % acetic acid 500 µl 37 % formaldehyde per litre
Washing solution	30 % EtOH
Thiosulfate solution	0.02 % sodium thiosulfate
Silver nitrate solution	0.2 % silver nitrate 75 µl 37 % formaldehyde per 100 ml (prepared just before usage)
Developing solution	3 % sodium carbonate 0.0004 % sodium thiosulfate 500 µl 37 % formaldehyde per litre
Stop solution	50 mM EDTA

3.4.9 Western Blot analysis

Proteins that have been previously separated by electrophoretic methods can be detected and identified by applying the immunological method of Western blotting (also: immunoblotting). For this purpose the proteins are transferred to a nitrocellulose or polyvinylidene fluoride (PVDF) membrane in a strong electric field. Those molecules bound to the membrane are subsequently recognized and bound by specific antibodies, which are in turn detected by secondary antiimmunoglobulin antibodies. The latter are most commonly coupled to horseradishperoxidase (HRP) or alkaline phosphatase (AP) which allows convenient detection via the enzymatic activity visualized by means of chromogenic or fluorogenic substrates.

Western blotting was performed as follows. After electrophoresis gels were equilibrated with transfer buffer for 10 minutes at room temperature. Meanwhile, a PVDF membrane of respective size was activated by incubation in 100 % methanol (MeOH) for 1 minute and ddH_2O for 5 minutes and finally soaked in transfer buffer for 10 minutes. Two sheets of thick blotting paper were soaked with transfer buffer. One sheet of blotting paper, the PVDF membrane, the gel and the second sheet of blotting paper were placed in a tank blotting or a semi-dry blotting apparatus and air bubbles were removed. Blotting was performed at 25 V with a current of 70 mA per gel for 30 minutes for semi-dry blots or at 100 V for 1 hour for tank blots.

Subsequently, the membranes were blocked with 3 % bovine serum albumin (BSA) in TBS-T for 1 hour at room temperature. All incubation steps were performed on a shaker at room temperature. The primary antibody was employed in 3 % BSA, TBS-T, for 1 hour. After washing with TBST 3 times for 5 minutes, the membranes were incubated in 3 % BSA, TBS-T containing the secondary antibody for 30 minutes. This step was followed by washing in TBS-T three times for 5 minutes. For visualisation the membranes were equilibrated with AP buffer for 5 minutes and incubated in AP staining solution until the desired staining intensity was obtained. The membranes were dried over night prior to evaluation.

Buffers:

Transfer buffer	15 mM TRIS 120 mM glycine 20 % methanol 0.2 % SDS pH 8.3
TBS-T	20 mM TRIS 150 mM NaCl 0.05 % TWEEN-20 pH 7.5
AP buffer	100 mM TRIS 100 mM NaCl 5 mM $MgCl_2$ pH 9.5
Staining solution	10 ml AP-buffer 66 µl NBT (50 mg/ml in 70 % DMF) 33 µl BCIP (50 mg/ml in 100 % DMF)

3.4.10 Proteolytic digest of model substrates

To follow the degradation of the model substrates α-casein, ß-casein and Tau 1 µM HTRA1 were incubated with 20 µM casein or 8 µM Tau respectively at 37 °C. At certain time points aliquots were taken and the reaction was stopped by adding 5x SDS loading dye. Subsequently, the aliquots were incubated for 5 minutes at 95 °C and analyzed by SDS-PAGE. Proteins were detected by Coomassie Brilliant Blue staining.

3.4.11 Proteolytic digest of model substrates in the presence of different compounds

Degradation of model substrates by HTRA1 was followed in the presence of different compounds. 1 µM HTRA1 were incubated with different ratios of the respective compound at 37 °C for 30 minutes. Subsequently 20 µM casein or 8 µM Tau, respectively, were added to the samples followed by continuous incubation at 37 °C. Samples were taken at appropriate timepoints and degradation products were analyzed on SDS-PAGE.

3.4.12 pNA (para-Nitroanilin)-assay

pNA (para-Nitroanilin)-assays are used to quantify the specific activity of a protease. In order to determine the proteolytic activity of HTRA1 a substrate containing the RseA-derived amino acid sequence “VFNTLPMMGKASPV” conjugated to pNA was used. Proteolytic cleavage by the protease results in the release of the free pNA-group. Increasing release of pNA was measured by absorption spectophotometry at a wavelength 405 nm.

All measurements were conducted in TRIS, 150 mM NaCl, pH 8. 1 µM HTRA1 were incubated with different concentrations of compounds at 37 °C for 30 minutes. Subsequently 500 µM pNA-substrate were added to the samples and absorbance was continuously measured at a wavelength of 405 nm. Measurements were conducted for 2 hours.

$$\text{Specific activity} = (\Delta A_{405} \times V)/(m \times \varepsilon \times t)$$

Δ_{405}: absorbance difference
V: reaction volume [ml]
m: amount of protease [mg]
ε: molar extinction coefficient of pNA [8.800 M^{-1} x cm^{-1}]
t: time [min]
d: layer thickness [cm]

3.4.13 Mass spectrometry analysis of proteolytic digests

In order to identify HTRA1 cleavage sites peptides generated in proteolytic digests were subjected to mass spectrometry analysis. Peptides were derived from proteolytic degradation of the model substrates β-casein and Tau as described in section 3.4.10. Samples were taken at defined time points (0, 10 and 40 minutes for β-casein and 0, 30 and 240 minutes for Tau) and proteins were precipitated via addition of ice-cold acetone p.a. at a ratio of 6:1 followed by overnight incubation at -20 °C. To separate the generated peptides from the remaining proteins samples were centrifuged at 21000 x g, 4 °C for 1 hour. Supernatants were subsequently lyophilized in an Eppendorf 5301 concentrator. The resulting pellet was resuspended in 0.1 % formic acid and applied to C18 tips for further purification. Separation of the purified peptides was performed on a Thermo easy-nLC 1000 equipped with a Thermo Nanospray Flex ion source and masses were analyzed via an Orbitrap Elite 100 LC-MS ion trap spectrometer. Mass spectrometry analysis was carried out in collaboration with the Analytics Core Facility, University of Duisburg-Essen. Data were processed using the Utilities for Mass Spectrometry Analysis of Proteins (UMSAP) analysis software developed by Kenny Bravo-Rodriguez at the University of Duisburg-Essen (Bravo-Rodriguez *et al.* 2018).

3.4.14 Glutaraldehyde crosslinking

Determination of the oligomeric state of HTRA1 and different HTRA1 mutants was achieved via chemical crosslinking prior to gel electrophoresis. Covalent fixation is a prerequisite for oligomeric state analysis via non-native SDS-PAGE, since the non-covalent nature of the interface contacts within the HTRA1 trimer would lead to the dissociation of oligomers under denaturing conditions. From a multitude of commercially available crosslinkers glutaradehyde was chosen as a suitable reagent for this set of experiments. Glutaraldehyde is a highly effective, stable and inexpensive crosslinking reagent. It carries two reactive carbonyle groups, which facilitate the formation of covalent bonds with primary amino groups. The length of the crosslinking arm is not constant, because glutaraldehyde is also known to form polymers. This allows for the crosslinking of further distant molecules, especially in the presence of higher glutaraldehyde concentrations (> 2.5 %) (Azem *et al.* 1998). Due to its reactivity with primary amino groups the spectrum of buffers that can be used in glutaraldehyde crosslinking reactions is limited. However, buffer substances carrying primary amino groups (e.g. TRIS) can be utilized as ‘stop reagents’, that will cause termination of the reaction.

For the following experiments suitable conditions were tested for optimal crosslinking results and good resolution of oligomers on the gel. Relevant parameters are the concentration of both glutaraldehyde and protein as well as temperature and duration of the crosslinking reaction. In this study 0.5 µM HTRA1 were incubated in reaction buffer at 350 rpm, 37 °C for 5 minutes prior to the crosslinking reaction. Subsequently 0.5 % glutaraldehyde were applied. The reaction was stopped via incubation with 75 mM TRIS for 15 minutes at 500 rpm, room temperature and subsequent incubation at 40 °C for 3 minutes. Samples were analyzed via electrophoresis on NuPage Novex TRIS Acetate gels (3-8 %) followed by silver staining.

Reaction buffer	50 mM HEPES
	121 mM NaCl
	pH 7.5

3.4.15 Analytic size exclusion chromatography

Analytic size exclusion chromatography (SEC) was utilized to determine the oligomeric state of different HTRA1 constructs. Proteins were loaded onto a Superdex 200 5/150 GI column (GE Healthcare) equilibrated with buffer A. Chromatography was carried out at room temperature using an ÄKTAmicro FPLC system (GE Healthcare). Protein peaks were determined by measuring the optical density at 280 nm and subsequent analysis of the eluted fractions via SDS-PAGE electrophoresis and Western blot. Calibration of the ultilized column with an FPLC Gelfiltration LMW&HMW Standard (GE Healthcare) in the same buffer allowed for the calculation of approximate molecular weights of the eluted protein complexes.

Buffer A	50 mM NaPi
	50 mM NaCl
	pH 8

3.4.16 Determination of diffusion coefficients via NMR DOSY experiments [1]

Diffusion Ordered Spectroscopy (DOSY) experiments were performed at 25 °C on a Bruker 700 MHz Avance Ultrashield NMR spectrometer (Bruker, Germany) equipped with a 5 mm CPTCI ^{1}H-^{13}C/^{15}N/D cryoprobe with z-gradient. The variable gradient diffusion data was acquired as a pseudo-2D data set using a stimulated echo pulse sequence from the Bruker pulse program library, which was modified with a presaturation water suppression, with a diffusion delay (Δ) of 100 milliseconds and a diffusion gradient length (δ) of 6 milliseconds. Thirty-two gradient experiments were acquired for each data set with the gradient strength incremented from 5-95 % of the maximum gradient strength (50.4 G/cm for a smoothed square gradient pulse) in 32

[1] NMR DOSY experiments were performed in collaboration with Dr. Christine Beuck, Hendrik Kirschner and Prof. Peter Beyer, Department of Structural and Medical Biochemistry, University of Duisburg-Essen.

steps using a linear ramp. The number of transients was chosen according to protein concentration (table 3.16).

Table 3.16 Number of transients used in DOSY-NMR spectra

Conc. HTRA1	Transients
100 µM	32
50 µM	96
25 µM	256
10 µM	640
25 µM + ligand	800

The spectra were Fourier transformed and phased in Topspin 3.5. The integration of signals as a function of gradient strength was performed using the built-in T1T2 Dynamics module. The first data point was excluded due to irregular phasing and the last 4 data points were excluded due to low signal/noise. For free HTRA1 protein, the normalized I/I_0 values of four signals (3.0 ppm, 1.6 ppm, 1.4 ppm and 0.8 ppm) were averaged. For the VDAC2 peptide only two signals (3.2 ppm and 0.7 ppm) and for ligand MKL2 three signals (1.6 ppm, 1.4 ppm and 0.8 ppm) could be averaged because other protein signals overlapped with the signals of ligands or impurities found in the ligand preparations.

Plotting and fitting of the linearized data according to the Stejskal-Tanner equation (Stejskal and Tanner 1965; Altieri *et al.* 1995) was performed in GraphPad Prism 5. Error bars for the averaged data points represent the standard deviation. The error of the diffusion coefficient represents the standard error of the fit.

$$\ln\left(\frac{I}{I_0}\right) = -\gamma^2\delta^2\left(\Delta - {}^{\delta}/_{3}\right)\cdot D\cdot G^2$$

I = signal intensity

I_0 = signal intensity at gradient strength 0

γ = gyromagnetic ratio of the ^1H nucleus

δ = diffusion gradient pulse length

Δ = diffusion delay

G = gradient strength

D = translational diffusion coefficient.

3.4.17 Circular Dichroism (CD) spectroscopy [2]

Circular Dichroism (CD) spectroscopy is based on the unequal absorption of left- and right-handed circularly polarized light by asymmetric structure elements causing the light wave to be elliptically polarized as it passes through the sample. If the structure to be analyzed is a protein polarization is mainly effected via its peptide bonds and aromatic structures.

CD can be applied to analyze secondary structure elements, folding parameters and binding characteristics of large molecules. In this study, however, it was utilized to follow the unfolding of proteins as a function of temperature. Since structural elements such as α-helices and β-sheets are lost upon thermal unfolding of proteins, the technique allows for deductions regarding their stability and the kinetics underlying their structural decomposition. To acquire the CD melting curves for wildtype HTRA1 and various CARASIL-relevant HTRA1 mutants the absorption of circularly polarized light was measured at a defined wavelength over a temperature gradient ranging from 25 to 80 °C. In the course of thermal unfolding the loss of secondary structural elements as well as the melting of higher oligomeric structures can be followed as a gradual decrease in the CD signal thus allowing for the calculation of melting temperatures and deductions on the thermal stability of individual proteins and protein complexes.

For the study illustrated here samples containing 25 µM HTRA1 in 50 mM NaPi pH 6.7 were measured using a Jasco J-710 CD spectrometer. Data were collected at 222 nm in 0.2 °C steps and melting curves were generated by plotting the changes in ellipticity as a function of temperature thus portraying the thermodynamics of the proteins' thermal unfolding.

[2] CD spectroscopy was performed in collaboration with Dr. Christine Beuck, Hendrik Kirschner and Prof. Peter Beyer, Department of Structural and Medical Biochemistry, University of Duisburg-Essen.

4 Results

4.1 Protein Purification

4.1.1 Purification of 6x His-tagged HTRA1

In order to gain deeper insights into the molecular mechanisms underlying CARASIL (Cerebral Autosomal Recessive Arteriopathy with Subcortical Infarcts and Leukoencophalopathy), wildtype HTRA1 as well as constructs containing different CARASIL-relevant mutations were purified for biochemical assays. In the course of this study a number of constructs containing different domains of the full length protein were used. Since the function of the N-terminal domain is not yet known and purification of the full length protein from *E. coli* is limited presumably due to a structural relevance of disulfide bonds in this domain, the full length protein itself was not utilized in this work. Previous studies conducted in this laboratory (Truebestein *et al.* 2011) showed that constructs lacking the N-terminal domain (residues 158-480) as well as constructs lacking both the N-terminal and the PDZ domain (residues 158-375) could be purified in large quantities and showed reproducible proteolytic activities. This study will refer to these constructs as HTRA1 and HTRA1prot respectively. In addition to these constructs, proteolytically inactive variants, in which the active site serine 328 was mutated to alanine were purified and will be referred to as $HTRA1_{S328A}$ and $HTRA1prot_{S328A}$.

To illustrate the purification procedure for 6x His-tagged proteins the purification of wildtype HTRA1 containing a C-terminal His-tag will be described in the following section. All other 6x His-tagged HTRA1 constructs were purified according to the same protocol.

HTRA1 containing a C-terminal 6x His-tag was purified from *E. coli* BL 21 (DE3) Rosetta 2. The purification procedure was based on a protocol established by Truebestein *et al.* (2011). Following expression the cells were harvested via centrifugation and lysed in a French Pressure Cell. In order to obtain purified HTRA1

from the cell lysate a two step procedure comprising a nickel-nitrilotriacetic acid (Ni-NTA) affinity and size exclusion chromatography (SEC) column was performed.

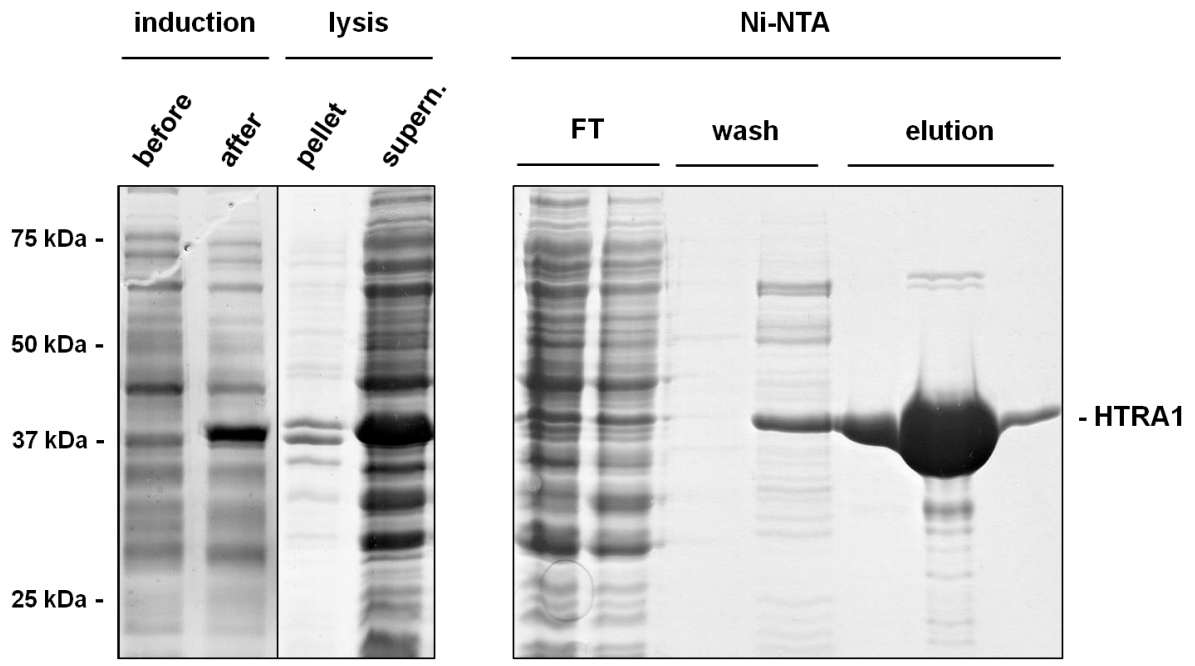

Figure 4.1 Ni-NTA purification of 6x His-tagged HTRA1
Samples collected from induction, cell lysis and Ni-NTA purification were subjected to SDS-PAGE and proteins were visualized via Coomassie Brilliant Blue staining. Lane 1 and 2 show whole cell lysates before and after induction. Lanes 3 and 4 show pellet and supernatant following lysis. Flowthrough (FT), wash and elution fractions from Ni-NTA chromatography are shown in the following lanes.

In the first step the cell lysate was applied to a Ni-NTA column (GE Healthcare) (figure 4.1). In order to remove unspecifically bound proteins the column was washed with 30 mM imidazole. HTRA1 was subsequently eluted via application of an imidazole gradient. Eluted fractions containing HTRA1 were collected and concentrated using a Vivaspin centrifugal device. Following concentration the samples were subjected to size exclusion chromatography on a Superdex 200 prep grade gel filtration column (GE Healthcare) (figure 4.2).

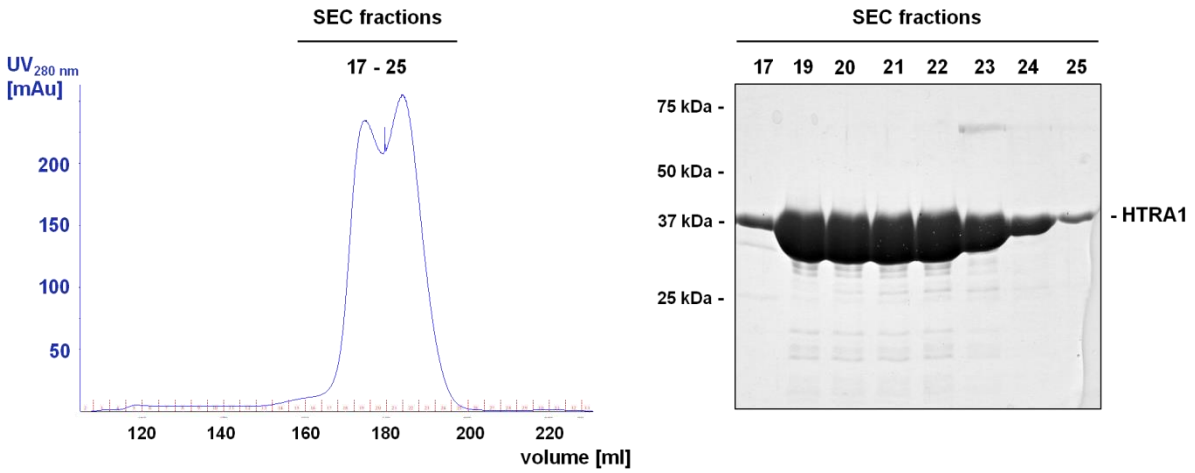

Figure 4.2 SEC purification of 6x His-tagged HTRA1
The elution peak from Ni-NTA chromatography was concentrated and applied to a Superdex 200 26/60 column (GE Healthcare) equilibrated with 50 mM NaPi, 100 mM NaCl, pH 8. Fractions indicated in the elution profile (left panel) were analyzed by SDS-PAGE and subsequent Coomassie Brilliant Blue staining (right panel). Fractions 19-24 were pooled, concentrated and stored at -80 °C.

The resulting gel filtration profile showed a small aggregation peak eluting in the void volume (data not shown), which probably contained higher oligomers of HTRA1 and aggregates, a second peak corresponding to HTRA1 and a third peak containing slightly lower amounts of HTRA1. The molecular mass of the second peak was 120 kDa according to the calibration of the column hence corresponding to an HTRA1 trimer. SDS-PAGE analysis of this peak fraction indicated that the protein preparation was approximately 95 % pure (Fig. 4.2, right panel). After purification fractions collected from the trimer peak were concentrated for biochemical assays. Bradford analysis and comparison of Coomassie Brilliant Blue stained bands after SDS-PAGE with bands of a serial dilution standard of BSA showed a protein concentration of circa 25 mg/ml.

4.1.2 Purification of tag-less HTRA1

Via the purification procedure described above for His-tagged HTRA1 large quantities of protein could be purified in a short amount of time. However, the C-terminal 6x His-tag interfered with NMR experiments due to its inherent flexibility, since the high signal generated by the flexible tag decreased the overall sensitivity of the experiment. Thus in this study a purification procedure was established, that would yield untagged

HTRA1 of high purity. To obtain tag-less HTRA1prot the HTRA1 protease domain (residues 158-375) was cloned into a modified pET41b vector, in which the thrombin cleavage site between the glutathione-S-transferase (GST)-tag and the multiple cloning site was exchanged for a PreScission cleavage site. The construct was subsequently expressed from *E. coli* BL21 (DE3) Rosetta cells and purified via a three step purification procedure consisting of a glutathione-sepharose column, a reverse glutathione-sepharose column and a final gel filtration step. To outline the purification procedure purification of wildtype HTRA1prot will be described as a representative for all constructs purified via this strategy.

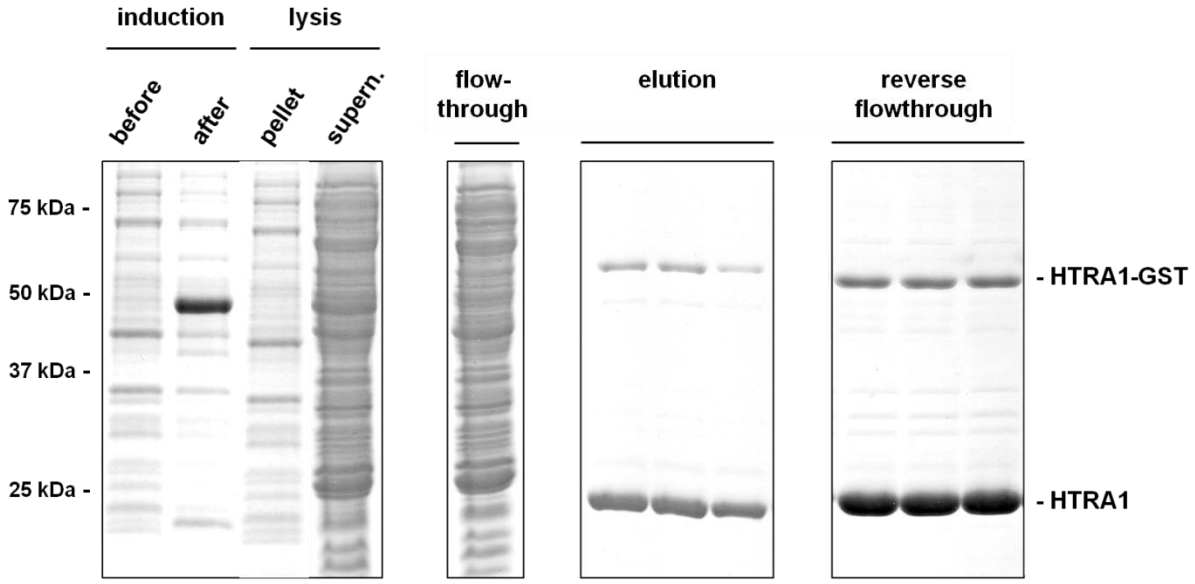

Figure 4.3 Glutathione-sepharose purification of tag-less HTRA1prot
Samples collected during induction, lysis and glutathione-sepharose purification were subjected to SDS-PAGE and proteins were visualized via Coomassie Brilliant Blue staining. Lane 1 and 2 show whole cell lysates before and after induction. Lanes 3 and 4 show pellet and supernatant following lysis. Samples of the flowthrough (FT), elution and reverse FT fractions from glutathione-sepharose chromatography are shown in the following lanes.

Following expression, harvesting and lysis as described above for 6x His-tagged HTRA1 the lysate was applied to a glutathione sepharose 4 Fast Flow column (GE Healthcare) (figure 4.3). In order to remove residual chaperones the column was washed with 250 µM ATP. Subsequently 100 U of PreScission protease diluted in 80 ml of lysis buffer were loaded onto the column to facilitate cleavage at the PreScission cleavage site, that is located between the N-terminal GST-tag and HTRA1prot thus releasing tag-less HTRA1prot from the column. Following overnight cycling of the PreScission protease on the column at 1 ml/min cleaved HTRA1 was eluted with 3 column volumes of lysis buffer and the eluted fractions were collected

and concentrated using a Vivaspin centrifugal device. In order to remove residual proteins binding to the column in an unspecific manner as well as uncleaved GST-HTRA1prot a reverse glutathione-sepharose purification step was carried out. In this step HTRA1 was collected in the flowthrough, whereas unspecific proteins were retained on the column.

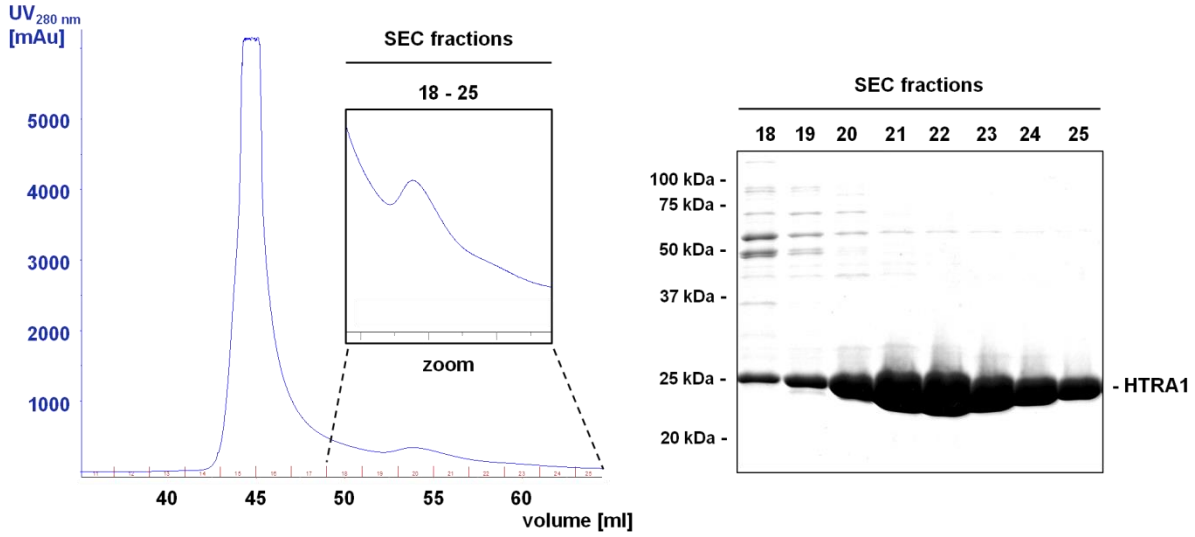

Figure 4.4 SEC purification of tag-less HTRA1prot
The elution peak from glutathione-sepharose chromatography was concentrated and applied to a Superdex 75 column (GE Healthcare) equilibrated with 50 mM NaPi, 100 mM NaCl, pH 8. Fractions indicated in the elution profile (left panel) were analyzed by SDS-PAGE and subsequent Coomassie Brilliant Blue staining (right panel). Fractions 21-25 were pooled, concentrated and stored at -80 °C.

Following concentration, the flowthrough containing HTRA1 was subjected to size exclusion chromatography on a Superdex 75 preparation grade gel filtration column (GE Healthcare). The SEC elution profile as well as selected samples subjected to SDS-PAGE analysis are given in figure 4.4. Higher molecular weight impurities still present after glutathione sepharose affinity chromatography were successfully removed during this purification step resulting in an HTRA1prot preparation of high purity.

4.1.3 Purification of Tau-2N4R

In order to follow the digest of a native HTRA1 substrate (Tennstaedt *et al.* 2012) *in vitro* the human protein Tau was purified for biochemical assays. Due to its involvement in Alzheimer's disease Tau is not only a native, but also a disease relevant substrate. In this study the Tau-2N4R isoform containing four repeat motives as well as the self assembly regions was utilized.

Tau was purified from BL21 (DE3) Rosetta 2 cells in a three step procedure consisting of a boiling step, a hydroxyl apatite (HAP) and a size exclusion (SEC) chromatography that was first established by Poepsel *et al.* (2015). Induction with isopropyl-β-D-thiogalactoside (IPTG) resulted in the induction of a distinct protein band on SDS-PAGE gels migrating at approximately 55 kDa, whereas the calculated molecular weight for Tau is 47 kDa. However, Tau belongs to the group of intrinsically disordered proteins, which tend to show a characteristic shift to higher apparent molecular weights when subjected to SDS-PAGE electrophoresis (Grundke-Iqbal *et al.* 1988).

Due to its intrinsically disordered nature Tau was found to be extremely soluble even at high temperatures (Hagestedt *et al.* 1989) allowing for a separation from other proteins by boiling and subsequent centrifugation. During this centrifugation step the lysate was cleared from heat-precipitated proteins, whereas Tau remained in the supernatant. As can be seen in figure 4.5 a large proportion of bacterial proteins could be removed in this first purification step. Nevertheless, a considerable number of proteins remained in the soluble fraction, giving rise to a plethora of additional bands upon SDS-PAGE analysis. The majority of these bands migrated below the 55 kDa Tau band.

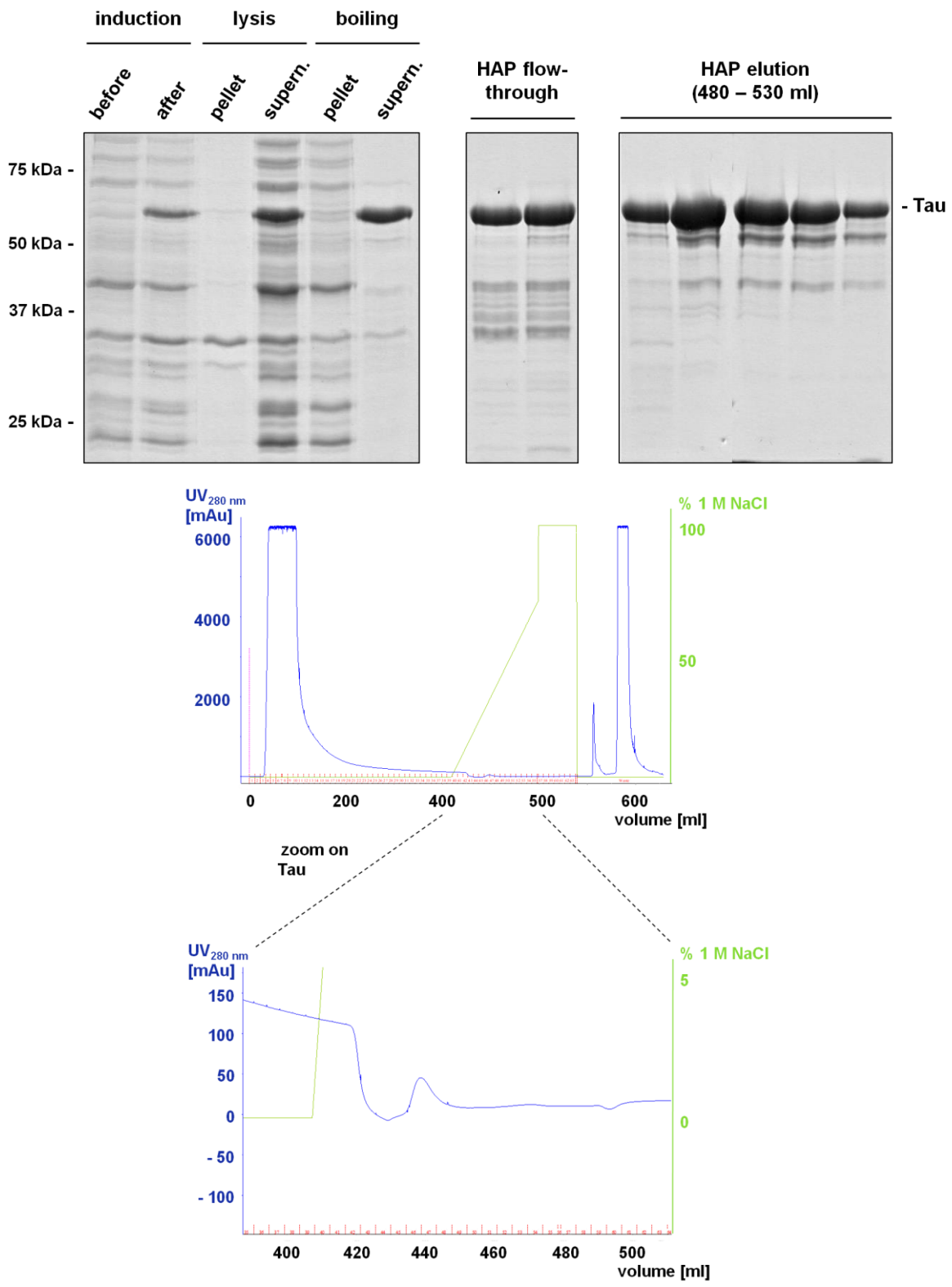

Figure 4.5 Purification of Tau-2N4R
Fractions collected during HAP purification were subjected to SDS-PAGE and proteins were visualized via Coomassie Brilliant Blue staining (upper panel). Lane 1 and 2 show full cell lysates before and after induction. Lanes 3 and 4 show pellet and supernatant following lysis. Lanes 5 and 6 show pellet and supernatant after boiling. Samples of the flowthrough (FT) and elution fractions from HAP chromatography are shown in the following lanes. The lower panel shows the UV absorption profile at 280 nm of the HAP chromatography including a zoom into the Tau peak, which displays a low UV signal due to its low intrinsic absorption coefficient. UV absorption at 280 nm is shown in blue, NaCl concentrations are shown in green.

To achieve further purification the sample was subjected to HAP chromatography. Due to its basic character (calculated pI = 8.24) Tau binds to the column and can be eluted via a sodium chloride gradient. However, large amounts of Tau were found in the flowthrough together with the majority of bacterial proteins from the lysate presumably due to inefficient binding to the resin (figure 4.5). Therefore fractions from the flowthrough were subjected to the column again in order to increase Tau yield. Due to the absence of tryptophane residues from the Tau sequence the UV signal generated by Tau during NaCl elution was very weak. Yet large quantities of Tau could be detected in the elution fractions subjected to SDS-PAGE electrophoresis and subsequent Coomassie Brilliant Blue staining. The main proportion of Tau eluted at an NaCl concentration of approximately 300 mM.

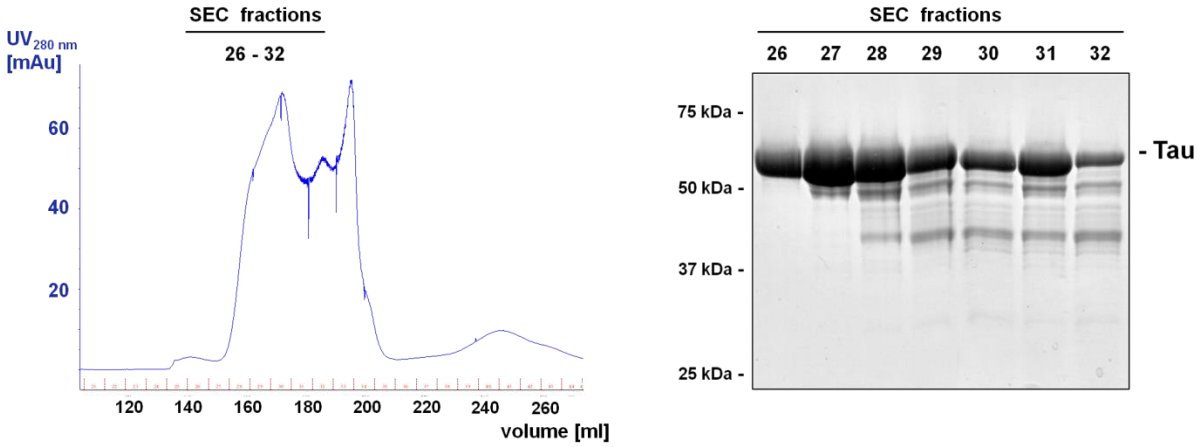

Figure 4.6 SEC purification of 4R Tau
The elution peak from HAP chromatography was concentrated and applied to a Superdex 200 26/60 column (GE Healthcare) equilibrated with 10 mM HEPES, 50 mM $(NH_4)_2SO_4$, pH 7.5. Fractions indicated in the elution profile (left panel) were analyzed by SDS-PAGE and subsequent Coomassie Brilliant Blue staining (right panel).

Samples containing Tau were subsequently subjected to SEC chromatography in order to remove remaining impurities as well as aggregated Tau and smaller Tau fragments. From the gel filtration column Tau eluted in three peaks corresponding to a monomer (180-190 ml), a dimer (160-180 ml) and a 4-6 mer (147-160 ml) (figure 4.6). Samples containing these peaks were combined, concentrated and stored at -80 °C.

4.2 Biochemical Characterization of CARASIL-relevant HTRA1 mutants

4.2.1 Localization of CARASIL-relevant mutations in HTRA1

CARASIL is a monogenic disease associated with loss of function mutations in the *HTRA1* gene. The loss of function phenotype is typically linked to mutations immediately affecting the proper positioning of the active site (e.g. $HTRA1_{A252T}$) or to premature stop codons causing either mRNA decay (e.g. $HTRA1_{R370X}$) or severe truncations of the resulting protein ($HTRA1_{R302X}$) (Hara *et al.* 2009).

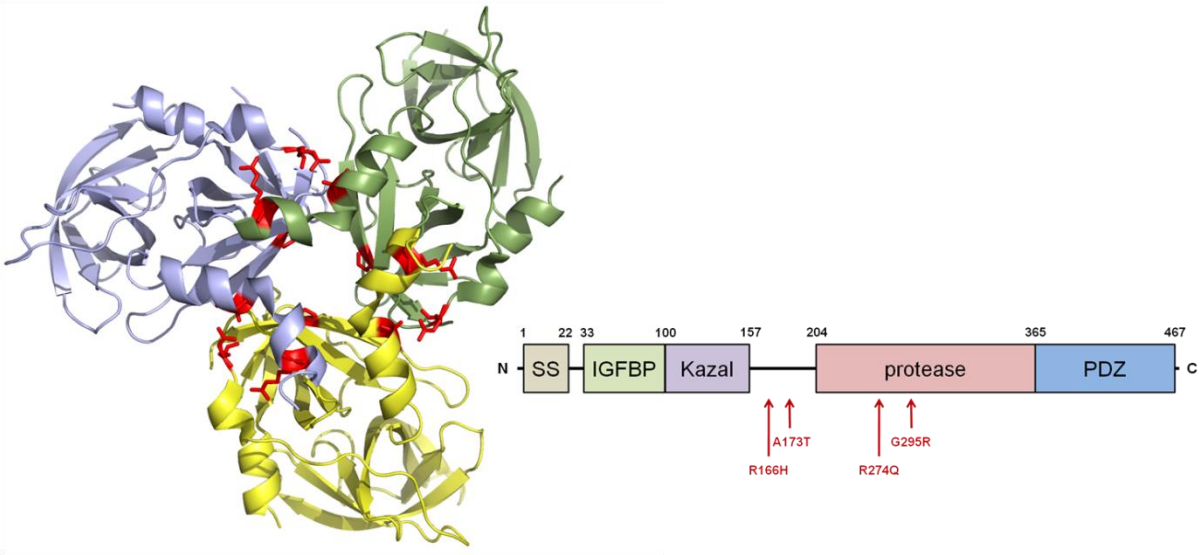

Figure 4.7 Localization of CARASIL-relevant interface mutations in the HTRA1 trimer
The left panel gives a structural representation of the HTRA1 trimer. Separate protomers are coloured in blue, yellow and green. The positions of the interface mutations investigated in this study (R166H, A173T, R274Q and G295R) are highlighted in red. The representation is based on the structure of the HTRA1 trimer solved by Truebestein *et al.* (2011) (PDB Code: 3NWU). The right panel shows the domain architecture of HTRA1 with the CARASIL-relevant interface mutations highlighted in red.

However, recently another set of disease-relevant mutations ($HTRA1_{R166H}$, $HTRA1_{A173T}$, $HTRA1_{R274Q}$ and $HTRA1_{G295R}$) has been discovered, that were found to cause neither direct effects on active site positioning, nor a premature stop codon, but were situated at the trimer interface of HTRA1. Mapping of the mutations onto the HTRA1 structure (figure 4.7) as well as molecular dynamics simulations and free

energy calculations [3] showed that the affected residues are implicated in interactions between two adjacent HTRA1 protomers suggesting that mutations at these positions would have detrimental effects on trimer stability.

In the following the interface mutations will be characterized biochemically regarding their impact on proteolytic activity and oligomeric state in order to gain deeper insights into the mechanisms underlying the disease causing effects of these mutations. Furthermore, different protein repair strategies will be investigated regarding their potential to restore the mutants' proteolytic activity.

4.2.2 Proteolytic activity of CARASIL mutants

In order to acquire and compare basic activities of the disease-relevant interface mutants time dependent degradation of β-casein was followed on SDS-PAGE (figure 4.8). The wildtype enzyme as well as an HTRA1 construct carrying the A252T mutation, that is not implicated in trimerization, but in the proper folding of the active site, were used as controls.

[3] Computer-based structural analyses were conducted Dr. Kenny Bravo-Rodriguez, Department of Microbiology II, University of Duisburg-Essen.

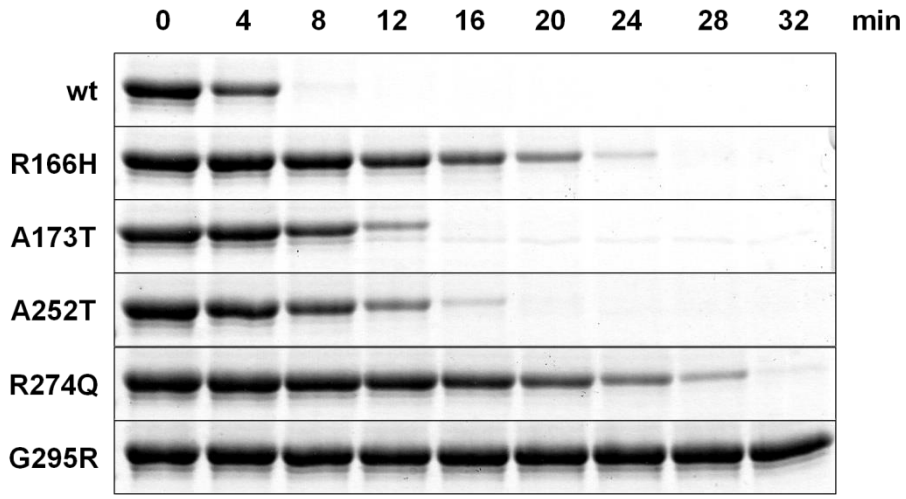

Figure 4.8 β-casein degradation by wildtype HTRA1 and CARASIL-relevant HTRA1 mutants
Time dependent degradation of β-casein was followed on SDS-PAGE. 1 µM HTRA1 were incubated with 20 µM β-casein in 50 mM NaPi, 50 mM NaCl, pH 8 at 37 °C for 32 minutes and samples were taken at indicated time points. Samples were subjected to SDS-PAGE followed by Coomassie Brilliant Blue staining. A 20-fold surplus of β-casein was sufficiently cleaved by wildtype HTRA1 within 8 minutes, while the CARASIL mutants required longer incubation to degrade the same amount of substrate.

Whereas the wildtype enzyme degraded a 20-fold surplus of β-casein within 8 minutes, all tested CARASIL-relevant mutants displayed decreased proteolytic activities. However, the extent of activity loss varied depending on the type of mutation. While most mutants displayed only a partial loss of proteolytic activity, the G295R mutation rendered HTRA1 completely inactive, as could be seen in an over night digest of β-casein (data not shown). In contrast to this, the A173T and A252T substitutions showed the highest residual activities with only a 1-fold decrease in degradation speed, whereas the R166H and R274Q mutants displayed a 2.5 or 3-fold decrease respectively. Degradation assays utilizing α-casein and pNA (para-nitroaniline)-assays using a substrate based on the RseA-derived amino acid sequence “VFNTLPMMGKASPV” rendered comparable results (data not shown).

To assess the mutations' effects regarding the degradation of a physiological HTRA1 substrate further assays were conducted using the native substrate Tau. To follow the digest of Tau HTRA1 was incubated with an 8-fold surplus of the Tau-2N4R isoform and samples were taken at indicated time points followed by SDS-PAGE analysis and Coomassie Brilliant Blue staining (figure 4.9).

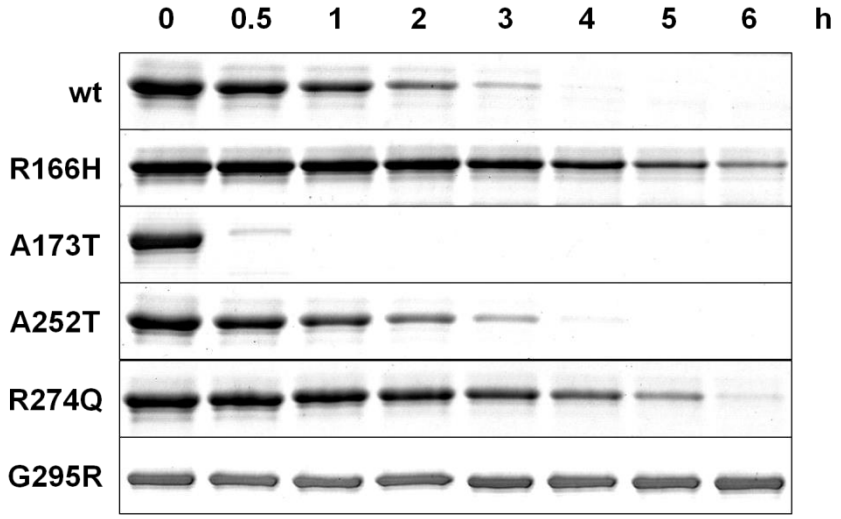

Figure 4.9 Tau degradation by wildtype HTRA1 and CARASIL-relevant HTRA1 mutants
Time dependent degradation of Tau was followed on SDS-PAGE. 1 µM HTRA1 were incubated with 8 µM Tau in 50 mM TRIS pH 8 at 37 °C for 6 hours and samples were taken at indicated time points. Samples were subjected to SDS-PAGE followed by Coomassie Brilliant Blue staining. An 8-fold surplus of β-casein was sufficiently cleaved by wildtype HTRA1 within 4 hours. Degradation velocities obtained for the CARASIL-relevant mutants varied depending on the type of mutation.

For both the wildtype enzyme and the A252T mutant degradation was completed within 4 hours of incubation indicating that in contrast to degradation of the model substrate β-casein Tau proteolysis is not affected by the A252T mutation. Neither HTRA1$_{R166H}$, nor HTRA1$_{R274Q}$ were able to completely digest an 8-fold surplus of Tau within 6 hours, though a considerable degree of degradation could be observed within this timespan. Consistent with the results observed for the degradation of β-casein the G295R mutant remained inactive. Remarkably the A173T mutant was found to digest Tau approximately 6 times faster than the wildtype enzyme.

4.2.3 Analysis of oligomeric states via glutaraldehyde crosslinking

Mapping of the mutations R166H, A173T R274Q and G295R onto the structure of HTRA1 as well as computational analyses suggested that the residues affected by these amino acid substitutions are implicated in trimer stability and are thus likely to cause trimerization defects. In order to demonstrate that the decrease in proteolytic activity observed for the corresponding enzymes was indeed due to a loss of trimer formation crosslinking experiments were performed.

From a variety of commercially available crosslinkers glutaradehyde, which carries two reactive carbonyle groups to facilitate the formation of covalent bonds with primary amino groups, was chosen as a appropriate reagent for this analysis. Suitable conditions were tested for optimal crosslinking results and good resolution of oligomers on the gel. In this study 0.5 µM HTRA1 were incubated at 350 rpm, 37 °C for 5 minutes prior to the crosslinking reaction. Subsequently 0.5 % glutaraldehyde were applied. The reaction was stopped via addition 75 mM TRIS. Crosslinked complexes were subsequently separated by SDS-PAGE and visualized via silver staining. Again the wildtype enzyme and the A252T mutant were used as controls.

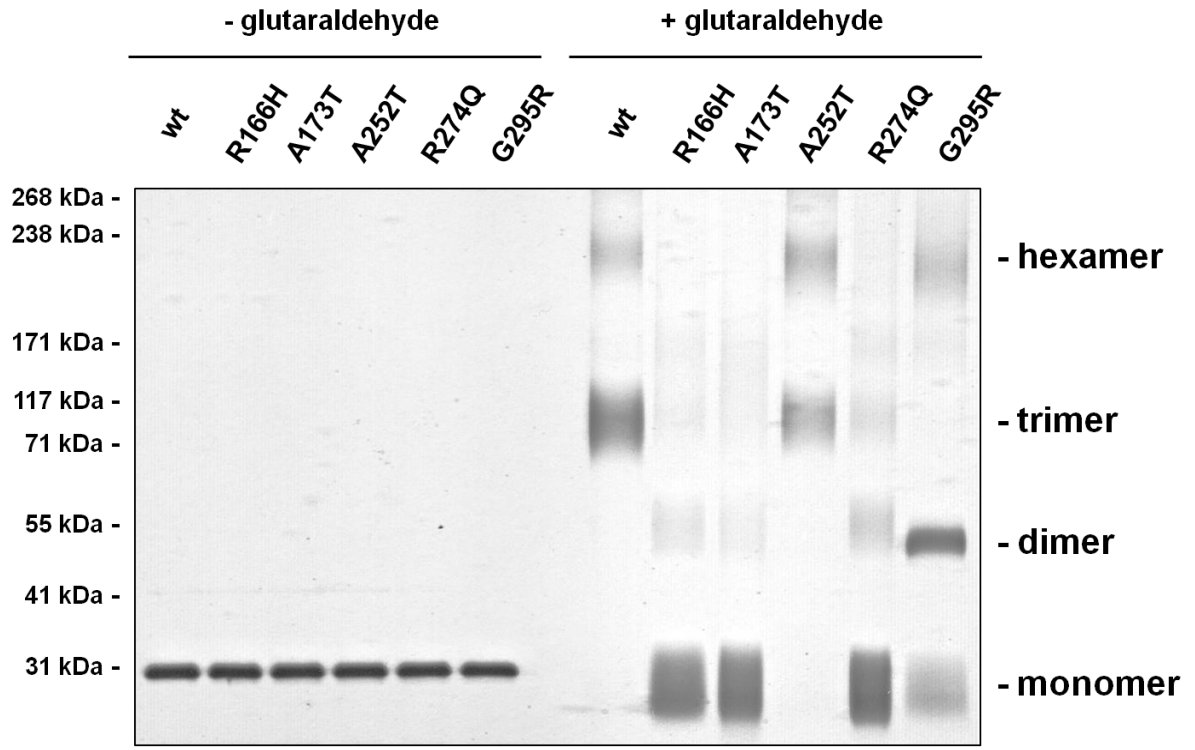

Figure 4.10 Oligomeric states of wildtype HTRA1 and CARASIL-relevant mutants analyzed via glutaraldehyde crosslinking
0.5 µM HTRA1 were incubated at 37 °C for 5 minutes prior to crosslinking with 0.5 % glutaraldehyde. The reaction was stopped via addition of 75 mM TRIS. Crosslinked complexes were separated via SDS-PAGE and visualized via silver staining. Wildtype HTRA1 and HTRA1$_{A252T}$ migrated primarily as trimeric bands, HTRA1$_{R166H}$, HTRA1$_{A173T}$ and HTRA1$_{R274Q}$ migrated as monomers and HTRA1$_{G295R}$ showed an intense dimer band.

As can be seen in figure 4.10 HTRA1$_{A252T}$ showed a migration pattern similar to that of the wildtype enzyme with a distinct band migrating at the height of the trimer (111 kDa) and another slightly less intense one on the hexamer level (222 kDa), whereas monomeric bands could not be detected for either enzyme, confirming that the A252T mutation is indeed not affecting trimer stability as computational analysis had

suggested. In contrast to this all constructs carrying mutations located at the trimer interface showed a different migration pattern. In accordance with the results derived from computational modeling HTRA1$_{R166H}$, HTRA1$_{A173T}$ and HTRA1$_{R274Q}$ could all be detected as monomeric bands (37 kDa) following glutaraldehyde crosslinking. Additionally another less intense band could be observed on dimer level (74 kDa) and another even lighter one on trimer level. HTRA1$_{G295R}$, however, predominantly gave rise to a compact band migrating on dimer level, whereas only a weak band could be detected on the height of the monomer.

In addition to the analysis of the disease relevant mutations found in CARASIL patients two synthetic amino acid substitutions at position 274 were characterized regarding their oligomeric states in order to further assess the importance of residue 274 on trimer assembly. In the first construct the long positively charged arginine was substituted for the short uncharged residue alanine, whereas in the second construct it was exchanged for the negatively charged residue glutamate. These substitutions were chosen under the assumption that the side chain of the alanine residue would be too short to interact with its binding pocket on the opposing protomer consisting of aspartate 174* and glutamate 177*, while the negatively charged glutamate would be repelled by the negative charge of these residues. Thereby both mutations would cause a disruption of the inter-monomer salt bridge.

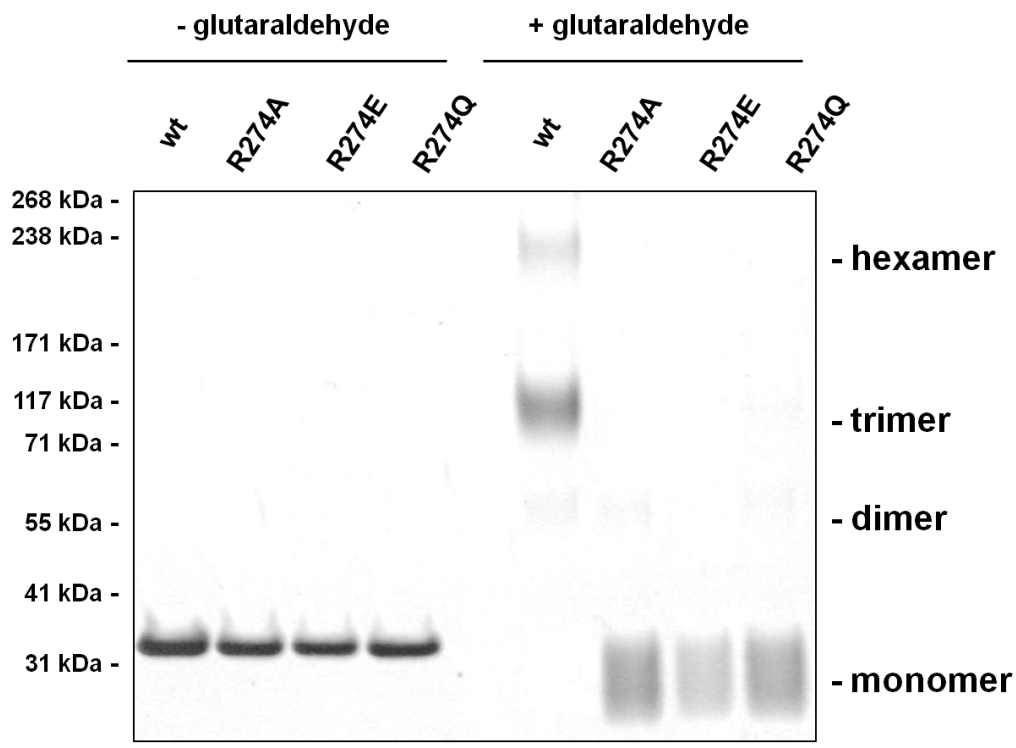

Figure 4.11 Oligomeric states of wildtype HTRA1, HTRA1$_{R274A}$, HTRA1$_{R274E}$ and HTRA1$_{R274Q}$ analyzed via glutaraldehyde crosslinking
0.5 µM HTRA1 were incubated at 37 °C for 5 minutes prior to crosslinking with 0.5 % glutaraldehyde. The reaction was stopped via addition of 75 mM TRIS. Crosslinked complexes were separated via SDS-PAGE and visualized via silver staining. Wildtype HTRA1 migrated primarily as a trimeric band, whereas HTRA1$_{R274A}$, HTRA1$_{R274E}$ and HTRA1$_{R274Q}$ migrated as monomers.

In order to test this hypothesis both constructs were treated with the chemical crosslinker glutaraldehyde as described above and analyzed via SDS-PAGE electrophoresis and subsequent silver staining. The wildtype enzyme and the original mutant HTRA1$_{R274Q}$ were used as controls. As shown in figure 4.11 both constructs display the same migration pattern as the original mutant with a prominent band migrating at the height of monomeric HTRA1 (37 kDa) thus revealing an oligomerization defect similar to that of HTRA1$_{R274Q}$ and highlighting the importance of arginine 274 in trimer assembly.

4.2.4 Concentration dependence of oligomeric states

As could be observed in the previous crosslinking experiments both wildtype HTRA1 and the constructs carrying CARASIL-relevant mutations display a pattern of multiple bands reflecting a mixture of different oligomeric forms. These data indicate that

neither enzyme exists in just one distinct oligomeric state. Rather the oligomeric states appear to exist at an equilibrium. This observation gave rise to the idea that one could observe a concentration dependent shift of the equilibrium towards a particular oligomeric state.

In order to test this hypothesis the oligomeric states of both wildtype HTRA1 and HTRA1$_{R274Q}$ were assessed via analytical gel filtration chromatography using an ÄKTAmicro FPLC system. To prevent autoproteolysis of the enzymes in the course of the assay the inactive S328A variants were utilized in this set of experiments. Both wildtype HTRA1 and the R274Q mutant were injected into the FPLC system at different concentrations ranging from 25 to 100 µM. The resulting fractions were subsequently subjected to SDS-PAGE analysis and blotted onto a polyvinylidene fluoride (PVDF) membrane. Bands were visualized using a primary antibody directed against HTRA1 and a secondary antibody coupled to alkaline phosphatase. Previous calibration of the column using the GE Healthcare LMW and HMW calibration kits allowed for the allocation of the resulting bands to an approximate molecular weight. The resulting distribution of bands is displayed in figure 4.12.

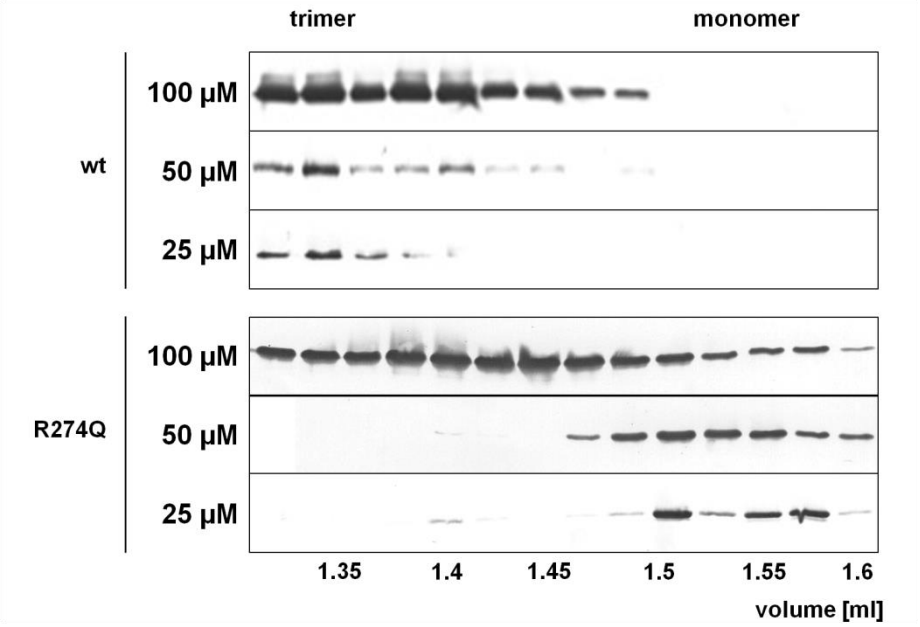

Figure 4.12 Concentration dependence of oligomeric states analyzed via size exclusion chromatography
Wildtype HTRA1 and HTRA1$_{R274Q}$ were subjected to a Superdex 200 5/150 GI column (GE Healthcare) connected to an Äkta micro FPLC system at 25, 50 and 100 µM. Fractions were subsequently submitted to SDS-PAGE followed by Western blot analysis. Whereas wildtype HTRA1 eluted as a trimer, HTRA1$_{R274Q}$ displayed a shift towards the monomeric state at lower protein concentrations.

Whereas wildtype HTRA1, which eluted at approximately 1.35 ml (110 kDa) in all runs, remained in the trimeric state within the tested concentration range, a clear shift towards the monomeric form could be observed for $HTRA1_{R274Q}$ at lower protein concentrations (25 and 50 µM). While at a concentration of 100 µM the protein's elution profile displayed a range of oligomeric states with bands appearing in both the monomeric (1.55 ml, 45 kDa) and the trimeric (1.35 ml, 110 kDa) fractions, the application of lower concentrations resulted in a distinct shift towards the monomeric state as can be concluded from the absence of bands within the trimer fractions. These results demonstrate that $HTRA1_{R274Q}$ exists at a dynamic equilibrium of different oligomeric forms and that the equilibrium can be shifted in a concentration dependent manner.

In order to verify the above results the oligomeric states of wildtype HTRA1 and $HTRA1_{R274Q}$ were additionally assessed via determination of their respective diffusion coefficients using NMR DOSY experiments. The DOSY experiment combines NMR radio frequency pulses with magnetic field gradients encoding spacial information [4]. In the course of the experiment a magnetic field gradient pulse is applied to a previously excited sample resulting in the dispersion of the magnetization vectors thus cancelling out the total signal. After a defined period of time a refocusing pulse is applied. However, refocusing can only be achieved for those nuclei that have not moved too far away from their original position. Thus the spacial movement of nuclei in solution decreases the effectiveness of the refocusing pulse and thereby the intensity of the resulting signal. Integration of signals as a function of gradient strength renders the diffusion coefficient. Since the diffusion coefficient is dependent on the molecular weight of a molecule and correlates with the natural logarithm of the resulting signal intensity in an antiproportional manner, recording of the diffusion spectra should enable us to distinguish different oligomeric states of HTRA1.

In the course of the experiment 2D spectra were recorded for wildtype HTRA1, $HTRA1_{R166H}$, $HTRA1_{A173T}$ and $HTRA1_{R274Q}$ at different concentrations ranging from 10

[4] NMR DOSY experiments were performed in collaboration with Dr. Christine Beuck, Hendrik Kirschner and Prof. Peter Beyer, Department of Structural and Medical Biochemistry, University of Duisburg-Essen.

to 100 µM. For each data-set 32 gradient experiments were acquired with the gradient strength ranging from 5-95 % of the maximum gradient strength (50.4 G/cm for a smoothed square gradient pulse). Measurements were performed at 25 °C on a Bruker 700 MHz Avance Ultrashield NMR spectrometer (Bruker, Germany) equipped with a 5 mm CPTCI ^{1}H-$^{13}C/^{15}N/D$ cryoprobe with z-gradient. The first data point was excluded due to irregular phasing and the last 4 data points were excluded due to low signal to noise ratio.

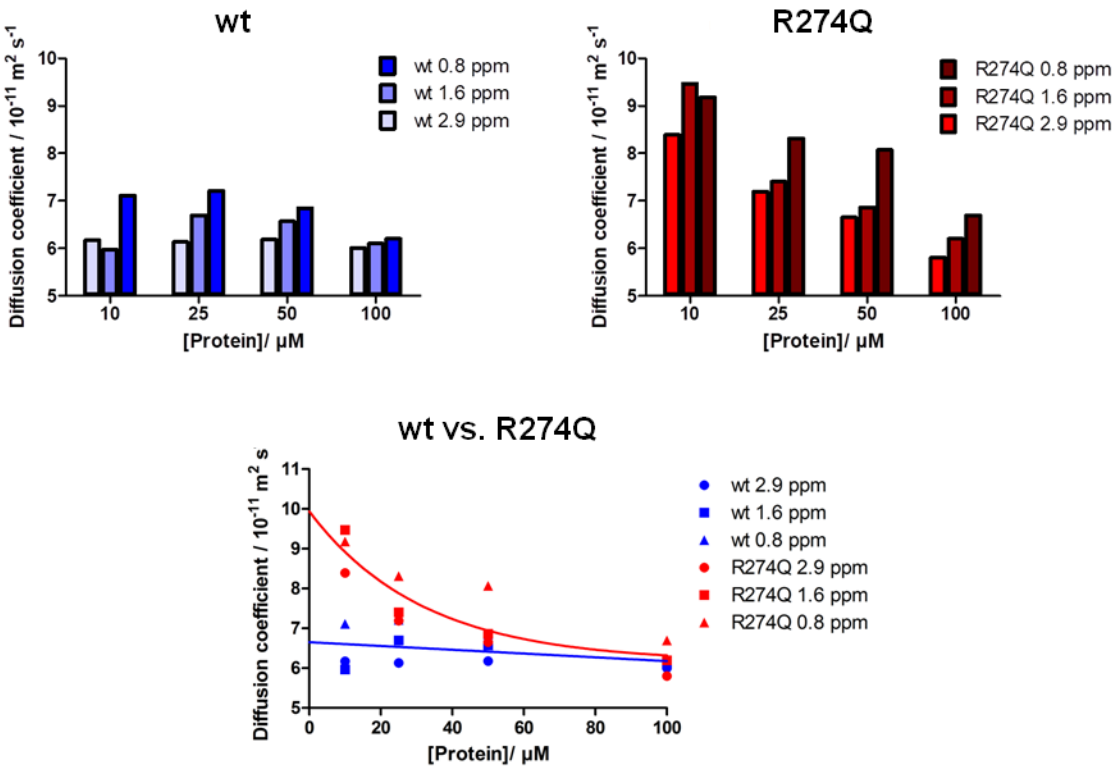

Figure 4.13 Concentration dependence of oligomeric states analyzed via NMR DOSY experiments
The upper left panel shows the diffusion coefficients for HTRA1protSA wildtype determined from three independent signals recorded at 0.8 ppm (dark blue), 1.6 ppm (medium blue) and 2.9 ppm (light blue). The upper right panel displays the diffusion coefficients for HTRA1protSA$_{R274Q}$ determined from three independent signals recorded at 0.8 ppm (dark red), 1.6 ppm (medium red) and 2.9 ppm (light red). A unified representation for both proteins is given in the bottom panel. Protein concentrations are indicated on the x-axis and the corresponding diffusion coefficients are given on the y-axis.

The graphs shown in figure 4.13 display the averaged diffusion coefficients calculated from three signals selected from the 1D-spectrums (2.9 ppm, 1.6 ppm, and 0.8 ppm) of wildtype HTRA1 and HTRA1$_{R274Q}$ respectively. Plotting of the diffusion coefficient against the protein concentration was used to visualize concentration dependent changes of oligomeric states. Whereas for wildtype HTRA1 there are no significant changes in the diffusion coefficient within the tested concentration range (10 to

100 µM), the interface mutant HTRA1$_{R274Q}$ displays a distinct increase in the diffusion coefficient with decreasing protein concentrations. At 100 µM the mutant's diffusion coefficient is comparable to that of the wildtype suggesting that at this concentration it exists in its trimeric form. Yet lower concentrations are associated with higher deviations of the diffusion coefficient from that of the wildtype indicating a shift towards the monomeric state at lower concentrations.

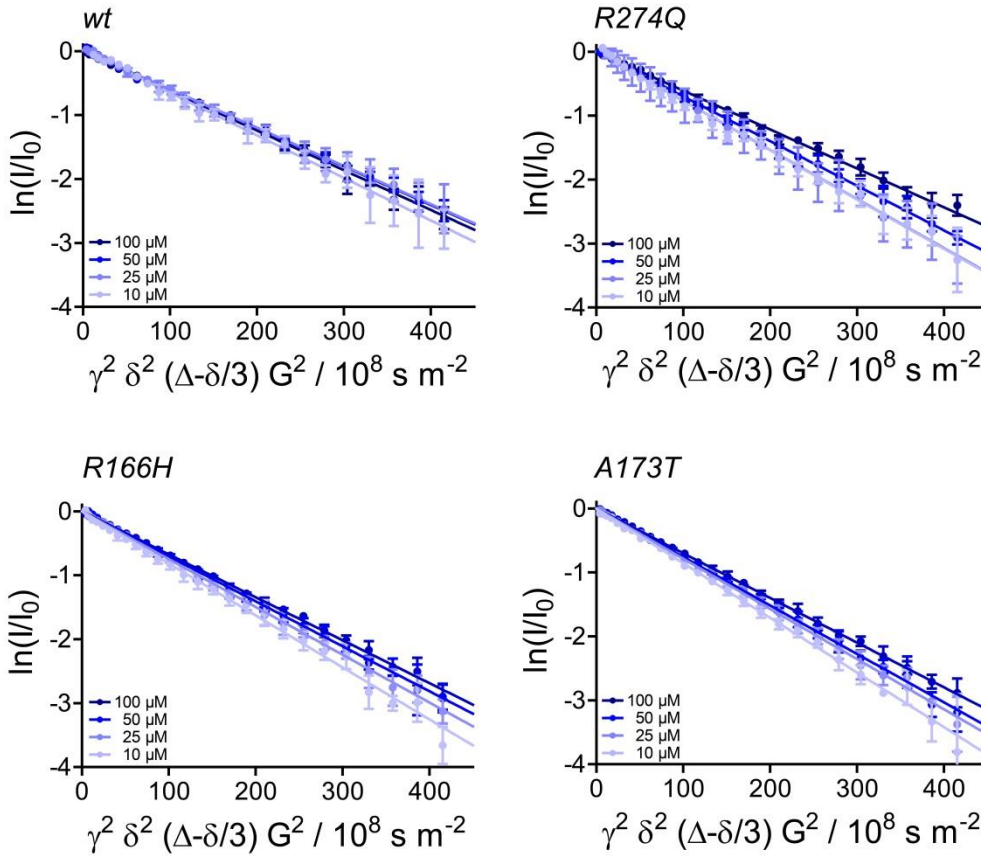

Figure 4.14 Stejskal-Tanner plots of the concentration dependence of oligomeric states analyzed via NMR DOSY experiments
The Stejskal-Tanner plots display the normalized signal intensities of the protein peaks (y-axis) as a function of gradient strength (x-axis) with the slope corresponding to the protein's diffusion coefficient. Signals were recorded at 0.8 ppm, 1.6 ppm and 2.9 ppm. Protein concentrations ranged from 10 to 100 µM. Error bars indicate the standard error of the mean. All interface mutants displayed a shift towards higher diffusion coefficients at lower concentrations.

The Stejskal-Tanner plots in figure 4.14 display the normalized signal intensities derived from wildtype HTRA1, HTRA1$_{R166H}$, HTRA1$_{A173T}$ and HTRA1$_{R274Q}$ as a function of gradient strength at different concentrations with the slope corresponding to the proteins' diffusion coefficients. As described above, the diffusion coefficient and thus the oligomeric state observed for wildtype HTRA1 remained unaltered over a broad concentration range indicating the presence of a stable trimer. In contrast, the interface

mutants displayed a concentration dependence of their diffusion coefficients with a distinct shift towards higher values at decreasing concentrations. This concentration dependent shift of the equilibrium towards the monomeric state is most profound for $HTRA1_{R274Q}$ with a complete shift towards the monomeric form occurring already at 25 µM, whereas for $HTRA_{R166H}$ and $HTRA1_{A173T}$ concentrations as low as 10 µM were required to observe a comparably low diffusion coefficient. This result indicates that among the monomer-forming interface mutants the R274Q mutation shows the highest impact on trimer stability and is in accordance with the finding that $HTRA1_{R274Q}$ had also displayed the most severe impairment in proteolytic activity in β-casein degradation assays.

4.2.5 Temperature stability of oligomeric states analyzed via Circular Dichroism (CD)-melting experiments

To further determine the implications of CARASIL-relevant mutations on protein stability, data were collected from circular dichroism (CD) melting experiments [5]. CD is a well-established method applied to analyze secondary structure elements, folding parameters and binding characteristics of large molecules like proteins and DNA. It is based on the unequal absorption of left- and right-handed circularly polarized light by asymmetric structural elements such as α-helices and β-sheets resulting in an elliptical polarization of the light wave as it passes through the sample. Since these structural elements are lost upon thermal denaturation the unfolding of proteins can be followed as a function of temperature allowing for deductions regarding their stability and the kinetics underlying their structural decomposition.

[5] CD spectroscopy was performed in collaboration with Dr. Christine Beuck, Hendrik Kirschner and Prof. Peter Beyer, Department of Structural and Medical Biochemistry, University of Duisburg-Essen.

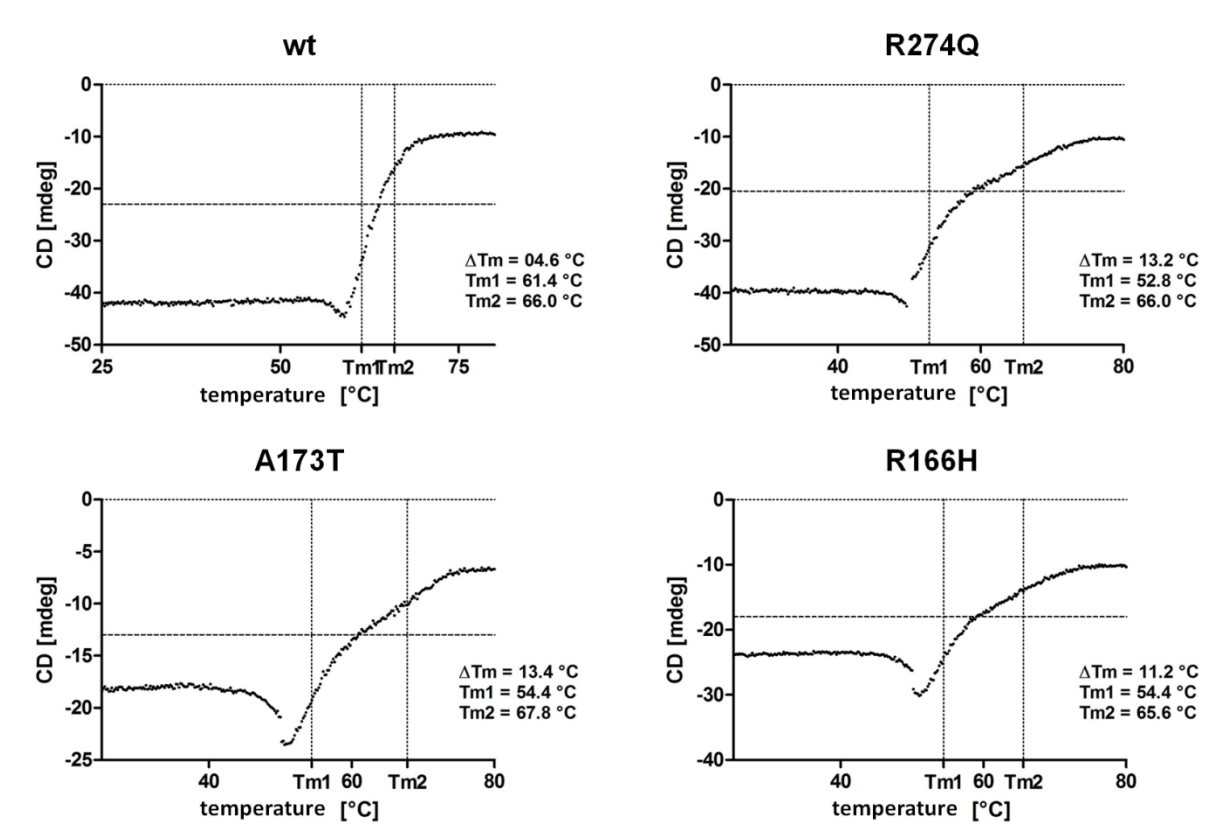

Figure 4.15 Changes in ellipticity of HTRA1, HTRA1$_{R166H}$, HTRA1$_{A173T}$ and HTRA1$_{R274Q}$ as a function of temperature
Changes in ellipticity were monitored at 222 nm (α-helices) over a temperature gradient ranging from 25 to 80 °C. The y-axis shows the CD signal in millidegrees recorded at different temperatures (x-axis). The two sigmoidal curves are separated via the horizontal dotted lines. Inflection points are indicated by the vertical dotted lines. Tm1, Tm2 and ΔTm are depicted for each curve.

Figure 4.15 represents the changes in ellipticity determined for wildtype HTRA1, HTRA1$_{R166H}$, HTRA1$_{A173T}$ and HTRA1$_{R274Q}$ as a function of temperature thus portraying the thermodynamics of their thermal unfolding. Ellipticity was monitored at 222 nm over a temperature gradient ranging from 25 to 80 °C. Notably, all curves display two points of inflection each representing a folding transition between two distinct states. This finding indicates that thermal unfolding of the HTRA1 trimer is a two-step procedure involving a transient intermediate. Assuming that this folding intermediate represents monomeric HTRA1 the graph can be divided into two sigmoidal curves with the first point of inflection representing the transition from the trimeric to the monomeric state and the second one displaying the final transition to the fully unfolded protein. From the position of these inflection points on the x-axis two distinct melting temperatures (Tm1 and Tm2) can be derived. Remarkably, Tm1, which represents the trimer-monomer transition, varies considerably between the wildtype enzyme and the CARASIL-mutants, whereas Tm2 depicting the transition from the monomeric to the

fully unfolded state remains unaffected by the mutations. This finding confirms that the interface mutations effectively compromise thermodynamic stability of the trimer yet have no impact on overall protein stability. While for the wildtype enzyme the first transition point was close to that of the final transition to the unfolded state (ΔTm = 4.6 °C), HTRA1$_{R274Q}$ displayed the most profound shift in Tm1 and therefore the largest difference in melting temperatures (ΔTm = 13.2 °C). This observation indicates a particularly low trimer stability for this mutant thus validating the results obtained in NMR diffusion experiments. Due to aggregation of the unfolded protein at high temperatures refolding-curves could not be recorded.

4.3 Restoration of proteolytic activity via molecular clamps

4.3.1 Restoration of proteolytic activity assayed via the degradation of the model substrate β-casein

The above data obtained from crosslinking assays, analytical gelfiltration chromatography, NMR DOSY experiments and CD spectroscopy suggest that impaired trimer assembly is the main mechanism underlying loss of protein function in the CARASIL-relevant mutants HTRA1$_{R166H}$, HTRA1$_{A173T}$, HTRA1$_{R274Q}$ and HTRA1$_{G295R}$. Furthermore, it could be shown that the different oligomeric forms exist at an equilibrium that appears to be shifted towards the monomeric state in these mutants. These findings raised the idea of shifting the equilibrium back towards the trimeric form via the chemical modulation of protein-protein interactions thus restoring trimerization and hence the proteolytic activity of trimer-interface CARASIL mutants.

To restore proper oligomer formation in the HTRA1 mutants a strategy was chosen based on the observation that in the HTRA1 trimer there is a high prevalence of negatively charged residues on both sides of the protomer interface. Therefore, it should be possible to bridge the gap between two monomers using a compound with positive charges on either side (molecular clamps), that bind to the anionic hotspots on either side of the interface thus stabilizing the trimer. In order to address this hypothesis we chose to investigate compounds carrying two guanidinio carbonyle

pyrrole (GCP) motives connected by linkers of various sizes. The GCP motive is a synthetic arginine analogue developed by the group of Carsten Schmuck, University of Duisburg-Essen (Jiang *et al.* 2013), that was designed to recognize and bind oxyanions. The interaction of the GCP motive with oxyanions is based on a multitude of hydrogen bonds and ionic interactions. This feature makes it an optimal candidate for binding to the various aspartate and glutamate residues located at the HTRA1 interface region thus bridging the gap between two individual protomers.

In order to screen for potential candidate molecules restoring HTRA1 trimerization we chose an indirect approach assaying the restoration of proteolytic activity rather than retrimerization. The main advantage of this indirect approach is, that it allows us to exclude those compounds *ab initio*, that restore trimer formation, but on the other hand interfere with proteolytic activity. Furthermore, assaying the mutants' proteolytic activity in presence of the compounds is an efficient means to assess their effectiveness yielding fast and reproducible results in a quantitative manner.

In order to assess the ligands' effects on proteolytic activity β-casein degradation assays were performed with the CARASIL-relevant interface mutant $HTRA1_{R274Q}$. Following preincubation of the enzyme with 2.5 mM of the respective compound at 37 °C for 30 minutes time dependent degradation of a 20-fold surplus of the substrate β-casein was analyzed as described in section 4.2.2. Wildtype HTRA1 as well as samples preincubated in the absence of compound were used as negative controls.

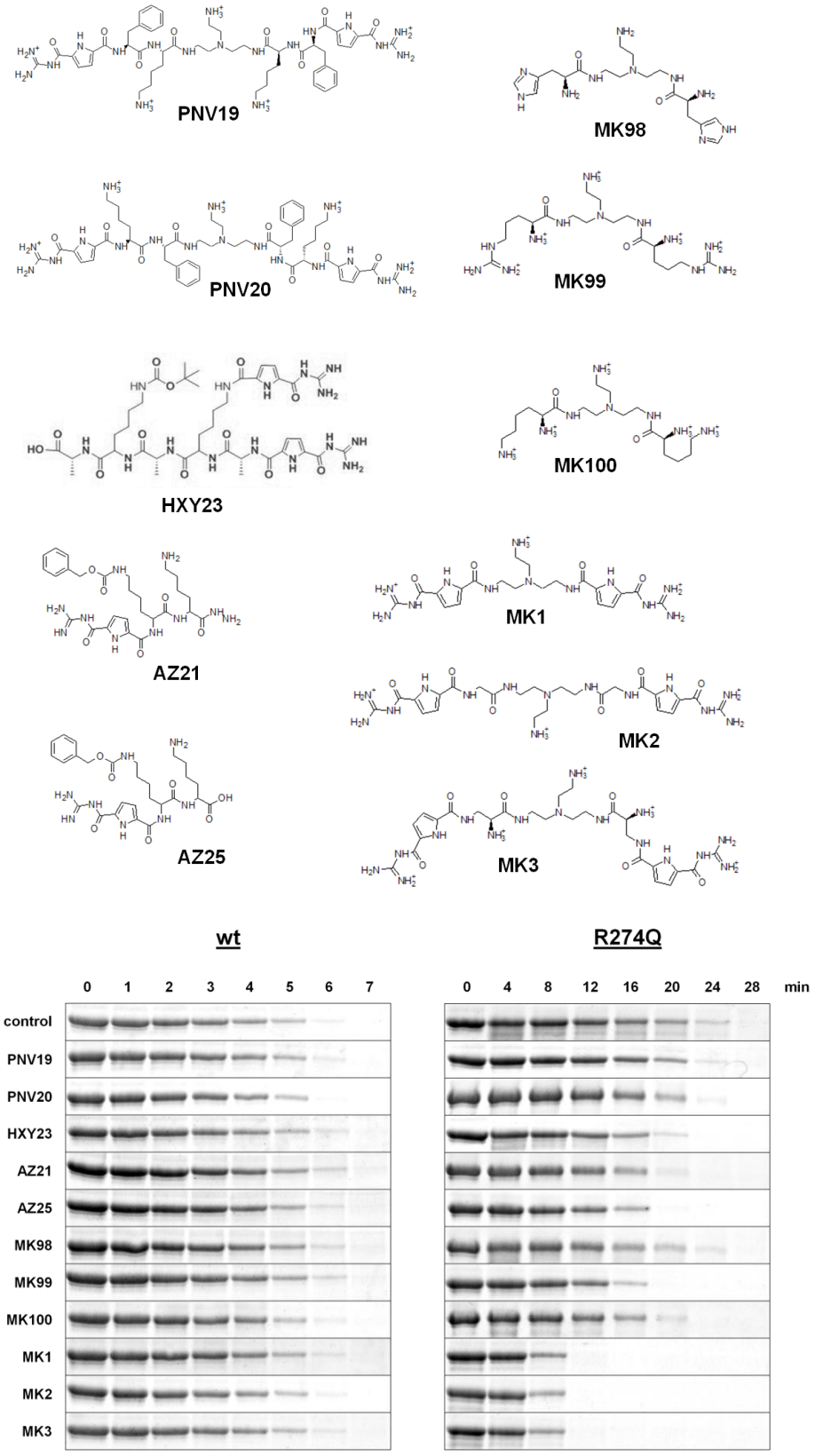

Figure 4.16 β-casein degradation by wildtype HTRA1 and HTRA1$_{R274Q}$ in the presence of clamp compounds

Time dependent degradation of β-casein was followed on SDS-PAGE. Following preincubation with the respective compound 1 µM wildtype HTRA1 or HTRA1$_{R274Q}$ were incubated with 20 µM β-casein in 50 mM NaPi, 50 mM NaCl, pH 8 at 37 °C for 7 or 28 minutes, respectively. Samples were taken at indicated time points and subjected to SDS-PAGE followed by Coomassie Brilliant Blue staining.

Compounds MK1, MK2 and MK3 significantly increased proteolytic activity of $HTRA1_{R274Q}$, but displayed no effect on wildtype HTRA1.

Compounds MK1, MK2 and MK3 are synthetic ligands designed to fit the requirements for bridging the inter-monomer gap by binding to the anionic hotspots on either side of the interface via complementary electrostatic interactions. They consist of a central tris(2-aminoethyl)amine core connected to two arms each comprising a flexible linker with a terminal GCP unit. The length of the linker region is varied with compound MK1 containing the shortest and compound MK3 the longest linker in order to assess the effects of linker length on binding affinity. Figure 4.16 shows that whereas in the absence of compound $HTRA1_{R274Q}$ cleaves a 20-fold surplus of β-casein within 28 minutes, it is able to digest the same amount of substrate within 12 minutes in presence of the ligands, indicating that the supramolecular clamps indeed cause a partial restoration of proteolytic activity. Furthermore, it could be shown that the presence or absence of glycine and thus the length and flexibility of the linker had no significant effect as seen by the comparison of the three ligands. Importantly neither compound displayed an effect regarding the activity of wildtype HTRA1. This finding confirms that the observed effects are restricted to the R274Q mutant alone and that the compounds do not interfere with the intrinsic proteolytic activity of the wildtype.

Remarkably control compounds, in which the GCP motive is exchanged for histidine (MK98), arginine (MK99) or lysine (MK100) respectively, showed no (MK98) or very weak (MK99 and MK100) effects indicating that the synthetic recognition unit GCP significantly increases binding affinity compared to the proteinogenic amino acids.

In addition, a set of control compounds, that were chosen from an internal library, were tested regarding their effects on the proteolytic activities of wildtype HTRA1 and the monomeric mutant. These compounds either carried a guanidino group coupled to a pyrridine ring via an amide bond at both their termini (PNV19 and PNV20) or a combination of this and other motives such as carboxylic (HXY23) or toluol groups (AZ21 and AZ25). Similar to MK98, MK99 and MK100 these compounds did not render significant effects on the proteolytic activity of either HTRA1 construct.

To demonstrate that the compounds' effects can indeed be attributed to their binding to the protease domain we repeated the above experiment with an $HTRA1_{R274Q}$

construct lacking the PDZ domain - a regulatory domain frequently addressed by allosteric regulators of HTRA activity.

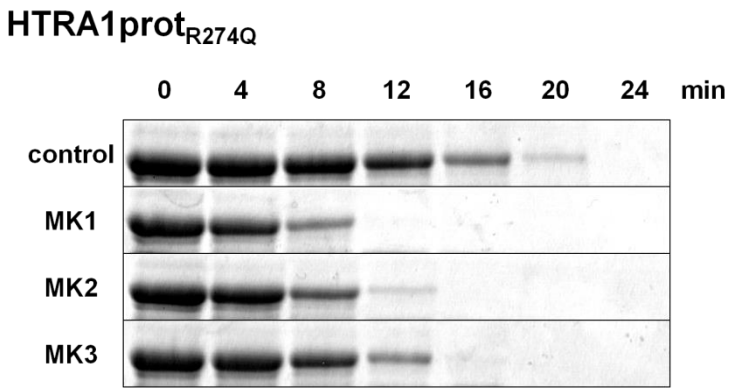

Figure 4.17 β-casein degradation by HTRA1prot$_{R274Q}$ in the presence of compounds MK1, MK2 and MK3
Time dependent degradation of β-casein was followed on SDS-PAGE. Following preincubation with the respective compound 1 µM HTRA1prot$_{R274Q}$ were incubated with 20 µM β-casein in 50 mM NaPi, 50 mM NaCl, pH 8 at 37 °C for 24 minutes. Samples were taken at indicated time points and subjected to SDS-PAGE followed by Coomassie Brilliant Blue staining. Compounds MK1, MK2 and MK3 significantly increased proteolytic activity of HTRA1prot$_{R274Q}$.

Figure 4.17 shows that similar to HTRA1$_{R274Q}$ HTRA1prot$_{R274Q}$ displays an approximately 2-fold increase in proteolytic activity when preincubated with the clamp compounds. These results demonstrate that the compounds‘ effects are independent of the PDZ domain. Thus the ligands‘ effects can indeed be ascribed to their binding to the proteolytic domain rather than an allosteric effect mediated via the PDZ domain.

In order to demonstrate that the effects of the clamp compounds are not allele specific, but extend to other CARASIL-relevant interface mutants displaying defects in trimerization β-casein degradation assays were performed for HTRA1$_{R166H}$, HTRA1$_{A173T}$ and HTRA1$_{R274Q}$ in the presence of ligands MK1, MK2 and MK3. Additionally, dose-response curves were generated for each mutant-ligand combination to further analyze their concentration-dependent effects and assess their effective concentration range.

Prior to proteolytic digests the monomeric mutants were incubated with varying concentrations of each compound covering a concentration range from 0 to 2.5 mM. Bands obtained via SDS-PAGE gel electrophoresis were quantified using the ImageJ analysis software. The normalized decrease in band intensities was plotted against the

respective compound concentrations. HTRA1$_{A252T}$ and samples preincubated in the absence of compound were used as negative controls.

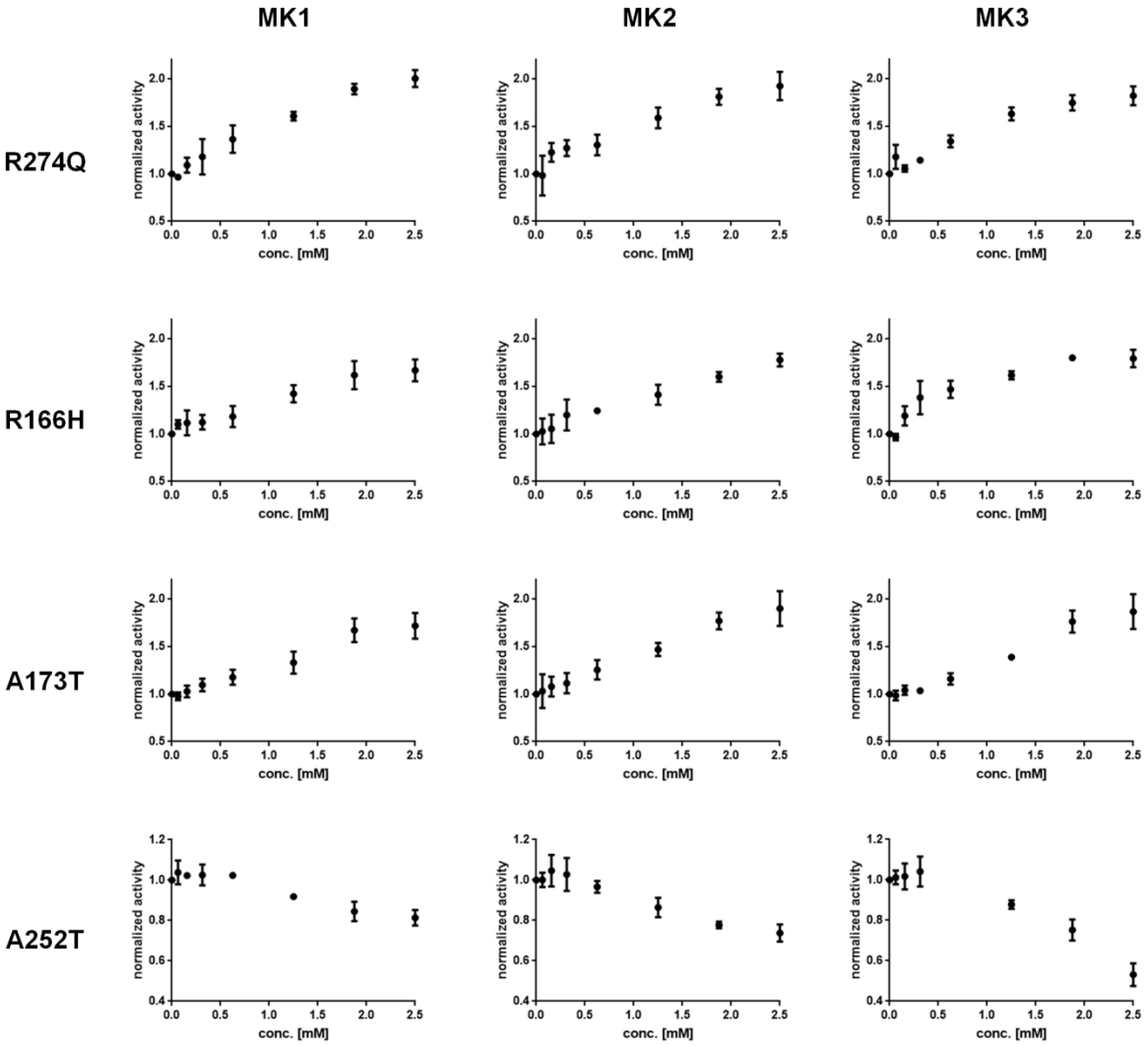

Figure 4.18 β-casein degradation by CARASIL-relevant HTRA1 mutants in the presence of compounds MK1, MK2 and MK3
Time dependent degradation of β-casein was followed on SDS-PAGE. Following preincubation with different concentrations of the respective compounds ranging from 0 to 2.5 mM 1 µM HTRA1 were incubated with 20 µM β-casein in 50 mM NaPi, 50 mM NaCl, pH 8 at 37 °C. Samples were subjected to SDS-PAGE followed by Coomassie Brilliant Blue staining and band intensities were subsequently quantified via ImageJ. Plotting of the normalized activities (y-axis) against compound concentrations (x-axis) rendered the dose-response curves. The error bars display the deviations calculated from two independent experiments.

The dose-response curves demonstrate an augmentative effect on the proteolytic activity of those HTRA1 mutants whose loss of activity is attributable to defects in trimer assembly (figure 4.18). The observed effect is concentration-dependent and appears to reach a plateau phase at compound concentrations of approximately 2 to 2.5 mM. At these concentrations reaction velocities are approximately twice as high as the

enzymes' basal activities. However, the restoration of proteolytic activity is most profound for HTRA1$_{R274Q}$. In contrast to the interface mutants the active site mutant HTRA1$_{A252T}$ displays a reduction in proteolytic activity when preincubated with the clamp compounds. This inhibitory effect is most pronounced for compound MK3.

In order to gain deeper insights into the clamp compounds' binding mode combination studies were performed. In cases, where compounds address different and distinct binding sites on the target protein additive effects should be observed, when two or more different compounds are added to the reaction.

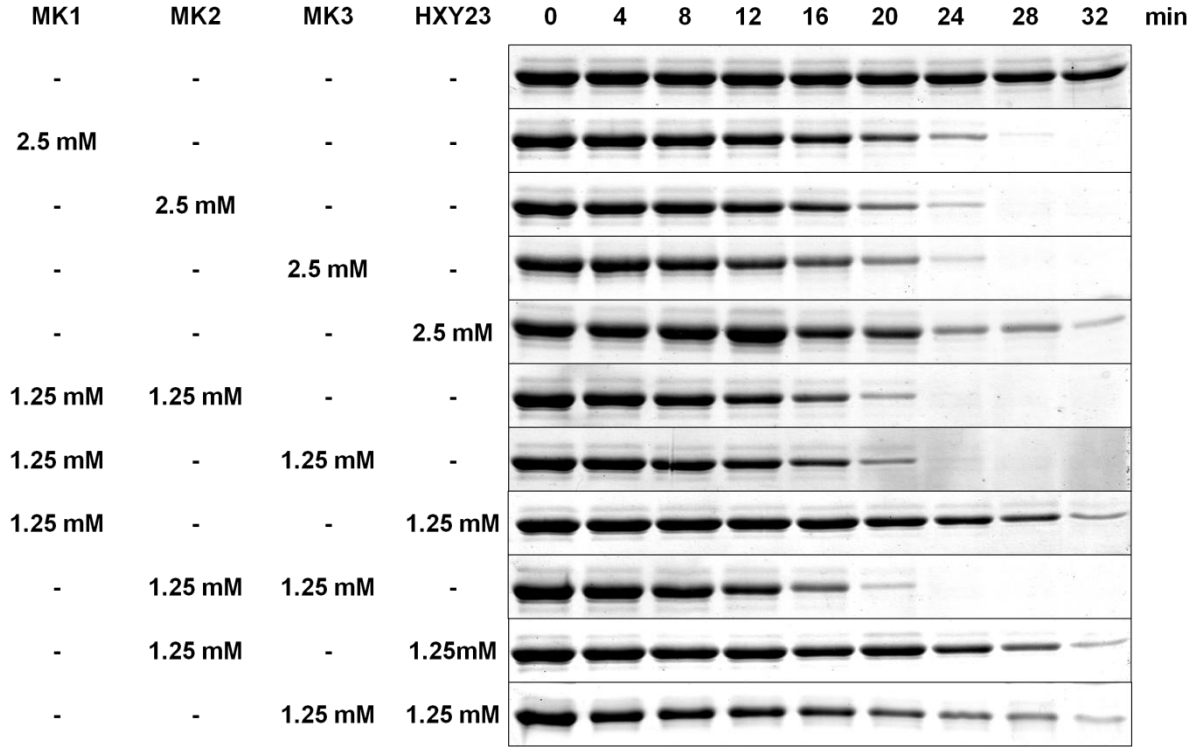

Figure 4.19 β-casein degradation by HTRA1prot$_{R274Q}$ in the presence of different compound combinations
Time dependent degradation of β-casein was followed on SDS-PAGE. Following preincubation with the respective compound combination 1 µM HTRA1$_{R274Q}$ were incubated with 20 µM β-casein in 50 mM NaPi, 50 mM NaCl, pH 8 at 37 °C for 32 minutes. Samples were taken at indicated time points and subjected to SDS-PAGE followed by Coomassie Brilliant Blue staining. No additive effects were observed.

To determine whether additive effects can be observed for the clamp compounds HTRA1$_{R274Q}$ treated with either ligand MK1, MK2, MK3, HXY23 or a combination of the four was subjected to β-casein degradation assays as described above. As shown in the previous experiments MK1, MK2 and MK3 exhibited a significant effect on degradation velocity, whereas HXY23 displayed only a minor effect (figure 4.19). When

two of the three clamp compounds (MK1, MK2 or MK3) were combined only a minor additional increase in degradation speed could be obtained indicating that the three compounds presumably interact with the target enzyme via the same or similar binding sites. However, a combination of MK1, MK2 or MK3 with the weak activator HXY23 rendered a reaction velocity similar to that obtained with the weaker activator alone suggesting that HXY23 competes with MK1, MK2 and MK3 for the same binding sites thus alleviating their effects. Yet to gain deeper insights into the compounds‘ binding sites more detailed experimental and computational studies will be needed.

4.3.2 Restoration of trimer formation analyzed via NMR diffusion experiments

As shown in the previous experiments the molecular clamps MK1, MK2 and MK3 are able to restore proteolytic activity in the monomeric CARASIL mutants, but do not render any effects on proteolysis by wildtype HTRA1. However, assessing the restoration of proteolytic activity is only an indirect indicator for the restoration of trimer formation. Since the high compound concentrations required to observe a restoration of proteolytic activity display a major challenge in most conventional experimental set-ups used to assess complex sizes and oligomeric states, we decided to assess the oligomeric state of HTRA1 in the absence and presence of the molecular clamps via NMR DOSY experiments [6]. Based on the observation that $HTRA1_{R274Q}$ displays the most profound defect in oligomerization and proteolytic activity compared to the other monomeric interface mutants this mutant was chosen as a representative for the analysis of trimer restoration. Furthermore, ligand MK2 was selected as a model compound for this set of experiments due to its inherent stability and the feasibility of its synthesis.

Spectra were recorded for both $HTRA1_{R274Q}$ and the wildtype enzyme at different concentrations ranging from 10 to 100 µM as described previously in section 4.2.4. An

[6] NMR DOSY experiments were performed in collaboration with Dr. Christine Beuck, Hendrik Kirschner and Prof. Peter Beyer, Department of Structural and Medical Biochemistry, University of Duisburg-Essen.

additional 1D-spectrum was recorded for compound MK2 in the absence and presence of HTRA1 in order to determine where its signals overlap with those derived from the enzyme.

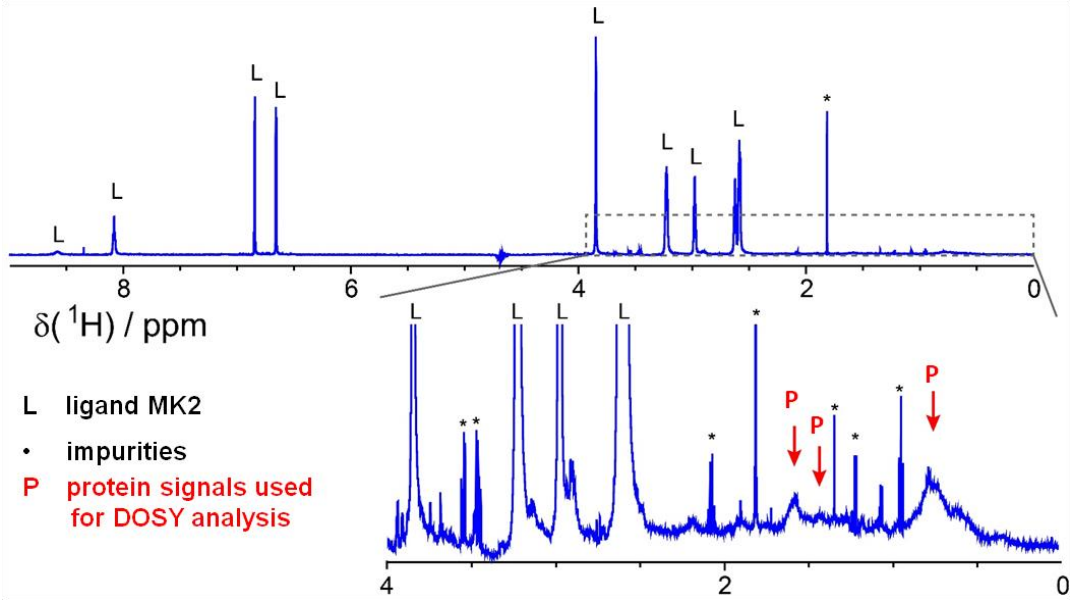

Figure 4.20 1D-^{1}H-spectrum for HTRA1protSA$_{R274Q}$ and compound MK2
An 1D-^{1}H-spectrum was recorded for 25 µM HTRA1prot$_{R274Q}$ in presence of 2.5 mM MK2. Given are the signal intensities recorded at 9-0 ppm including a zoom covering 4-0 ppm. The red Ps indicate the protein-derived signals, Ls indicate signals derived from the ligand and * mark impurities present in the ligand preparation.

In order to assess a protein's diffusion coefficient as a function of signal decrease as described in section 4.2.4 it is crucial to find sufficiently high protein signals, which do not overlap with the compound signals. However, the high compound concentrations required to observe a restoration of proteolytic activity (see section 4.3.1) massively increase the intensity of the ligand signals thus limiting the overall sensitivity of the experiment. Hence as shown in figure 4.20 only three protein derived signals recorded at 1.6 ppm, 1.4 ppm and 0.8 ppm met the above requirements and could therefore be considered in the following experiments.

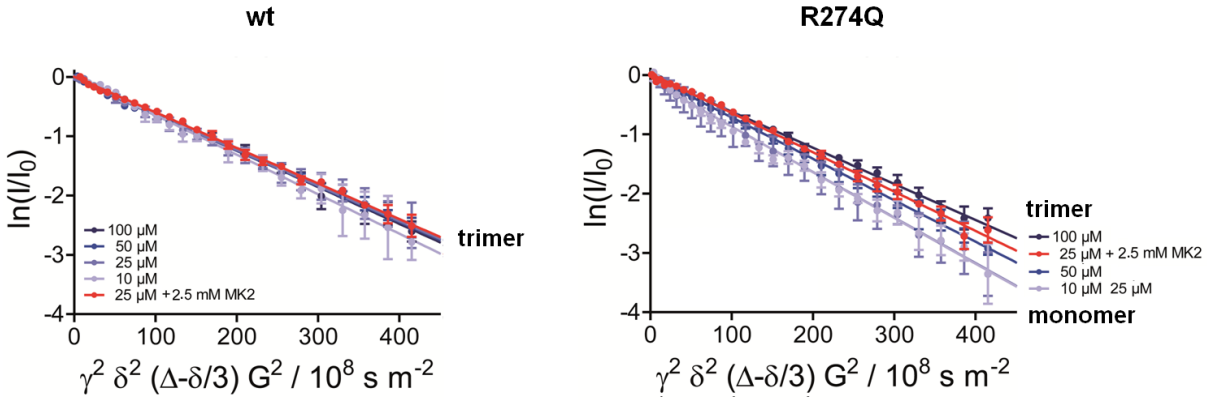

Figure 4.21 Stabilization of the trimer in presence of MK2 analyzed via NMR DOSY experiments
The Stejskal-Tanner plots display the normalized signal intensities of the protein peaks (y-axis) as a function of gradient strength (x-axis) with the slope corresponding to the protein's diffusion coefficient. The left panel shows the diffusion coefficients for HTRA1protSA wildtype. The right panel displays the diffusion coefficients for HTRA1protSA$_{R274Q}$. Signals were recorded at 0.8 ppm, 1.6 ppm and 2.9 ppm. Signal intensities acquired in the absence of compound are shown in blue, those observed for 25 µM protein in the presence of 2.5 mM compound MK2 are highlighted in red. Error bars indicate the standard error of the mean. Upon addition of compound MK2 HTRA1protSA$_{R274Q}$ displays a distinct shift towards the trimeric state, whereas no effect could be observed on the wildtype protein.

Figure 4.21 shows the normalized signal intensities of the protein peaks as a function of gradient strength (Stejskal-Tanner plot) with the slope corresponding to the protein's diffusion coefficient. For free HTRA1 protein the normalized I/I_0 values of four signals (3.0 ppm, 1.6 ppm, 1.4 ppm and 0.8 ppm) were averaged. For HTRA1 in presence of ligand MK2 three signals (1.6 ppm, 1.4 ppm and 0.8 ppm) could be averaged, since other protein signals overlapped with the signals of the ligand or impurities found in the ligand preparation. As described previously in section 4.2.4 no concentration dependent changes in the diffusion coefficient could be observed for wildtype HTRA1 indicating that it exists as a stable trimer within the tested concentration range. In accordance with this observation and the results obtained from proteolysis assays no changes were detected upon addition of compound MK2. In contrast, HTRA1$_{R274Q}$ displayed a significant concentration dependence of its diffusion coefficients. Whereas at a concentration of 100 µM the slope and thus the diffusion coefficient corresponds to that of the wildtype enzyme, a significant decrease can be observed at lower concentrations showing that the monomer-trimer ratio increases with lower protein concentrations. However, for 10 µM HTRA1$_{R274Q}$ no additional decrease of the diffusion coefficient could be detected suggesting that the equilibrium is entirely shifted towards the monomeric state at concentrations as low as 25 µM. These data indicate that the concentration dependent shift from the trimeric to the monomeric form occurs within a concentration range between 25 and 100 µM. However, upon addition of ligand

MK2 to 25 µM HTRA1$_{R274Q}$ the mutant displays a distinct shift towards the trimeric form with the diffusion coefficient almost resembling that of the wildtype protein. This finding demonstrates that the compound is indeed able to restore trimer formation in the CARASIL-relevant interface mutant.

4.4 Restoration of proteolytic activity via VDAC peptides

4.4.1 Restoration of proteolytic activity assayed via the degradation of the native substrate Tau

Following the successful restoration of enzymatic activity via molecular clamps a second approach to restore the CARASIL mutants' proteolytic function was investigated in the course of this study. This approach is based on the observation that HTRA1 activity can be modulated allosterically via small peptides binding either to its PDZ or directly to the proteolytic domain.

To identify potential activators of the CARASIL-relevant mutants peptides chosen from our laboratory portfolio of already known HTRA1 activators were investigated regarding their potential to restore proteolytic activity in the CARASIL mutants. The portfolio is based on a peptide screen conducted at the Institute for Medical Immunology, Charité Berlin [7]. In this screen a library containing the eleven C-terminal amino acids of 6.223 human proteins was spotted onto a nitrocellulose membrane using the inverted peptide method. The membrane was subsequently incubated with proteolytically inactive HTRA1$_{S328A}$ and binding of HTRA1 was visualized via immunodetection. Hits derived from the screen were then evaluated regarding their potential physiological relevance and selected peptides were further validated and characterized via isothermal titration experiments and proteolytic digests. In the following the peptides will be named according to their respective proteins for reasons of simplification.

[7] The peptide screen was conducted by Prisca Boisguerin and Rudolf Volkmer, Charité Berlin.

For the identification of peptides restoring the proteolytic activity of the CARASIL-relevant mutants the most potent activators found for wildtype HTRA1 were investigated regarding their impact on the activity of $HTRA1_{R274Q}$. In a previous study (Rey 2018) the tested peptides were subdivided into two groups: The first group comprises those peptides binding to the PDZ domain of HTRA1. A representative of this group is the CCNH-peptide derived from the C-terminus of Cyclin H, a regulator of Cyclin Dependent Kinase 7 (Dhulipala *et al.* 2006). Furthermore, a derivative of the original CCNH-peptide optimized for binding to the PDZ domain (CCNH-CFD.1) was analyzed. The second group comprises peptides affecting the proteolytic activity of HTRA1 in a PDZ-independent manner. Among these there are the C-termini of the three Voltage Dependent Anion-selective Channel (VDAC) isoforms (VDAC1, VDAC2 and VDAC3) – a class of β-barrel channels situated in the outer mitochondrial membrane (Ponnalagu and Singh 2017). Additionally, a derivative of the Calpain2 C-terminus (CAPN2.1) was tested, in which the valine residue at position -1 was exchanged for aspartate and the cysteine residue at position -5 was substituted by serine in order to increase solubility and prevent the formation of inter-peptide disulfide bonds. Representatives of both groups were taken into account in the course of this study. Furthermore, derivatives comprising sequences from both groups were investigated. The N-terminus of these derivatives equals that of CCNH, whereas its C-terminus is derived from VDAC2 (CCNH.2) or a variation of the VDAC2-peptide (CCNH-VDAC2AL) respectively. Previous studies (Rey 2018) showed that these mixed derivatives activate HTRA1 in a PDZ-dependent manner.

To assess the peptides' activation efficacy on $HTRA1_{R274Q}$ proteolytic digests were conducted using the native HTRA1 substrate Tau. Degradation of Tau was followed over six hours. The wildtype enzyme was used as a control.

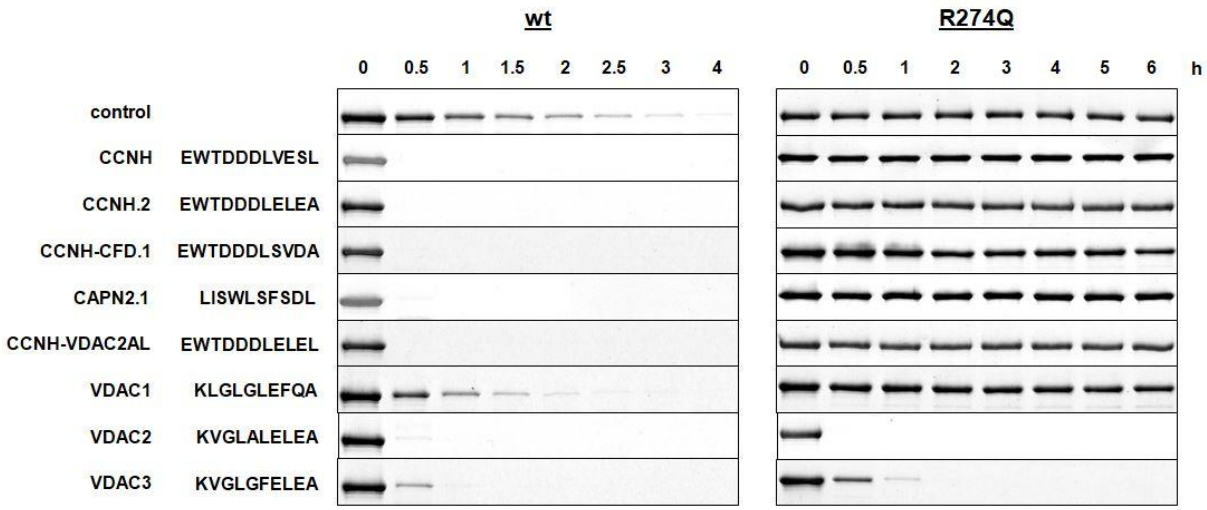

Figure 4.22 Tau degradation by wildtype HTRA1 and HTRA1$_{R274Q}$ in the presence of peptides
Time dependent degradation of Tau was followed on SDS-PAGE. Following preincubation with 50 µM of the respective peptides 1 µM wildtype HTRA1 or HTRA1$_{R274Q}$ were incubated with 8 µM Tau in 50 mM TRIS pH 8 at 37 °C for 4 or 6 hours, respectively. Samples were taken at indicated time points and subjected to SDS-PAGE followed by Coomassie Brilliant Blue staining. Peptides VDAC2 and VDAC3 significantly increased the proteolytic activity of HTRA1$_{R274Q}$.

Whereas wildtype HTRA1 degraded an 8-fold surplus of Tau within 4 hours, its degradation rate could be massively increased via addition of the peptides with VDAC1, which only rendered a mild increase in proteolytic activity, being the only exemption (figure 4.22). The CARASIL-relevant interface mutant HTRA1$_{R274Q}$, however, did not show any significant degradation within the surveyed time frame of six hours in the absence of compound. Remarkably, upon addition of the peptides VDAC2 and VDAC3 a complete digest of Tau could be observed already within 30 and 60 minutes, respectively. Thus both VDAC2 and VDAC3 were able to enhance the proteolytic activity of HTRA1$_{R274Q}$ to an extent, that exceeds the basal activity of the wildtype enzyme. In contrast peptides, whose activation mode was previously shown to depend on the PDZ domain (CCNH, CCNH.2 and CCNH-VDAC2AL) (Rey 2018), as well as the PDZ-independent activator CAPN2.1 displayed no effect on the activity of the interface mutant.

In order to demonstrate that the VDAC-peptides' effects on the proteolytic activity of HTRA1$_{R274Q}$ are indeed PDZ-independent the above experiment was repeated using a construct deleted for the PDZ domain (HTRA1prot$_{R274Q}$).

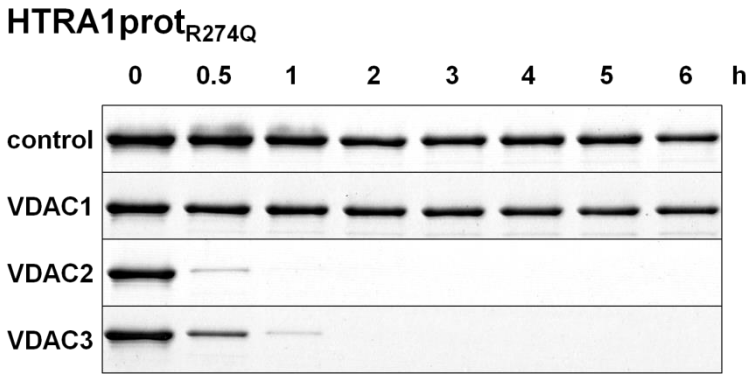

Figure 4.23 Tau degradation by HTRA1prot$_{R274Q}$ in presence of VDAC1, VDAC2 and VDAC3
Time dependent degradation of Tau was followed on SDS-PAGE. Following preincubation with 50 µM of the respective peptides 1 µM HTRA1prot$_{R274Q}$ were incubated with 8 µM Tau in 50 mM TRIS pH 8 at 37 °C for 6 hours. Samples were taken at indicated time points and subjected to SDS-PAGE followed by Coomassie Brilliant Blue staining. Peptides VDAC2 and VDAC3 significantly increased proteolytic activity of HTRA1prot$_{R274Q}$.

As shown in figure 4.23 proteolytic activity of HTRA1prot$_{R274Q}$ was dramatically increased upon addition of VDAC2 and VDAC3 and the extent of activation was comparable to that previously observed for HTRA1$_{R274Q}$. Thus binding to the PDZ domain can be excluded as a cause for the peptide-induced increase in proteolytic activity.

To further investigate the effects of VDAC2 dose-response assays were performed. Prior to proteolytic digests of the native substrate Tau both wildtype HTRA1 and HTRA1$_{R274Q}$ were incubated with varying concentrations of the peptide ranging from 0 to 50 µM. Samples taken at different time points during the reaction were subjected to SDS-PAGE.

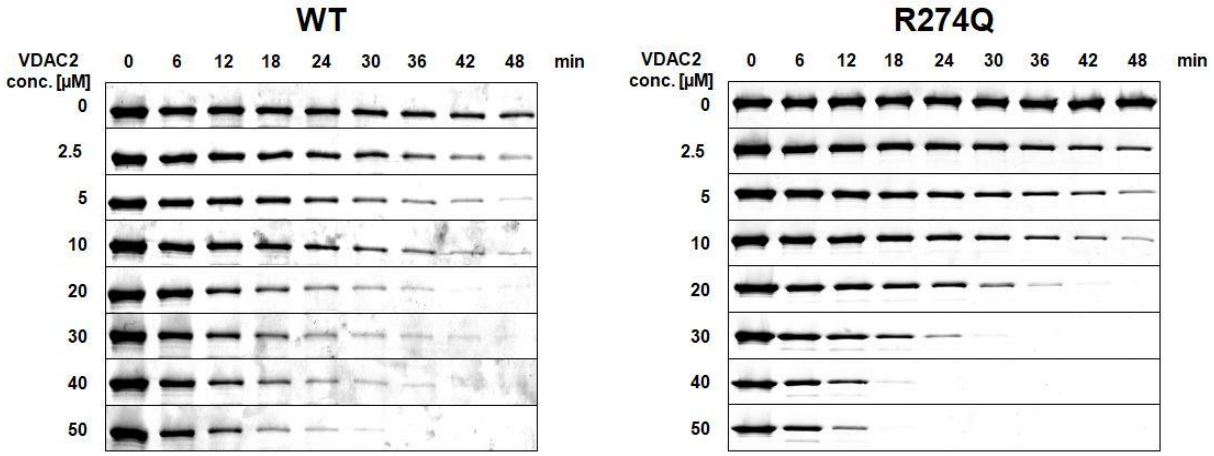

Figure 4.24 Concentration dependent effects of VDAC2 on Tau degradation by wildtype HTRA1 and HTRA1$_{R274Q}$
Time dependent degradation of Tau was followed on SDS-PAGE. Following preincubation with different concentrations of VDAC2 ranging from 0 to 50 µM 1 µM wildtype HTRA1 or HTRA1$_{R274Q}$ were incubated with 8 µM Tau in 50 mM TRIS pH 8 at 37 °C for 48 minutes. Samples were taken at indicated time points and subjected to SDS-PAGE followed by Coomassie Brilliant Blue staining.

As shown in figure 4.24 VDAC2 exhibits a concentration dependent effect on both wildtype HTRA1 and the R274Q mutant, which enters a plateau phase at a concentration of approximately 50 µM. Notably, the activating effect observed on HTRA1$_{R274Q}$ is significantly more pronounced than that on the wildtype enzyme.

In order to extend the concept of peptide-induced activation the effects of the VDAC peptides on other CARASIL-relevant HTRA1 mutants were investigated. The experimental set-up was designed as described above.

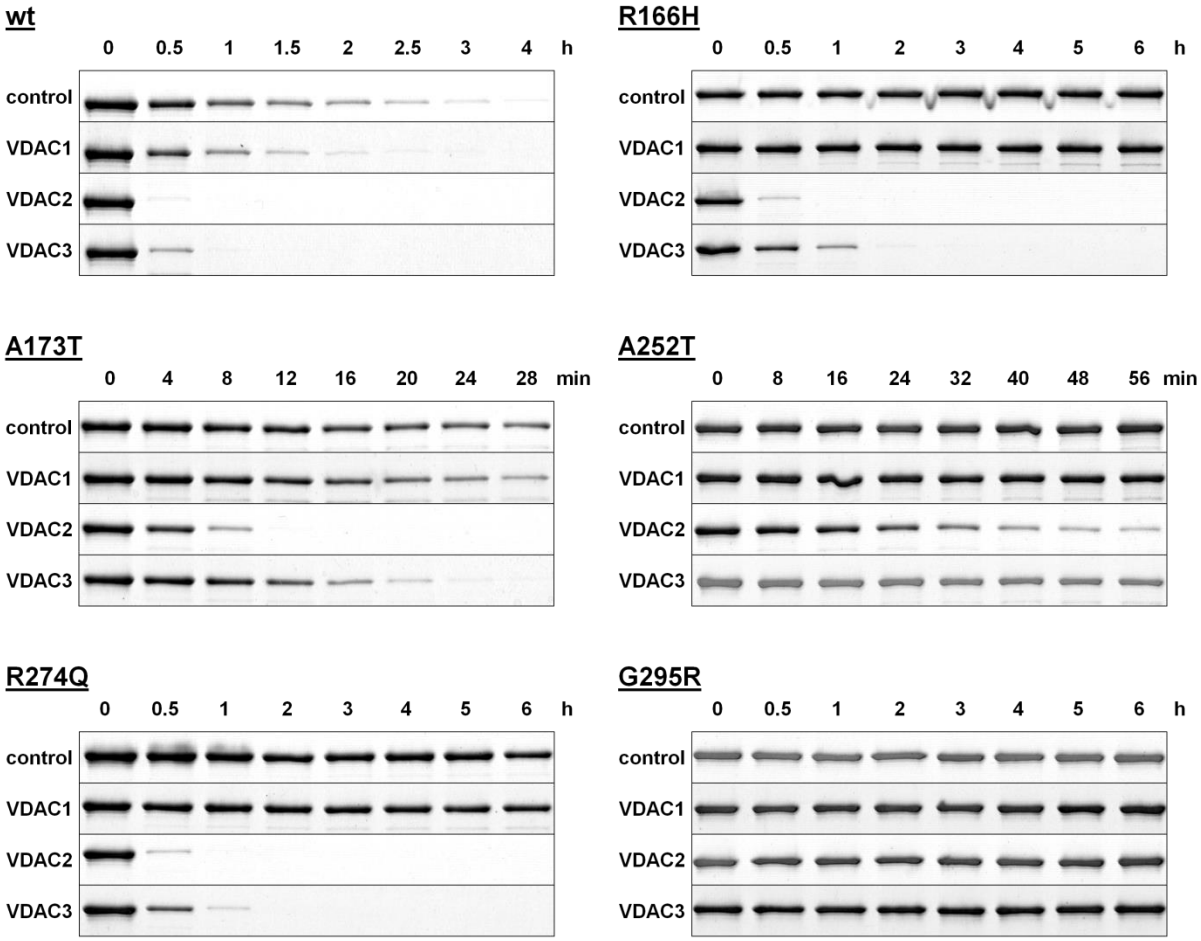

Figure 4.25 Tau degradation by CARASIL-relevant HTRA1 mutants in presence of VDAC1, VDAC2 and VDAC3
Time dependent degradation of Tau was followed on SDS-PAGE. Following preincubation with 50 µM of the respective peptides 1 µM HTRA1 were incubated with 8 µM Tau in 50 mM TRIS pH 8 at 37 °C for 28 minutes, 56 minutes, 4 hours or 6 hours. Samples were taken at indicated time points and subjected to SDS-PAGE followed by Coomassie Brilliant Blue staining. Peptides VDAC2 and VDAC3 significantly increased the proteolytic activity of HTRA1R_{166H}, HTRA1$_{A173T}$ and HTRA1$_{R274Q}$. Minor effects were observed on HTRA1$_{A252T}$ and no effects were obtained for HTRA1$_{G295R}$.

As shown in figure 4.25 all tested mutants displayed severely impaired proteolytic activities. For HTRA1$_{R166H}$, HTRA1$_{A173T}$ HTRA1$_{A252T}$ and HTRA1$_{R274Q}$ the defects in proteolytic activity were alleviated upon addition of VDAC2 and VDAC3. However, the extent of activity restoration varied depending on the type of mutation. For HTRA1$_{R166H}$ the effect was comparable to that observed for HTRA1$_{R274Q}$ with the overall time span required for complete proteolysis covering 30 to 60 minutes respectively. For HTRA1$_{A173T}$ the effect was slightly less pronounced. However, for all three mutants the activity increase observed upon addition of both VDAC2 and VDAC3 exceeded the basal activity of the wildtype enzyme showing that the concept of activity restoration via peptidic modulation can be extended to these disease-relevant mutants. In contrast

only a mild activity increase could be detected for HTRA1$_{A252T}$, whereas none was observed for HTRA1$_{G295R}$.

Allosteric activation mediated via the PDZ domain is considered to occur in a trimer-dependent fashion, since signal propagation to the active site is thought to involve interactions between the PDZ and loop L3, which subsequently passes the signal to loop LD* of the adjacent protomer. Unlike HTRA1$_{R274Q}$ the R252T mutant did not display defects in trimer formation thus suggesting a possibility for allosteric activation via peptidic modulators binding to the PDZ domain. To further address the responsiveness of HTRA1$_{A252T}$ to allosteric activity modulation Tau proteolysis was performed in the presence of the peptidic effector CCNH.2 (figure 4.26), which has previously been identified as a potential activator of HTRA1 acting in a PDZ-dependent manner.

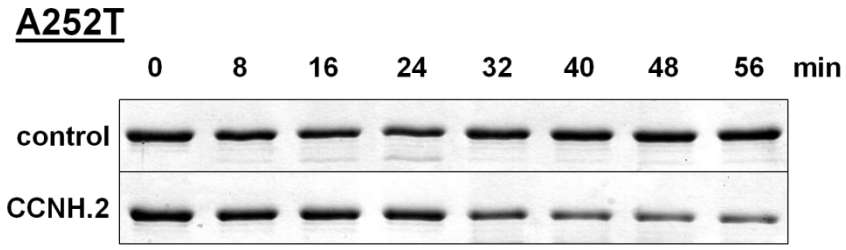

Figure 4.26 Tau degradation by HTRA1$_{A252T}$ in presence of CCNH.2
Time dependent degradation of Tau was followed on SDS-PAGE. Following preincubation with 50 µM CCNH.2 1 µM HTRA1prot$_{A252T}$ were incubated with 8 µM Tau in 50 mM TRIS pH 8 at 37 °C for 6 hours. Samples were taken at indicated time points and subjected to SDS-PAGE followed by Coomassie Brilliant Blue staining. Similar to VDAC2 and VDAC3 application of CCNH.2 only led to a minor increase in proteolytic activity of HTRA1$_{A252T}$.

Remarkably, HTRA1$_{A252T}$'s responsiveness to allosteric activity modulation via CCNH.2 appeared dramatically reduced compared to the wildtype enzyme (see above figure 4.22). Thus the mutant's insusceptibility to allosteric regulation is not restricted to VDAC2 and VDAC3, but additionally extends to peptidic effectors acting in a PDZ-dependent manner. These findings suggest, that allosteric activation mechanisms appear generally compromised in HTRA1$_{A252T}$.

4.4.2 Impact of VDAC2 on HTRA1 cleavage sites in Tau

To assess the impact of VDAC2 on the cleavage pattern generated during HTRA1-catalyzed proteolysis, mass spectrometry analysis of proteolytic digests was performed. In contrast to previous experiments, which focused on the quantitative effects of VDAC2 on degradation velocity, mass spectrometric analysis of peptides generated in proteolytic digests would allow to infer information regarding its mechanistic implications in a qualitative manner. In the course of the experiment 1 µM HTRA1 (wildtype or R274Q) were incubated with 8 µM Tau in the absence or presence of 50 µM VDAC2 and samples were taken at different time points (0, 0.5 and 4 hours). Following acetone-precipitation of residual proteins and further purification steps samples were subjected to mass spectrometry analysis at the Analytics Core Facility, University of Duisburg-Essen. The generated data were processed using the Utilities for Mass Spectrometry Analysis of Proteins (UMSAP) analysis software developed by Kenny Bravo-Rodriguez at the University of Duisburg-Essen (Bravo-Rodriguez *et al.* 2018).

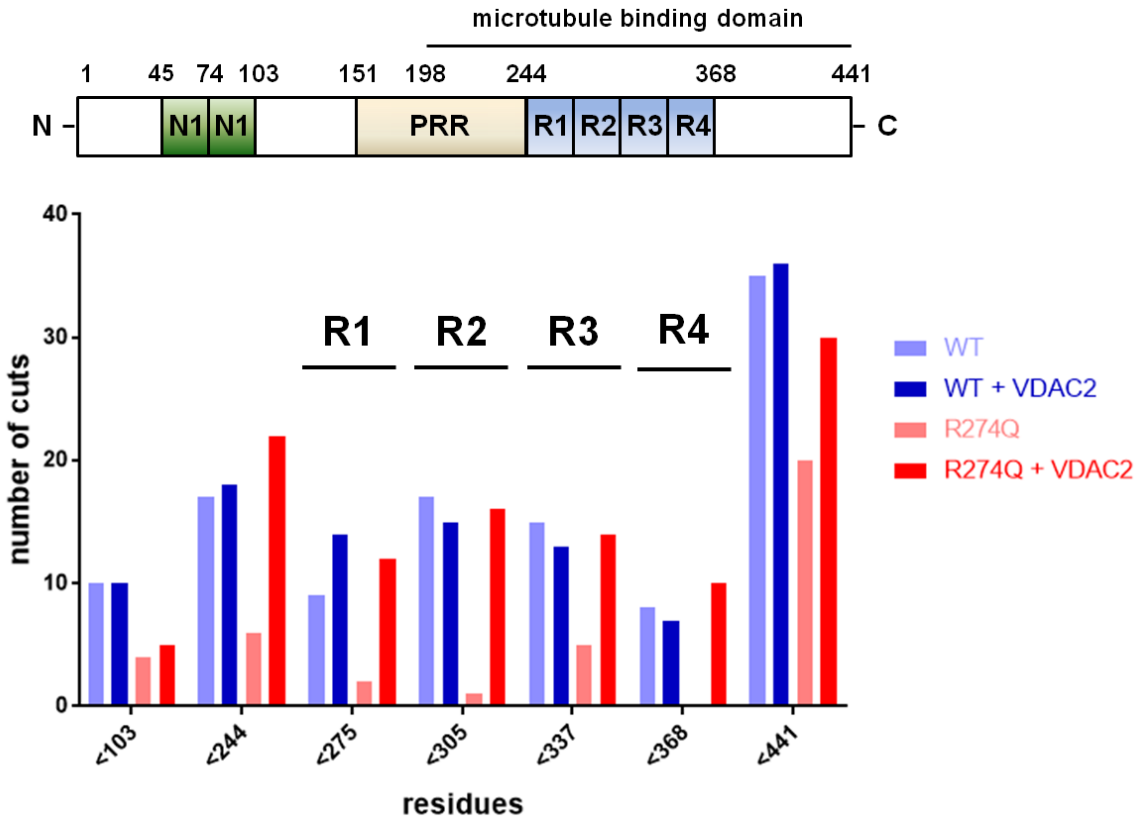

Figure 4.27 Analysis of HTRA1 cleavage sites in Tau in the absence and presence of VDAC2
8 µM Tau were incubated with 1 µM wildtype HTRA1 or HTRA1$_{R274Q}$ respectively in the absence or presence of 50 µM VDAC2 for 4 hours. Following acetone precipitation generated peptides were subjected to mass spectrometry analysis at the Analytics Core Facility, University of Duisburg-Essen. Experiments were conducted as triplicates. The upper panel illustrates the domain architecture of Tau-2N4R including the N-terminal inserts (N1 and N2), the proline rich region (PRR) and the repeat region (R1-R4) within the microtubule binding domain. The lower panel displays the number of cuts per region for wildtype HTRA1 (blue) or HTRA1$_{R274Q}$ (red) in the absence or presence of VDAC2.

The bar diagram in figure 4.27 displays the distribution of cleavage sites in Tau following incubation with wildtype HTRA1 or HTRA1$_{R274Q}$ for 4 hours. For the wildtype enzyme 111 cleavage sites could be identified, whereas the number of cleavage sites was dramatically reduced to 38 in the monomeric mutant. Upon addition of VDAC2 only a minor increase in the total number of cuts was observed for wildtype HTRA1 accompanied by a slight shift from the second, third and fourth towards the first repeat region, whereas the N-terminal region (aa 1-103) remained entirely unaffected. In contrast, a major increase in the total number of cleavage sites to 109 was observed for the R274Q mutant. This effect was visible in all domains of Tau. Yet it was most prominent in the repeat regions.

In addition to the analysis of cleavage patterns, the peptide's impact on amino acid preferences at the P1 and P1' residues was investigated (figure 4.28). As shown in

previous reports (Truebestein *et al.* 2011) wildtype HTRA1 displayed a distinct preference for small hydrophobic amino acids at position P1 with valine, isoleucine and leucine being the most prevalent residues. A similar preference could be observed for HTRA1$_{R274Q}$. Likewise addition of VDAC2 did not cause major changes at position P1.

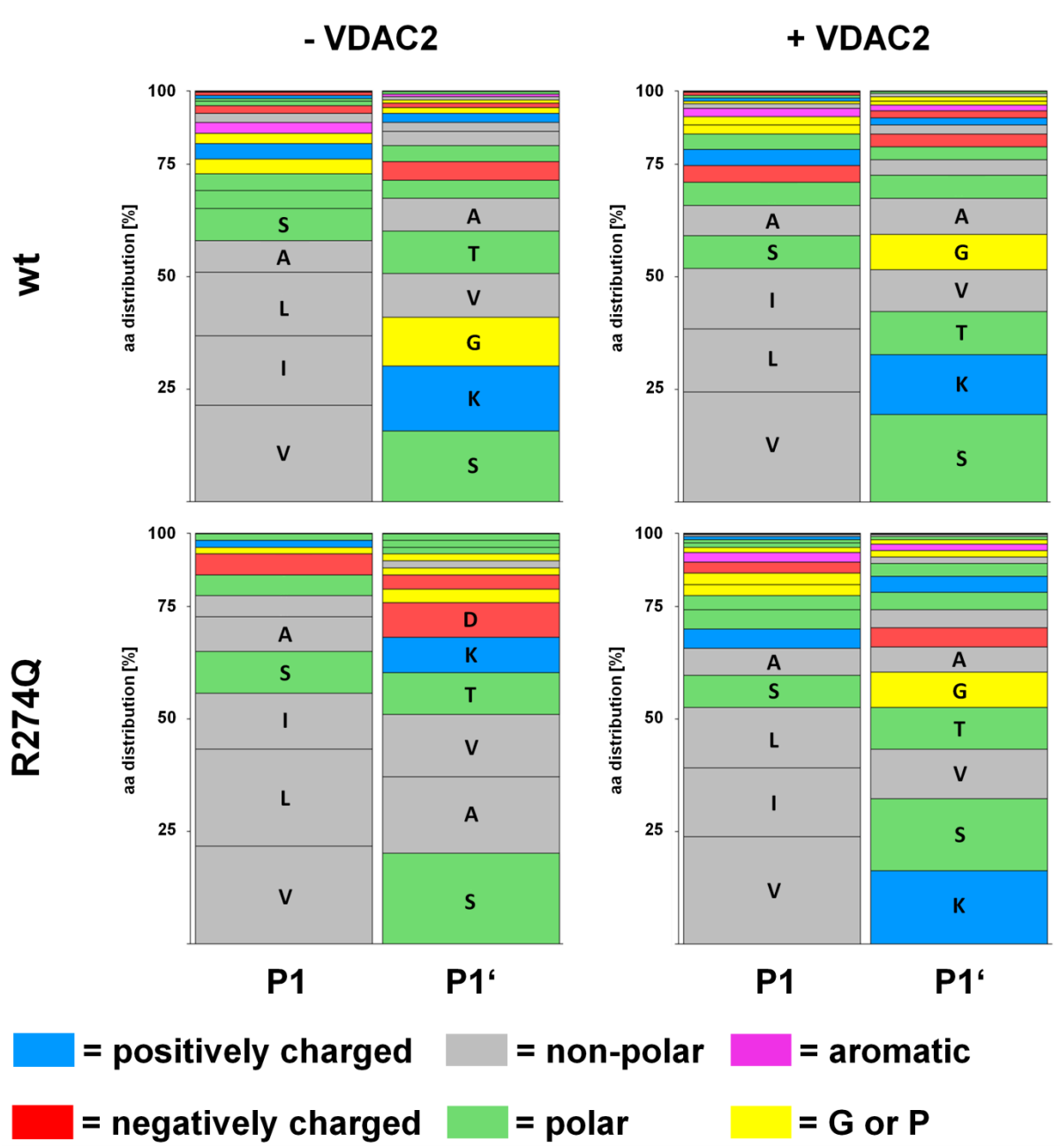

Figure 4.28 Analysis of amino acid preference in the absence and presence of VDAC2
The figure depicts the amino acid preference at P1 and P1' for wildtype HTRA1 and HTRA1$_{R274Q}$ in the absence and presence of VDAC2.

In stark contrast to this the amino acid preference at position P1' was significantly altered by both the mutation and the peptide. Both wildtype HTRA1 and HTRA1$_{R274Q}$

showed a marked preference for the polar residue serine in this position. Yet in the wildtype enzyme there was also a distinct preference for the positively charged residue lysine and the small amino acid glycine, whereas the R274Q mutant preferred the non-polar residues alanine and valine. Remarkably, addition of VDAC2 resulted in a significant shift of the mutant's amino acid preference at position P1'. The most apparent change is a major increase in the prevalence for the positively charged lysine residue. With lysine, serine, valine, threonine and glycine being the five most prevalent residues at position P1' the amino acid preference of HTRA1$_{R274Q}$ in presence of VDAC2 resembles that of the wildtype enzyme.

4.4.3 Specificity of the VDAC2 peptide

As demonstrated above application of the VDAC2 peptide resulted in a distinct increase in HTRA1 activity. Yet it remained to be investigated whether the effect is restricted to HTRA1 alone or shared among its homologues and other related serine proteases. To address the specificity of VDAC2-induced activation Tau degradation assays were performed for the human HTRA1 homologues HTRA2 and HTRA3. Furthermore, three additional serine proteases carrying the conserved chymotrypsin-like protease fold were included in the assay. Proteolysis of Tau in the absence and presence of 50 µM VDAC2 was followed over various time spans adjusted to the requirements of the respective enzymes.

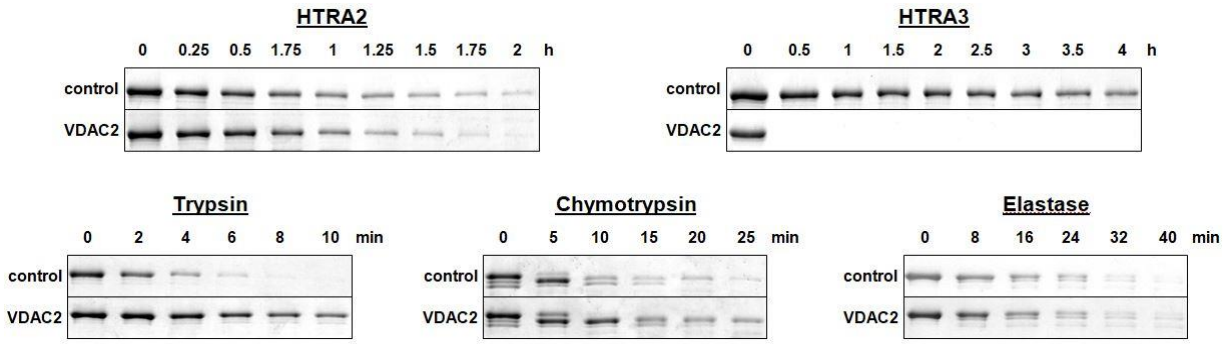

Figure 4.29 Tau degradation by trypsin-like serine proteases in presence of VDAC2

Time dependent degradation of Tau was followed on SDS-PAGE. Following preincubation with 50 µM VDAC2 1 µM HTRA2/HTRA3 or 0.01 µM Trypsin/Chymotrypsin/Elastase were incubated with 8 µM Tau in 50 mM TRIS pH 8 at 37 °C. Samples were taken at indicated time points and subjected to SDS-PAGE followed by Coomassie Brilliant Blue staining. VDAC2 significantly increased proteolytic activity of HTRA3, whereas no activating effects were observed on the other serine proteases.

As depicted in figure 4.29, for the cytosolic protease HTRA3 addition of VDAC2 resulted in a profound increase in proteolytic activity similar to that described for its homologue HTRA1, whereas no significant effect could be detected for the mainly mitochondrial protease HTRA2. Remarkably, activation was not observed for the non-HTRA serine proteases. Instead the proteolytic activity of both trypsin and chymotrypsin appeared mildly compromised in presence of the peptide, while that of elastase remained unaltered. Taken together these findings indicate, that the activating effect of the VDAC2 C-terminus is precisely confined to the two cytosolic HTRA homologues HTRA1 and HTRA3 suggesting a profoundly specific activation mechanism.

4.4.4 Determination of oligomeric states in the presence of VDAC2

Peptides corresponding to both the VDAC2 and VDAC3 C-termini were able to dramatically elevate the proteolytic activity of the CARASIL-relevant interface mutants HTRA1R_{166H}, HTRA1$_{A173T}$ and HTRA1$_{R274Q}$. Yet the mechanism underlying activity restoration remains unclear. Previous studies have shown that inter-monomer communication is essential for the proper positioning of the catalytic triad, the formation of the oxyanion hole and the shaping of the substrate specificity pocket thus making the formation of stable trimers a prerequisite for HTRA1 activity (Truebestein *et al.* 2011). Therefore, the observation, that the loss of function phenotype of the interface mutants is associated with a pathologic shift of the monomer-trimer equilibrium towards the monomeric form, led us to investigate whether recovery of proteolytic activity via the VDAC peptides is associated with restoration of trimer formation.

In order to assess the oligomeric state of wildtype HTRA1 and the disease-relevant mutants glutaraldehyde crosslinking experiments were performed. In the course of the experiment 0.5 µM HTRA1 were incubated with 50 µM VDAC2 peptide, which had

shown the most prominent effect on proteolytic activity in the previous experiments, at 350 rpm, 37 °C for 30 minutes prior to the crosslinking reaction. Following the application of glutaraldehyde the reaction was stopped via addition of 75 mM TRIS. Crosslinked complexes were subsequently separated via SDS-PAGE and visualized by silver staining.

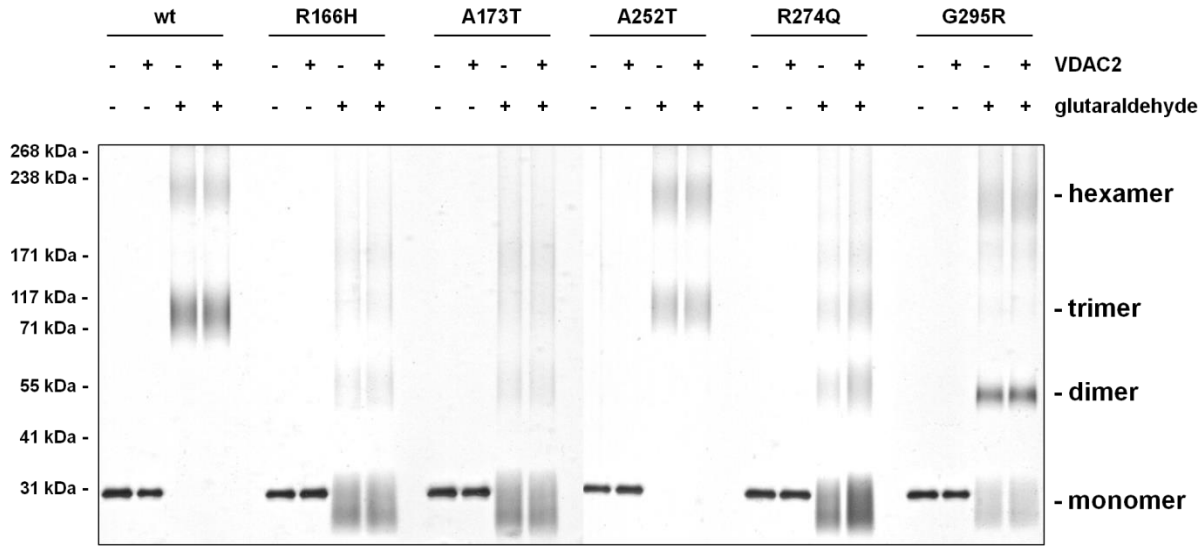

Figure 4.30 Oligomeric states of wildtype HTRA1 and CARASIL-relevant mutants analyzed via glutaraldehyde crosslinking in presence of VDAC2
The effects of VDAC2 on the oligomeric states of CARASIL-relevant HTRA1 mutants were investigated via glutaraldehyde crosslinking experiments. 0.5 µM HTRA1 were incubated with 50 µM VDAC2 at 37 °C for 5 minutes prior to crosslinking with 0.5 % glutaraldehyde. The reaction was stopped via addition of 75 mM TRIS. Crosslinked complexes were separated via SDS-PAGE and visualized via silver staining. VDAC2 displayed no effects on the oligomeric states of the tested HTRA1 constructs.

As described previously (see section 4.2.3) both wildtype HTRA1 and HTRA1$_{A252T}$ migrated predominantly as a trimeric band, whereas for HTRA1$_{R166H}$, HTRA1$_{A173T}$ and HTRA1$_{R274Q}$ the monomeric state prevailed and HTRA1$_{G295R}$ displayed a compact band migrating on dimer level. Remarkably, addition of the VDAC2 peptide did not affect the migration pattern of any of the tested proteins (figure 4.30) indicating that the restoration of proteolytic activity induced by the peptide is not accompanied by a transition to higher oligomeric forms.

Reportedly the trimer is the smallest functional unit for HTRA1 to exert its proteolytic activity. However, as shown previously by Truebestein *et al.* (2011) higher oligomeric forms have been observed in the presence of unfolded substrate. To determine whether substrate induced oligomer conversion plays a role in HTRA1 activation via

the VDAC2 peptide crosslinking experiments were performed in presence of both the VDAC2 peptide and the intrinsically unfolded substrate Tau.

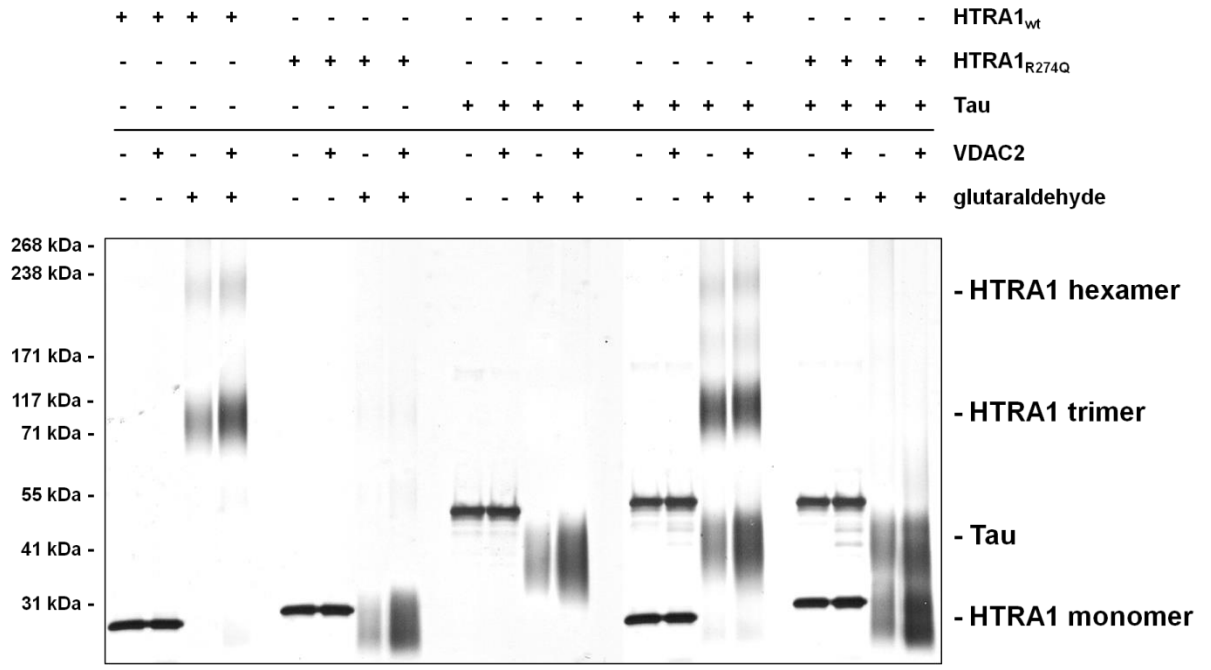

Figure 4.31 Oligomeric states of wildtype HTRA1 and HTRA1$_{R274Q}$ analyzed via glutaraldehyde crosslinking in presence of its native substrate Tau and the peptide VDAC2
The effects of VDAC2 on the oligomeric states of CARASIL-relevant HTRA1 mutants were investigated via glutaraldehyde crosslinking experiments in presence of the native HTRA1-substrate Tau. 0.5 µM HTRA1 were incubated with 50 µM VDAC2 and 0.5 µM Tau at 37 °C prior to crosslinking with 0.5 % glutaraldehyde. The reaction was stopped via addition of 75 mM TRIS. Crosslinked complexes were separated via SDS-PAGE and visualized via silver staining. Higher oligomeric species could be observed neither in the presence of Tau, nor upon application of VDAC2.

Figure 4.31 shows the migration pattern of wildtype HTRA1 and HTRA1$_{R274Q}$ upon preincubation with VDAC2 and the native substrate Tau and subsequent glutaraldehyde crosslinking. When incubated alone both enzymes displayed a migration pattern similar to that described in the previous experiment with wildtype HTRA1 migrating predominantly as a trimer and HTRA1$_{R274Q}$ migrating primarily as a monomer. Tau displayed a monomeric band at approximately 50 kDa. However, a conversion of HTRA1 to higher oligomeric species could be observed neither in the presence of Tau, nor upon application of the VDAC2 peptide, nor via a combination of the two.

In order to further investigate the effects of the VDAC2 peptide on trimer stability and verify the results obtained from crosslinking assays NMR DOSY experiments were

performed [8]. Since HTRA1$_{R274Q}$ displayed the most profound defect in oligomerization and proteolytic activity it was chosen as a model enzyme to investigate the effects of the VDAC2 peptide on trimer stability.

As described in section 4.2.4 spectra were recorded for both wildtype HTRA1 and HTRA1$_{R274Q}$ at different concentrations (10-100 µM). An additional 1D-spectrum was recorded for the VDAC2 peptide in the absence and presence of HTRA1 in order to determine, whether signals generated by the peptide overlap with those derived from the protein and assess the impact of peptide derived signals on the overall sensitivity of the experiment.

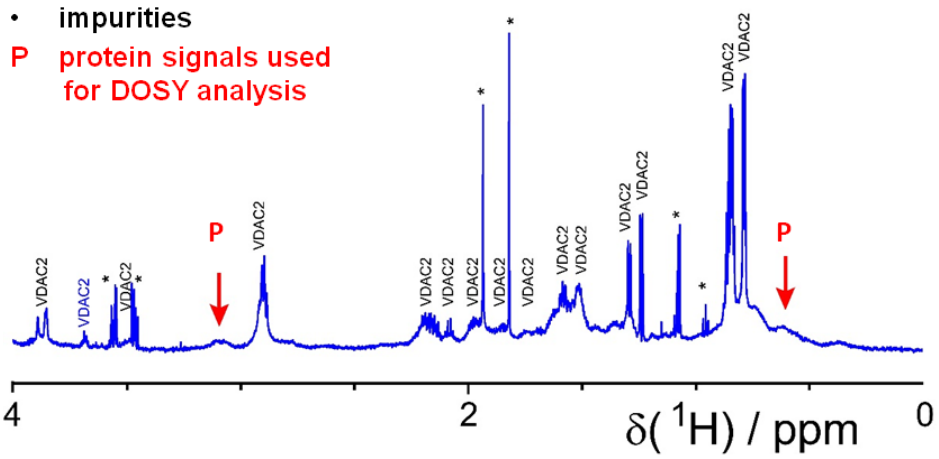

Figure 4.32 1D-^{1}H-spectrum for HTRA1protSA$_{R274Q}$ and VDAC2
An 1D-^{1}H-spectrum was recorded for 25 µM HTRA1prot$_{R274Q}$ in presence of 50 µM VDAC2. Shown are the signal intensities recorded at 4-0 ppm. The red Ps indicate the protein signals used for analysis of the DOSY data and * mark impurities present in the peptide preparation.

As shown in figure 4.32 there is a considerable overlap of the signals derived from the peptide and the enzyme. Furthermore, the sensitivity of the experiment appeared limited due to the high intensity of the peptide-derived signals compared to those generated by the protein. Thus only two HTRA1-derived signal peaks recorded at 3.2 ppm and 0.7 ppm, respectively, were considered for DOSY experiments.

[8] NMR DOSY experiments were performed in collaboration with Dr. Christine Beuck, Hendrik Kirschner and Prof. Peter Beyer, Department of Structural and Medical Biochemistry, University of Duisburg-Essen.

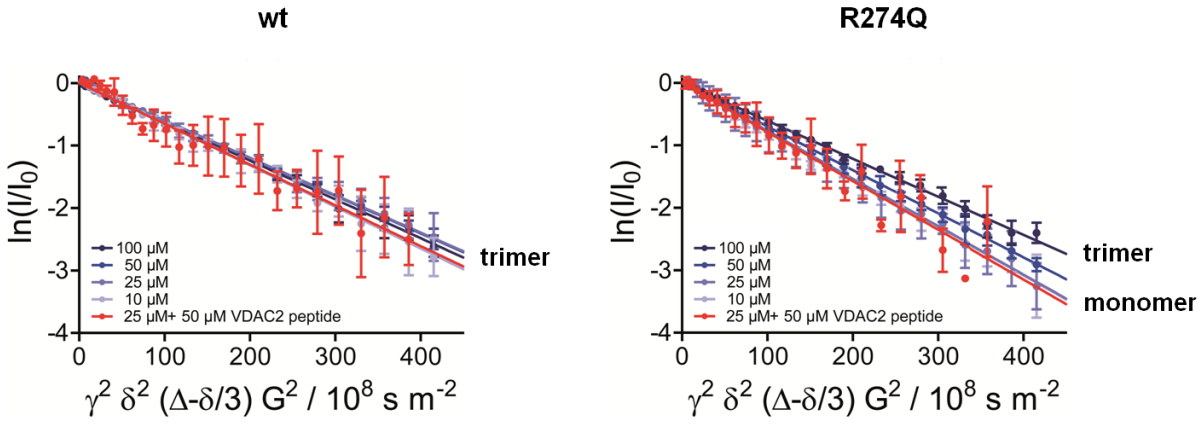

Figure 4.33 Concentration dependence of oligomeric states in the absence and presence of VDAC2 analyzed via NMR DOSY experiments
The Stejskal-Tanner plots display the integrated signals of the protein peaks (y-axis) as a function of gradient strength (x-axis) with the slope corresponding to the protein's diffusion coefficient. The left panel shows the diffusion coefficients for HTRA1protSA wildtype. The right panel displays the diffusion coefficients for HTRA1protSA$_{R274Q}$. Signals were recorded at 0.7 ppm and 3.2 ppm. Signal intensities acquired in the absence of compound are shown in blue, those observed in the presence of 50 µM VDAC2 are highlighted in red. Error bars indicate the standard error of the mean. No shifts were observed upon addition of VDAC2.

Figure 4.33 shows the normalized signal intensities of the protein peaks as a function of gradient strength (Stejskal-Tanner plot) with the slope corresponding to the protein's diffusion coefficient. As depicted in section 4.2.4 HTRA1$_{R274Q}$ displayed a concentration-dependent distribution of diffusion coefficients indicating a shift of the monomer-trimer equilibrium towards the monomeric form at lower protein concentrations. In contrast, no concentration dependent changes in the diffusion coefficient were detected for the wildtype enzyme suggesting that it exists as a stable trimer. In accordance with the results obtained from crosslinking experiments addition of 50 µM VDAC2 to 25 µM wildtype HTRA1 or HTRA1$_{R274Q}$ respectively did not render significant effects on the diffusion coefficient confirming that the peptide enhances the proteolytic activity of HTRA1 via a novel mechanism, that does not involve a transition to higher oligomeric species.

4.4.5 Derivatisation of the VDAC2 peptide

In order to gain deeper insight into the activation mechanism associated with VDAC2-binding and assess the functional significance of its individual residues a spotted

peptide array was performed [9]. Sequences analyzed in this screen were derived from the original VDAC2 peptide except for single amino acid substitutions replacing each of its 10 residues by one of the 20 residues belonging to the spectrum of canonical amino acids. Peptides were spotted onto a nitrocellulose membrane using the inverted peptide method. Following incubation with proteolytically inactive HTRA1SA the enzyme's binding was visualized via immunodetection utilizing an Alexa633-coupled antibody and binding affinities were evaluated based on the fluorescence intensities recorded for each peptide sequence (figure 4.34).

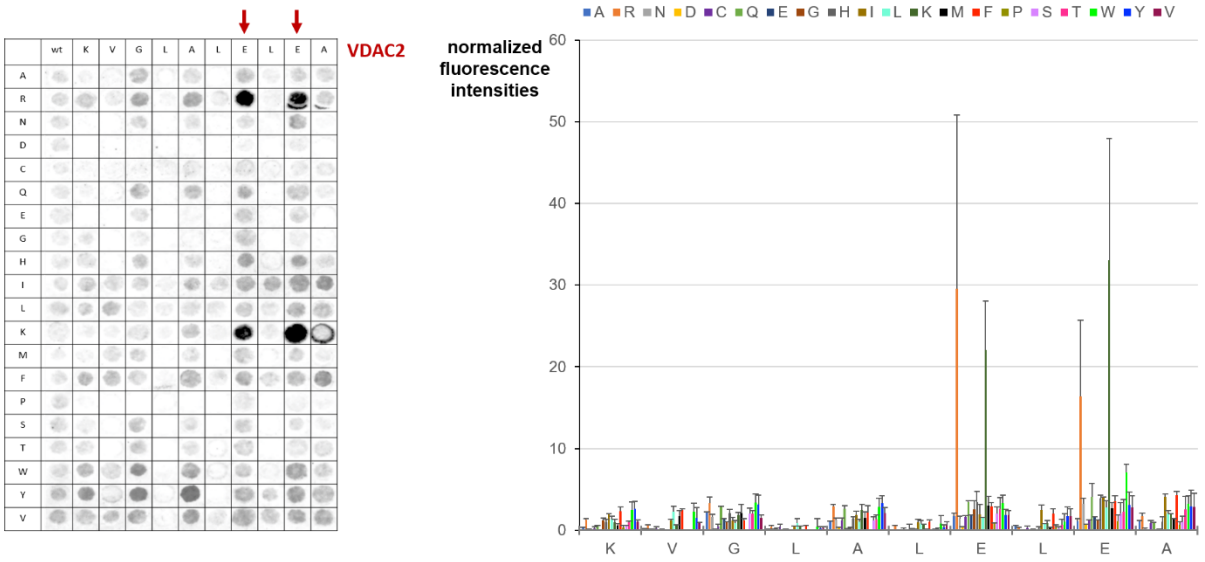

Figure 4.34 Assessment of the functional significance of individual residues in VDAC2 for HTRA1 binding
The functional significance of individual residues in VDAC2 for HTRA1 binding was assessed via a spotted peptide array (left panel). Each residue of the original VDAC2 peptide (upper row) was exchanged for one of the 20 canonical amino acids (left column). Sequences were spotted onto a nitrocellulose membrane and HTRA1 binding was viualized via immunodetection. The right panel shows the normalized fluorescence intensities (y-axis) recorded for each peptide sequence. Amino acid substitutions are colour-coded and depicted on the x-axis.

Plotting of the normalized fluorescence intensities revealed a strong preference for the positively charged residues arginine and lysine at position -1 and -3, respectively, followed by the aromatic amino acids tryptophane and phenylalanine. Based on this finding affinity-optimized derivatives were designed, whose effects were subsequently compared to those of the original peptide via Tau degradation assays. In the first derivative (VDAC2.1) the negatively charged glutamate at position -1 was substituted

[9] Peptide arrays were performed by Dr. Jasmin Schillinger, Institute of Microbiology II, University of Duisburg-Essen.

for a positively charged lysine, whereas that at position -3 was exchanged for an aromatic phenylalanine thus considering preferences for both positive charge and aromatic structure. Remarkably, this first derivative displayed considerable sequence similarity to the peptidic DPMFKLboroV inhibitor, which was utilized by Truebestein *et al.* (2011) to solve the structure of the active HTRA1 trimer. The inhibitor binds to the active site serine via its C-terminal boronic acid group forming a tetrahedral boronate complex and trapping the enzyme in its active state. Notably, the inhibitor itself was found to stabilize the active conformation via hydrophobic interactions between its leucine and phenylalanine residues with the L3 residues leucine 307, leucine 309 and tyrosine 316. In accordance with these structural features a second derivative (VDAC2.2) was designed, which was further optimized for binding and stabilizing the active site. In this derivative the aromatic amino acids tryptophane and tyrosine were placed in position -3 and -5 respectively thus allowing for additional ringstacking interactions. Furthermore, the C-terminal alanine residue was exchanged for valine due to the finding, that the valine residue of the boronic acid inhibitor was found to be deeply buried in the enzyme's S1 specificity pocket in the active ligand bound structure. Additionally, truncated versions of both derivatives lacking the four N-terminal amino acids (VDAC2.3 and VDAC2.4) were included in the experiment in order to investigate the N-terminal residues' impact on HTRA1 activation and possibly reduce the peptides' potential for unspecific interactions with other proteins.

To investigate the derivatives' effects on proteolytic activity Tau degradation assays were carried out for both wildtype HTRA1 and the CARASIL-relevant mutant $HTRA1_{R274Q}$. The peptides were added in equimolar amounts and preincubated with the enzyme for 30 minutes prior to the reaction. The original VDAC2 C-terminal peptide was used as a control.

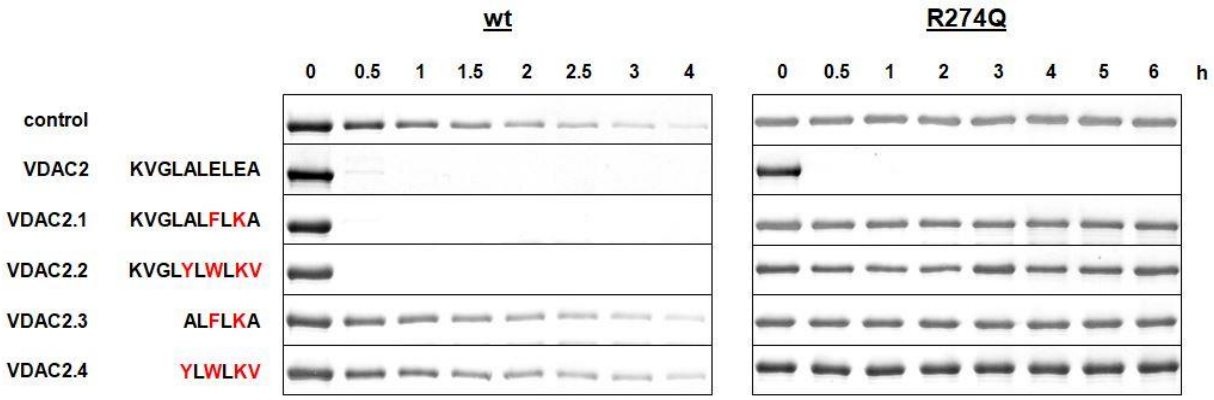

Figure 4.35 Tau degradation by wildtype HTRA1 and HTRA1$_{R274Q}$ in the presence of VDAC2 derivatives
Time dependent degradation of Tau was followed on SDS-PAGE. Following preincubation with 50 µM of the respective peptides 1 µM wildtype HTRA1 or HTRA1$_{R274Q}$ were incubated with 8 µM Tau in 50 mM TRIS pH 8 at 37 °C for 4 or 6 hours respectively. Samples were taken at indicated time points and subjected to SDS-PAGE followed by Coomassie Brilliant Blue staining. Peptides VDAC2.1 and VDAC2.2 significantly increased proteolytic activity of the wildtype enzyme, but not HTRA1$_{R274Q}$.

On wildtype HTRA1 both derivatives optimized for active site binding (VDAC2.1 and VDAC2.2) induced a distinct increase in proteolytic activity comparable to that observed for the original peptide, whereas activation of the monomeric mutant was abolished entirely. In contrast the N-terminally truncated variants (VDAC2.3 and VDAC2.4) did not show an effect on either enzyme (figure 4.35). These findings demonstrate that the N-terminal residues are indispensable for activity modulation. Furthermore, both wildtype HTRA1 and the monomeric R274Q mutant responded to peptide application in a distinct manner suggesting that the peptides modulate proteolytic activity via different mechanisms possibly addressing different binding sites.

4.5 Crystal structure of HTRA1$_{D174R/R274Q}$

In contrast to the previous chemical approaches, which utilized the effects of either supramolecular or small peptidic ligands to restore proteolytic activity in disease-relevant HTRA1 mutants, an additional strategy established by the group of Martin Dichgans (Institute for Stroke and Dementia Research, University Clinic Munich, unpublished) exploits the biological concept of compensatory mutations. The idea behind this approach is to achieve oligomer restoration via the introduction of compensatory amino acid substitutions within the opposite monomer interface. In a

screen of candidate mutations for their ability to functionally reconstitute the R274Q mutation coexpression of the disease-relevant interface mutant with HTRA1$_{D174R}$ was shown to restore both trimer formation and proteolytic activity. However, the mutation's effects were found to be strictly allele-specific, as functional restoration did not extend to any of the other HTRA1 interface-mutations investigated.

In order to determine the precise effects underlying the allele specific oligomer reconstitution a crystal structure of HTRA1 carrying both the disease causing and the compensatory mutation was established. In the experimental set-up an N-terminally shortened, inactive HTRA1-construct (residues 161-375), that was found to abolish the need for methylation prior to crystallization (Eigenbrot *et al.* 2012), was cloned into a pET28a-vector and purified from *E. coli*. The following crystallography studies were conducted by the group of Ingrid Vetter, Max-Planck Institute, Dortmund.

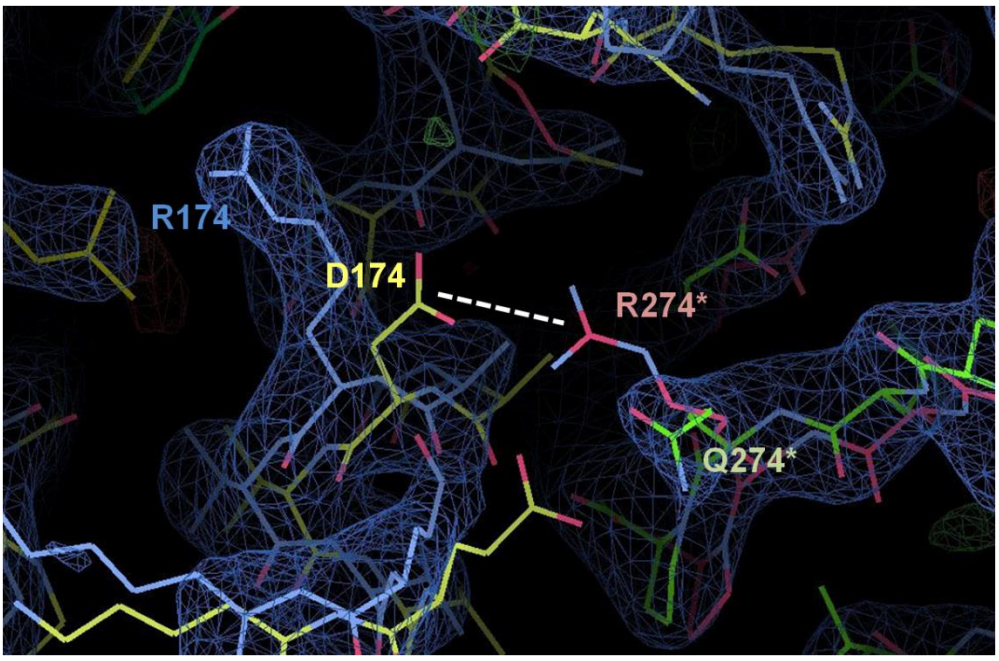

Figure 4.36 Structural overlay of HTRA1wt and HTRA1$_{D174R/R274Q}$
The amino acid sequence of HTRA1$_{D174R/R274Q}$ was fitted into the electron density map. The structure of the first HTRA1$_{D174R/R274Q}$ protomer is shown in blue and that of the neighbouring protomer* is shown in green. The structure of the wildtype protein (Truebestein *et al.* 2011) is displayed in yellow and red*. The inter-protomer salt bridge formed in the wildtype protein is presented as a dashed line.

The electron density map derived from the X-ray spectrum of the HTRA1$_{D174R/R274Q}$ crystal renders a symmetric trimeric structure that displays high similarity to that of the wildtype HTRA1 protease domain solved by Truebestein *et al.* (2011). A comparison of the HTRA1$_{D174R/R274Q}$ crystal structure to that of the wildtype protein, in which

aspartate 174 forms a stable salt bridge with arginine 274*, shows that in the mutant construct the arginine 174 residue is distant from glutamine 274* (figure 4.36) suggesting that the compensatory effect is not based on a direct interaction of the two mutated residues. Furthermore, the R174 residue is twisted away from the interaction surface thus excluding a direct interaction with the neighbouring protomer.

Table 4.1 Interaction surface areas in $HTRA1_{wt}$, $HTRA1_{R274Q}$ and $HTRA1_{D174R/R274Q}$
Interaction surfaces were calculated via the PISA (**P**roteins, **I**nterfaces, **S**tructures and **A**ssemblies) analysis software and averaged over all six interaction areas within the trimer. The calculation for the wildtype enzyme is based on the PDB-structure 3NWU and that of $HTRA1_{R274Q}$ on a model derived from the wildtype structure or that of $HTRA1_{D174R/R274Q}$, respectively.

Protein	**Interaction surface in Å²**
wildtype	970.8
R274Q (model derived from the wildtype structure)	943.3
R274Q (model derived from the structure of $HTRA1_{D174R/R274Q}$)	958.6
D174R/R274Q	975.3

Instead, calculating the interaction surface for each structure (table 4.1) reveals that the loss of the intermolecular salt bridge is compensated by a distinct increase in the contact area between the individual protomers. This increase in the interaction area might be the basis underlying the observed restoration of trimer formation and hence the recovery of proteolytic activity. Yet, the exact mechanisms underlying the allele specificity of the compensatory mutation remain to be determined.

5 Discussion

5.1 Implications of CARASIL-relevant point mutations within the trimer interface on the oligomeric state and activity of HTRA1

Cerebral Autosomal Recessive Arteriopathy with Subcortical Infarcts and Leucoencephalopathy (CARASIL) is a rare, hereditary disorder affecting the small vessels of the brain that is associated with loss of function mutations in the *HTRA1* locus (see section 1.2.4). In most cases the loss of function phenotype is caused by mutations that either immediately affect the proper positioning of the active site (e.g. $HTRA1_{A252T}$) or induce premature stop codons resulting in mRNA decay (e.g. $HTRA1_{R370X}$) or severe truncations of the resulting protein ($HTRA1_{R302X}$) (Hara *et al.* 2009). However, a small subset of clinically relevant mutations was found within the protomer interface indicating a potential effect on trimer stability.

To gain deeper insights into the functional implications of the interface mutations HTRA1 constructs carrying the respective amino acid substitutions were purified from *E. coli* and subjected to biochemical characterization. Measuring the mutants' proteolytic activities against a panel of substrates revealed significant defects in substrate processing confirming that a loss of proteolytic activity can be associated with mutations which are not located in the immediate vicinity of the activation domain (see section 4.2.2). The most profound effect was observed for $HTRA1_{G295R}$, which showed a complete loss of proteolytic activity against a large panel of substrates, followed by $HTRA1_{R274Q}$. The mildest effect was ascertained for $HTRA1_{A173T}$, which even displayed a slight increase in proteolytic activity compared to the wildtype enzyme in Tau degradation assays. Presumably these substrate-dependent differences in residual activity can be attributed to the mutants' different affinities towards individual substrates.

Crosslinking experiments revealed that the loss of proteolytic activity was associated with trimer assembly defects (see section 4.2.3). Whereas both the wildtype enzyme and a control construct carrying the A252T mutation, which is located in close proximity to the active site residue aspartate 250 thus presumably affecting the proper

positioning of the catalytic triad, retained their trimeric conformation, all characterized interface mutants displayed defects in trimer formation. Comparison of the detected bands to a protein standard revealed that HTRA1$_{R166H}$, HTRA1$_{A173T}$ and HTRA1$_{R274Q}$ existed predominantly as monomers, while HTRA1$_{G295R}$ migrated as a compact dimer band. Mapping of the G295R mutation onto the HTRA1 structure and molecular dynamics simulations [10] showed that the positively charged arginine residue is directed towards the inner cavity of the trimer, where it establishes an intra-monomer salt bridge with the negatively charged aspartate 320 thus disrupting its interaction with threonine 293* and threonine 294* on the other side of the protomer interface. However, the analysis of band patterns derived from crosslinking experiments revealed, that besides the predominant oligomeric species both wildtype HTRA1 and constructs carrying CARASIL-relevant mutations display numerous additional bands of varying intensity representing minor oligomeric forms. These findings demonstrate that each mutant exists at an equilibrium between different oligomeric species, rather than a single oligomeric state. This notion could be further substantiated via NMR DOSY experiments (see section 4.2.4), which also revealed a concentration-dependent shift of the equilibrium. Whereas at 100 µM the mutants' diffusion coefficients were comparable to that of the wildtype protein indicating a trimeric conformation, lower concentrations were associated with a distinct shift towards the monomeric form. This concentration dependent switch was most profound for HTRA1$_{R274Q}$ with a complete shift towards the monomeric form occuring already at 25 µM, while for HTRA$_{R166H}$ and HTRA1$_{A173T}$ concentrations as low as 10 µM were required to observe a comparably high diffusion coefficient. Further analysis via circular dichroism melting curves, which display the thermal unfolding of proteins as a function of temperature, demonstrated that the R274Q mutation also renders the most profound effect on thermal stability of the trimer. Taken together these findings strongly suggest that the R274Q mutation displays a particularly strong effect on trimer stability. Remarkably, the R274Q mutant also displayed the most profound effect on proteolytic activity among the monomer-forming mutants, when subjected to β-casein degradation assays. Thus the mutants' loss of proteolytic activity appears to be negatively correlated to residual trimer stability

[10] Computer-based structural analyses were conducted Dr. Kenny Bravo-Rodriguez, Department of Microbiology II, University of Duisburg-Essen.

indicating that trimer destabilization is indeed the causative factor for the loss of function phenotype.

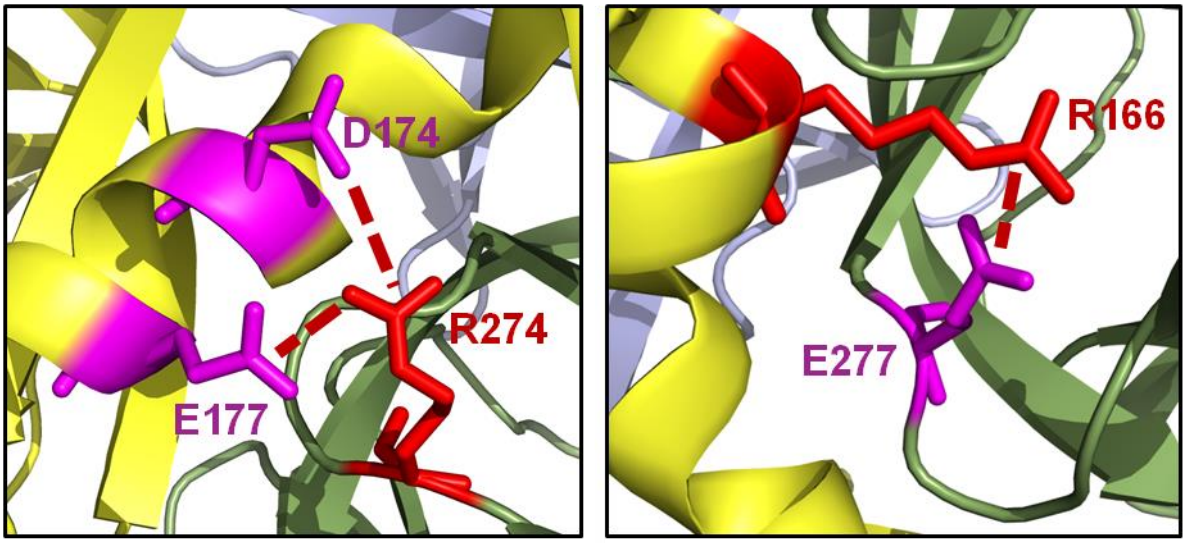

Figure 5.1 Inter-protomer salt bridges in HTRA1
Left panel: Close-up showing the interaction of arginine 274 (red) with aspartate 174 and glutamate 177 (magenta). Right panel: Close-up showing the interaction of arginine 166 (red) with glutamate 277 (magenta). The representations are based on the structure of the HTRA1 trimer solved by Truebestein *et al.*, 2011 (PDB Code: 3NWU).

Notably, these experimental results are in line with evidence gained from computational analyses. Mapping of the CARASIL-relevant interface mutations onto the HTRA1 structure shows that arginine 274 engages in the formation of salt bridges with both aspartate 174* and glutamate 177* on the opposing protomer interface (figure 5.1). Thus the R274Q mutation would result in the simultaneous loss of two trimer-stabilizing interactions. Furthermore, the mutation is located in close proximity to phenylalanine 278, which contributes to the hydrophobic cluster at the far tip of the trimer, and might thus interfere with the conserved ringstacking interactions that are essential for trimer stability. In contrast arginine 166 is only required for the formation of a single salt bridge formed with glutamate 277* of the adjacent protomer. Molecular dynamics simulations suggest, that upon loss of this salt bridge due to substitution of arginine 166 by histidine arginine 274* would undergo a distict shift translocating it to the vicinity of glutamate 227*. This rearrangement would cause the formation of an intra-monomer salt bridge, that competes with the inter-monomer salt bridge formed between arginine 274* and aspartate 174 or glutamate 177 under native conditions. However, histidine might be able to partially replace arginine 166 in its interaction with glutamate 277* thereby annihilating this effect to some extent. Mapping of the A173T

mutation reveals its location in close proximity to tyrosine 169 and phenylalanine 177, which together with phenylalanine 278 constitute the conserved, hydrophobic cluster that is essential for HTRA1 trimer stability. Although molecular dynamics simulations predict only a minor impact on this interaction network, even slight shifts within the α-helical segment containing alanine 173 might suffice to cause perturbations in this essential interaction. In accordance with these observations ΔΔG values derived from free energy perturbation calculations were significantly higher for $HTRA1_{R274Q}$ than for the other monomeric interface mutants indicating that destabilization of the trimer is most profound in this particular mutant.

Since the first cases of CARASIL were reported in individuals from consanguineous families, whose parents appeared unaffected, the disease was initially believed to follow a strictly recessive inheritance pattern (see section 1.2.4). Yet, three of the interface mutations (R166L, A173T and G295R) investigated in this study were reported to be symptomatic in both homo- and heterozygously affected individuals (Mendioroz *et al.* 2010; Menezes Cordeiro *et al.* 2015; Khaleeli *et al.* 2015; Verdura *et al.* 2015). A similar finding was also obtained for the mutation of glutamate 277, which engages in the inter-protomer salt bridge with arginine 166, to valine (Preethish-Kumar *et al.* 2017). Whereas homozygously affected patients displayed the classical symptoms of CARASIL, heterozygous mutation carriers presented with a weaker late-onset phenotype lacking the characteristic extraneuronal manifestations of the disease. Thus far it remains unknown whether the occurrence of a mild, late-onset phenotype in heterozygously affected individuals is a common feature in CARASIL pathogenesis or whether it is restricted to a certain subset of mutations causing the mutant allele to interfere with the physiological function of the remaining wildtype allele. However, for the interface mutants such an interference would be very likely, since interaction of the mutated protomer with the wildtype protein might hinder its efficient assembly into catalytically competent trimers. As trimer formation is essential for the initiation of the conserved HTRA activation cascade (L3 → LD* → L1*/L2*) and thus for the functional set-up of the active site (see section 1.1.3), such a disturbance would dramatically interfere with the enzyme's activity. Similar dominant negative effects that are restricted to mutations located within a protomer interface have already been described for other diseases. For example in Autosomal Recessive Osteopetrosis, which is caused by mutations in the trimeric receptor activator of nuclear factor-κB

ligand (RANKL), mutants carrying the interface-mutation G275R were shown to interact with wildtype RANKL thereby exerting a dominant-negative effect on its trimerization (Douni *et al.* 2012).

Notably, the mutations S284R, P285L and F286V, which Verdura *et al.* (2015) reported to cause a CARASIL-like syndrome in heterozygous carriers similar to the interface mutants (see section 1.2.4), are located within loop LD, which receives the activation signal from the sensor loop L3 of the neighbouring protomer. Thus both types of mutations presumably prevent signal relay across the protomer-protomer gap thereby interfering with the conserved activation cascade. This striking similarity might point towards a common pathologic mechanism underlying the dominant-negative phenotype shared by both the interface and the LD-loop mutants.

Remarkably, the observation that the interface mutants' loss of activity and hence the corresponding loss of function phenotype can be attributed to impaired oligomer assembly renders a potential route for functional restoration. Thus far therapeutic strategies in the treatment of CARASIL have been merely palliative focusing on the alleviation of symptoms, rather than causative approaches. Among the suggested therapeutic options there is the administration of TGF-β receptor blockers as is already common practice in the treatment of Marfan syndrome (Brooke *et al.* 2008). However, the exact implications of HTRA1 activity in the TGF-β pathway remain a matter of controversy and recent findings strongly suggest that pathologic inhibition of TGF-β signalling, rather than its upregulation is the key process driving disease progression (Beaufort *et al.* 2014). An additional, strictly allele specific approach focuses on the functional restoration of $HTRA1_{R370X}$, whose expression is dramatically reduced due to nonsense-mediated mRNA-decay, via compounds that suppress translation termination at in-frame premature termination codons (Zhou *et al.* 2013). This approach might be especially promising, since on the protein level the R370X truncation displays no significant effect on proteolytic activity (Shiga *et al.* 2011). However, no such approaches exist for any of the other CARASIL-relevant HTRA1 mutations highlighting the fundamental need for additional therapeutic options.

The fact that oligomer assembly in HTRA1 is a dynamic process might render the interface-mutants accessible to therapeutic intervention. Furthermore, investigating

the functional restoration of HTRA1 interface-mutants might not only yield potential treatment options for patients carrying CARASIL-relevant mutations located within the protomer-interface, but also serve as a proof of principle study to develop general concepts for the restoration of proteins displaying defects in oligomerization.

5.2 Restoration of trimer assembly via supramolecular clamp compounds

A first strategy to achieve a functional restoration of CARASIL-relevant interface mutants focuses on the stabilization of inter-protomer contacts via supramolecular clamp compounds. The idea behind this approach is to compensate the loss of intrinsic affinity via additional ionic interactions thereby bridging the inter-protomer gap and shifting the monomer-trimer equilibrium back towards the trimeric state.

The chemical modulation of protein-protein interactions has become a field of growing interest during the recent years. Yet, most approaches aim at the inhibition of inter-subunit contacts (Wilson 2009; Jubb *et al.* 2015), whereas studies investigating their stabilization are scarce. The supramolecular clamps used in this study are flexible conjunction modules carrying positively charged guanidinio carbonyle pyrrole (GCP) units on either end. The GCP motive is a synthetic arginine analogue designed to recognize and bind oxyanions via extensive complementary ionic interactions and hydrogen bonds (Jiang *et al.* 2013) thus making it an optimal candidate for binding to the anionic hotspots located on either side of the protomer-protomer interface.

An essential prerequisite for the functional restoration of the HTRA1 interface-mutants is that the applied ligands do not interfere with the enzyme's proteolytic activity. Thus in order to assess the clamp compounds' potential to restore trimer formation we chose to screen for activity restoration, rather than retrimerization, since this indirect approach would exclude ligands impairing enzymatic activity *ab initio*. Indeed, the GCP-clamps induced a substantial increase in the interface-mutants' proteolytic activities (see section 4.3.1). In line with our model, the wildtype enzyme remained unaffected and activity restoration was independent of the PDZ domain demonstrating

that the ligands' effects are indeed restricted to stabilizing protomer-protomer interactions. Remarkably, this approach was not allele specific, but extended to the full spectrum of monomer-forming HTRA1 mutants investigated in this study. However, the technique was not applicable to $HTRA1_{G295R}$, which was shown to assemble into dimers in previous glutaraldehyde crosslinking assays. This might be due to the circumstance, that the dimer forms a compact structure, which is not accessible to the supramolecular clamps. Furthermore, assaying the proteolytic activity of an HTRA1 construct carrying the A252T mutation, which is located in direct proximity to histidine 250, revealed a decrease in proteolytic activity upon application of the compounds. This might be due to a mutation-induced conformational shift rendering the catalytic residues more accessible thus increasing their susceptibility to external influences. Yet the exact mechanism underlying this effect requires further investigation.

In line with the restoration of proteolytic activity, the comparative assessment of diffusion coefficients from NMR DOSY experiments revealed a significant shift towards the trimeric form upon compound application (see section 4.3.2). This finding clearly demonstrates that the ligand's effects on the interface-mutants' proteolytic activities can indeed be ascribed to a restoration of their trimeric conformation.

Variations in linker length via incorporation of an additional glycine residue rendered no significant effects on the clamp compounds' activating properties. This finding indicates that the ligands are either able to address different binding sites across the protomer-protomer interface or that their inherent flexibility enables them to adapt various conformations allowing them to adjust to variable binding positions. Yet, a greater variety of different linker lengths needs to be studied in order to properly address this question.

Furthermore, comparison of the molecular clamps against a panel of other ligands carrying positively charged head-groups revealed that the GCP unit is essential for the functional restoration of proteolytic activity. Strikingly, compounds displaying the same molecular scaffold as the molecular clamps except for a substitution of the GCP moiety for the proteinogenic amino acids histidine, arginine and lysine were significantly less effective. This finding indicates that compared to the native amino acids the GCP motive is superior in the binding of anionic surfaces thus enabling it to significantly

improve the stabilizing effect of the molecular clamps. A similar effect has previously been observed in the development of peptidic inhibitors of β-tryptase, which bind to the anionic hotspots surrounding the enzyme's central pore thereby blocking substrate entrance to the active site. In this study ligands carrying the artificial GCP group at their termini appeared approximately two orders of magnitude more potent than those containing a positively charged proteinogenic residue at the same position (Jiang *et al.* 2013).

However, the compound concentrations required to achieve a restoration of trimerization and proteolytic activity are far beyond the physiologically feasible concentration range indicating a need for further improvement. Despite its superior anion-binding properties compared to the positively charged proteinogenic amino acids the affinity of a single GCP moiety towards an anionic protein surface is still low compared to conventional small molecule ligands. Thus further approaches should aim to address additional binding sites across the protomer-protomer interface via multi-armed ligands in order to achieve an increase in total binding affinity. Multivalent interactions, which are based on numerous simultaneous molecular binding events, can be exploited to systematically increase the overall affinity of an interaction network even when individual contacts are relatively weak. Whereas the on-rate of multivalent compounds does usually not differ from a monovalent one, their release from the protein surface (off-rate) is remarkably slow thus causing a considerable increase in binding affinities. Previous studies have shown that this multivalency approach can render a massive increase in overall ligand affinity (Maric *et al.* 2014; Choi and Jung 2018; Park 2014; Liese and Netz 2018). Besides the development of multi-armed ligands comprising numerous GCP units at their termini, an additional approach to achieve an increase in affinity would be the attachment of a highly affine PDZ-binding peptide via a flexible linker thereby incorporating different types of molecular recognition processes into a single molecule.

Taken together the above findings indicate that despite requiring further improvement the chemical modulation of protein-protein interactions is a promising approach for the functional restoration HTRA1 interface mutants. This strategy might be of particular interest due to its wide applicability to a variety of biological objectives involving

defective interactions between different subunits within a molecular interaction network.

5.3 Enhancement of proteolytic activity via C-terminal peptides derived from VDAC2 and 3

5.3.1 VDAC-induced activity enhancement proceeds independent of both the PDZ domain and inter-protomer communication

As described in the introductory section the proteolytic activity of HtrA family members is tightly regulated and depends on the elaborate interplay of both activating and inhibitory stimuli (see section 1.1). In line with this notion HTRA1 activity is modulated by a variety of processes including induced-fit substrate-binding, allosteric mechanisms triggered by peptidic modulators and presumably conversion to higher-order oligomers (Truebestein *et al.* 2011). Whereas nature uses these refined regulatory features as an efficient means to prevent uncontrolled, eventually deleterious proteolysis, they might also be utilized to artificially manipulate the enzyme's proteolytic function. This notion raises the possibility to exploit the activating features of regulatory peptide sequences to enhance the proteolytic activity of disease-relevant HTRA1 mutants in an allosteric fashion.

In order to identify potential activators of the CARASIL-relevant interface mutants a selection of activating peptides chosen from our laboratory portfolio containing C-terminal sequences from various proteins and their derivatives were studied regarding their effects on wildtype HTRA1 as well as the interface mutant HTRA1$_{R274Q}$. Among the tested peptides there were both sequences exerting their effects via the PDZ domain and those acting in a PDZ-independent manner. In the course of the experiment, peptides derived from the C-termini of both VDAC2 and VDAC3 were not only able to enhance the proteolytic activity of the wildtype enzyme, but also that of the monomeric mutant HTRA1$_{R274Q}$. In line with this finding the other monomer-forming CARASIL-mutants HTRA1$_{R166H}$ and HTRA1$_{A173T}$ were activated in a similar fashion showing that the effect is not allele-specific (see section 4.4.1). Remarkably, proteolytic

activities determined in presence of the peptides significantly exceeded the basal activity of the wildtype enzyme. The observed effects were most profound for the VDAC2 peptide, which was thus chosen for further investigation. Additional experiments revealed that the peptide's effects are not restricted to *in vitro* substrates, but extend to the CARASIL-relevant substrate latent TGF-β binding protein-1 (LTBP-1), as was shown is cell culture-based assays[11]. Since recent reports demonstrate that a lack of LTBP-1 processing by HTRA1 and the resulting downregulation of TGF-β bioavailability might be the critical event driving CARASIL-associated vascular pathology, these findings highlight not only the *in vivo* relevance of the observed effects, but also point to the peptide's potential to modulate disease progression. Taken together, these findings highlight the VDAC peptides' ability to functionally restore proteolytic activity in the monomer-forming CARASIL-mutants in a physiologically relevant manner.

In contrast, for peptides acting in a PDZ-dependent fashion the activating effect was restricted to the wildtype protein, whereas the monomeric mutants remained unaffected. This finding is in line with previous reports, which revealed that PDZ-dependent activation of HTRA1 requires inter-protomer communication. In the course of this process, the activation signal is passed from the PDZ domain to the sensor loop L3, which then interacts with the activation loop LD* of the adjacent subunit thereby initiating the rearrangement of the active site loops into the catalytically competent conformation. Notably, mutations of the L3 loop residues that are involved in signal relay consistently abolished the effects of PDZ-dependent activators (Rey 2018). This effect is in striking similarity to the interface mutations, since both interfere with the inter-protomer communication process triggered by peptide-binding to the PDZ domain.

Consistent with this finding VDAC2-driven activity enhancement was found to occur also in the absence of the PDZ domain (see section 4.4.1) indicating that its binding to the proteolytic domain is the event that triggers the activation process. However, the peptide did not render an activating effect on the closely related serine proteases

[11] Assays were conducted by Nathalie Beaufort, Institute for Stroke and Dementia Research, University Clinic Munich.

trypsin, chymotrypsin and elastase (see section 4.4.3), whose protease domains share the same conserved chymotrypsin-fold, suggesting that activity modulation via the VDAC2 peptide is a unique feature of the HTRA proteases, rather than a common characteristic of the conserved protease-fold.

Notably, the finding that the VDAC2 peptide activates not only wildtype HTRA1, but also the monomeric mutants HTRA1$_{R166H}$, HTRA1$_{A173T}$ and HTRA1$_{R274Q}$ is in striking contrast to the effects observed for the peptide CAPN2.1 (see section 4.4.1), which despite acting in a PDZ-independent fashion consistently activated the wildtype enzyme, yet rendered no effects on the monomeric mutants. This distinction suggests that activation via the CAPN2.1 peptide presumably proceeds via the conserved, trimer-dependent HtrA activation cascade, whereas activity modulation via the VDAC2 C-terminus occurs in a fashion that does not require inter-protomer communication. These findings highlight the diverse repertoire of activation mechanisms triggered by peptide-binding to the protease domain, which together with the PDZ-dependent regulatory mechanisms contribute to the finely-tuned adjustment of HTRA1's proteolytic activity.

Remarkably, activity enhancement induced by the VDAC2 peptide was not accompanied by a shift of the monomer-trimer equilibrium to higher oligomeric species (see section 4.4.4) indicating that the mechanism proceeds in a trimer-independent fashion. This finding is not only in stark contrast to the effects observed for the molecular clamps, which cause an up-regulation of the interface mutants' proteolytic activity by restoring trimer formation, but also to the classic model of trimer-dependent HtrA activation. Thus activation of the monomeric mutants by VDAC-derived peptides challenges the central dogma of HtrA activation, since it appears to proceed independent of the conserved inter-protomer communication cascade.

The observation that VDAC2-induced activity enhancement in the monomer-forming HTRA1 mutants does not involve trimer restoration raises the question whether the effect is based on a functional restoration of the monomeric species or on the activation of residual mutant trimers. Comparative titration experiments to quantify the peptide's effects on wildtype HTRA1 and the R274Q mutant revealed that the maximum degradation velocities observed upon application of the peptide are even higher for

HTRA1$_{R274Q}$ than for the wildtype enzyme (see section 4.4.1). Activity enhancement of residual trimers can therefore be excluded as a potential mode of action. Hence the gain of proteolytic activity is presumably based on the activation of individual protomers suggesting an activation mechanism that circumvents the conserved, trimer-dependent HtrA activation cascade, which requires signal relay from the sensor loop L3 to the activation loop LD* across the inter-protomer gap.

The observation that VDAC2-induced activity enhancement is even more pronounced for HTRA1$_{R274Q}$ might even indicate that the peptide's binding site is more accessible in the monomeric mutant than it is in the wildtype enzyme. In order to further investigate this hypothesis its binding affinities against wildtype HTRA1 and the monomer-forming mutants need to be determined. In this context we are currently setting up aggregation-induced emmission assays[12], in which the VDAC2-peptide is coupled to a luminophore, that fluoresces upon motional restriction thus allowing for a direct read-out and quantification of binding events (Riebe *et al.* 2017).

Remarkably, the effects of the VDAC2 peptide are not limited to an enhancement of processing rates, but also extend to the modulation of cleavage site specificities as can be derived from the cleavage patterns generated during proteolytic digests of the native HTRA1 substrate Tau (see section 4.4.2). Whereas the wildtype enzyme was able to introduce proteolytic cuts within all domains of the substrate, monomeric HTRA1$_{R274Q}$ displayed a profound lack of cleavage sites within the repeat regions. Strikingly, this difference in cleavage site specificities was almost completely abolished upon application of the VDAC2 peptide, which led to a major increase in the number of cuts introduced by HTRA1$_{R274Q}$ within this region. Whereas the number of cleavages was remarkably increased in the repeat regions upon VDAC2 peptide application, proteolysis of the N-terminal domain remained almost completely unaffected. This finding is in striking contrast to a previous study assessing the impact of PDZ-dependent activators on Tau proteolysis. As opposed to the results observed for the VDAC2 peptide, the increase in the number of cleavage sites upon application of the PDZ-binding effectors was most profound within the N-terminal domain (Rey 2018).

[12] Aggregation-induced emission assays will be performed in collaboration with the group of Jens Voskuhl, Institute for Organic Chemistry, University of Duisburg Essen.

This striking difference again highlights the diverse effects induced by different types of modulating stimuli which can be integrated by HTRA1 to generate a uniquely tailored proteolytic response.

Similarly, the analysis of amino acid preferences at the P1 and P1' residues revealed profound differences between HTRA1$_{R274Q}$ and the wildtype enzyme. Whereas at position P1' wildtype HTRA1 favoured both the uncharged amino acid serine and the positively charged residue lysine to an almost similar extent, the P1' preference of the monomeric mutant was restricted to small uncharged residues. Again this differential dispersion was largely alleviated upon application of the VDAC2 peptide. Hence both the wildtype-specific cleavage pattern and amino acid preference were restored upon application of the VDAC2 C-terminus demonstrating that the peptide's effects are not only restricted to quantitative activity enhancement, but also affect proteolysis in a qualitative manner.

5.3.2 Model of VDAC-induced activity enhancement

Whereas previous studies on HTRA1 activity modulation focused mainly on PDZ-driven mechanisms (Rey 2018), the data obtained in this study point to a novel form of activity enhancement proceeding in a fashion that appears uncoupled from of both the PDZ domain and the conserved, trimer-dependent HtrA activation cascade. The observation that the VDAC-derived peptides act in a PDZ-independent manner, suggests the existence of additional effector binding sites within the proteolytic domain, as has already been described for HTRA2 (see section 1.1.2).

In order to locate these additional binding sites docking analyses followed by molecular dynamics simulations were perfomed for both the VDAC2 peptide and its derivative VDAC2.2, which was optimised for binding to the active site [13]. The simulations revealed that both peptides could adopt various different binding poses on the protease

[13] Computational analyses were performed by Dr. Yasser Ruiz Blanco, Department of Computational Biochemistry, University of Duisburg-Essen.

surface. Among these potential binding sites, one was located immediately within the active site suggesting peptide-binding in a substrate-like manner, whereas another was situated at the far tip of the trimer. Indeed, both binding sites could be experimentally verified, since both an inhibitory antibody directed against the hydrophobic cluster at the trimer tip and a cyclodepsipeptide inhibitor, that binds directly to the active site, were able to competitively displace the VDAC2 peptide thus abolishing its activating effects in a concentration-dependent manner [14]. Remarkably, the observation that two potential binding sites can be addressed by VDAC2 might point to the existence of two separate activation mechanisms triggered by binding to either of the expected binding sites. Whereas binding to the active site in a substrate-like manner might trigger the conserved, trimer-dependent activation cascade resulting in substrate-induced active-site remodelling within the neighbouring protomers (Truebestein *et al.* 2011), binding to the alternative site at the trimer tip might induce a different, trimer-independent activation mechanism. In line with this hypothesis, the VDAC2-derivative VDAC2.2, which was optimized for active site-binding and found to display a higher number of binding poses and an increased relative free binding energy towards the active site in computational modeling, was unable to induce activity enhancement in $HTRA1_{R274Q}$, whereas its effects on the wildtype enzyme were comparable to that of the original peptide. This finding strongly suggests, that the VDAC2-induced activity increase in $HTRA1_{R274Q}$ is triggered by binding to the alternative binding site. Notably, in the monomeric mutant the activation mechanism would have to proceed in a fashion that abolishes the need for inter-protomer communication and the conserved interaction between loops L3 and LD*.

[14] Assays were performed by Annabell Roberti, Department of Microbiology II, University of Duisburg-Essen.

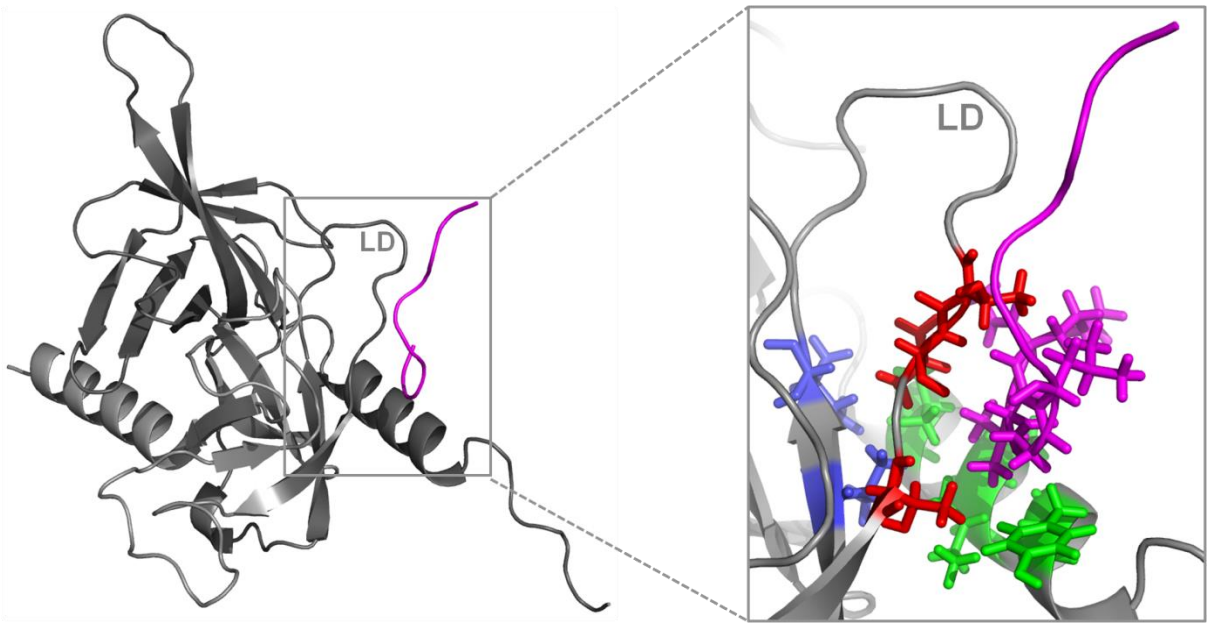

Figure 5.2 Potential interactions between HTRA1 and the VDAC2 peptide at the alternative binding site
The HTRA1 protease domain (grey) is shown in ribbon representation in the inactive conformation based on the PDB structure 3NUM (Truebestein *et al.* 2011). The VDAC2 peptide is displayed in magenta. The right panel shows a close-up of the calculated interactions involved in VDAC2-binding to the alternative interaction site. Residues contributing to the HTRA1-VDAC2 interaction are shown as sticks. Residues located at the trimer tip that interact with the peptide are shown in green. Residues stabilizing the hydrophobic cluster are coloured in blue. LD-residues interacting with the peptide are displayed in red. Figure based on a computational analysis by Yasser Ruiz Blanco, Institute of Computational Biochemistry, University of Duisburg-Essen (preliminary results).

Remarkably, computational analyses suggest that VDAC2-binding to the alternative binding site allows the peptide to interact simultaneously with both the protomer-protomer interaction interface located at the trimer tip and the activation loop LD (figure 5.2). This finding suggests that the VDAC2 C-terminal peptide might indeed be able to circumvent the conserved, trimer-dependent activation cascade by mimicking the L3-LD*-interaction thus inducing a conformational change in loop LD, which mediates further loop rearrangements culminating in the proper positioning of the activation domain. The peptide's interaction with the trimer tip is largely facilitated via its P2-valine, which in deeply burried within a hydrophobic cluster constituted by tyrosine 169, isoleucine 172, alanine 173 and valine 176 of the trimer tip and stabilized by valine 280 and isoleucine 282. Simultaneously the peptide engages in interactions with the activation loop LD via threonine 291, valine 292 and threonine 294. Notably, the peptide's C-terminal residues containing the carboxylate groups from the C-terminus as well as the P7- and P9-glutamates remain exposed to the solvent thus providing a low desolvation cost for the formation of the HTRA1-VDAC2 complex.

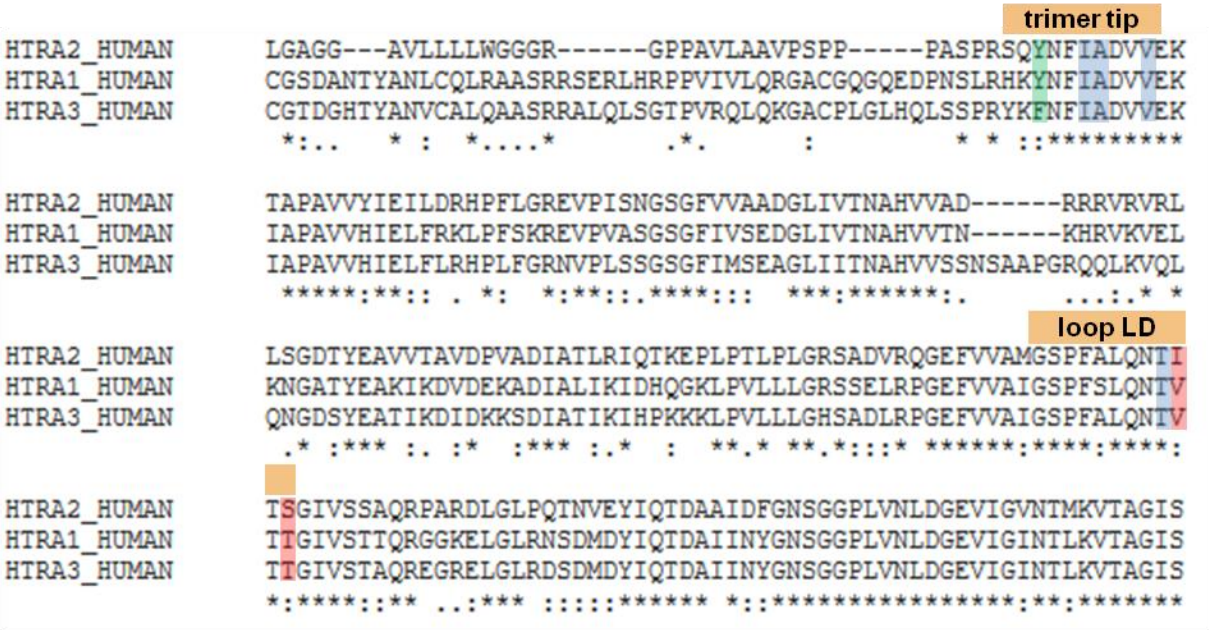

Figure 5.3 Alignment of HTRA1, HTRA2 and HTRA3 focusing on potential VDAC2 binding sites
The figure shows an alignment of HTRA1 (residues 119-352) with its human homologues HTRA2 and HTRA3. The location of the trimer tip and loop LD are marked with orange bars. The * indicates highly conserved amino acids, whereas the : indicates moderately conserved residues. Residues implicated in VDAC2-binding (based on docking studies and molecular dynamics simulations) are highlighted: blue = conserved in all three proteases, green = conserved in HTRA1 and HTRA2, but not in HTRA3, red = conserved in HTRA1 and HTRA3, but not in HTRA2.

A sequential alignment of HTRA1 with its human homologues HTRA2 and HTRA3 (figure 5.3) shows that among the three LD-residues immediately contributing to VDAC2-binding only one (threonine 291) is highly conserved among the three sequences. Yet the other two (valine 292 and threonine 294) are only conserved among HTRA1 and HTRA3, but differ in HTRA2 suggesting that LD-binding might be compromised in the mitochondrial HTRA homologue. This finding is in line with experimental data from proteolytic digests showing that HTRA1 and HTRA3, but not HTRA2 are activated by the VDAC2 peptide (see section 4.4.3). Based on this observation site-directed mutagenesis studies directed against valine 292 and threonine 294 should be conducted in order to experimentally verify the computationally calculated binding mode of the VDAC2 peptide and provide further insights into the precise mechanism underlying VDAC2-induced activation.

Notably, VDAC2-induced activation appeared slightly more pronounced in HTRA1$_{R274Q}$ compared to the wildtype enzyme (see section 4.4.1). With respect to the current binding model, this might be due to the circumstance that in the monomeric mutant the conserved interaction cluster at the trimer tip is much more accessible than in the

wildtype protein, in which this particular region engages in interactions with the neighbouring protomers. This finding further substantiates the notion that simultaneous binding to both the trimer tip and the activation loop LD facilitates VDAC2-induced activity enhancement.

Although the exact basis underlying VDAC-induced activation is still a topic of further investigation, the unusual mechanism underlying its effects greatly expands our knowledge regarding HTRA1 activity regulation from PDZ-dependent modulation via the conserved activation cascade (see section 1.1) to processes, that are strictly confined to a single protease domain and do not require inter-protomer communication. Taken together, these findings highlight the diverse repertoire of modulating stimuli that can be integrated by HTRA1 in order to achieve a finely tuned regulation of its proteolytic activity.

5.3.3 Limitations of VDAC-induced activation

The results provided in this study demonstrate that peptide sequences derived from the C-termini of VDAC2 and VDAC3 are able to enhance the proteolytic activity of HTRA1 via a novel mechanism that appears independent of both the PDZ domain and the conserved inter-protomer activation cascade thus rendering the peptides remarkable candidates for the functional restoration of HTRA1 mutants harbouring defects that compromise signal relay across the inter-protomer gap. Since the VDAC peptides were found to act in a PDZ-independent fashion, their effects might also be exploited to enhance the proteolytic activity of HTRA1 mutants carrying mutations within the PDZ domain that immunize them to the activating impact of PDZ-binding sequences.

However, the above results (see section 4.4.1) also point to possible limitations of this protein repair approach. Whereas addition of the VDAC2 and VDAC3 C-terminal peptides generates a major increase in the proteolytic activities of the monomer-forming CARASIL-mutants, their effects on $HTRA1_{A252T}$, in which trimer formation was not compromised, are comparatively weak. This observation might be due to the

circumstance that the highly conserved alanine 252 is located in direct proximity to the catalytic triad aspartate 250, which stabilizes the proton transfer from serine 328 to histidine 220 (see section 1.1.3). Although the mutation does not directly interfere with this interaction, minor shifts within the area surrounding aspartate 250 might suffice to partially compromise the function of the catalytic triad.

Remarkably, the A252T mutation did not only render HTRA1 less susceptible to VDAC-induced activation, but also to the effects of activating ligands acting in a PDZ-dependent fashion. This immunity to different forms of allosteric activity modulation suggests that allosteric activation mechanisms appear generally compromised in $HTRA1_{A252T}$. In accordance with the model of induced-fit substrate-binding suggested by Truebestein *et al.* (2011) effector-binding to allosteric sites presumably induces conformational rearrangements within the activation domain thereby stabilizing the catalytically competent conformation and predisposing it to substrate-binding. Hence mutations within close proximity of the catalytic residues might impede the steric rearrangements that facilitate the proper positioning of the catalytic triad upon effector-binding thus alleviating their activating effects. Notably, proteolysis assays with the model substrate β-casein revealed only a minor decrease of the A252T mutant's basal activity, whereas proteolytic digests of the physiological HTRA1 substrate Tau even remained unaffected by the mutation. Taken together these observations point to a pathomechanism that is based on a loss of susceptibility to allosteric activity modulation rather than on a general decrease in the protein's basal proteolytic activity. Apparently, this lack of responsiveness to modulating stimuli suffices to induce the clinical phenotype typically observed in CARASIL-patients thus suggesting a novel mechanism driving CARASIL-associated vascular pathology.

Notably, Verdura *et al.* (2015) report a patient carrying an HTRA1 mutation located within the PDZ domain ($HTRA1_{D450R}$), which manifests with CARASIL-like symptoms despite lacking the typical reduction in basal proteolytic activity. This striking similarity to the effects observed for $HTRA1_{A252T}$ as well as the PDZ domain's dispensability for basal proteolytic activity strongly support the hypothesis that the loss of allosteric activity modulation is sufficient to induce CARASIL-associated pathology. This finding is in line with the notion, that the basal activity observed for HTRA1 in the absence of modulating stimuli constitutes but a fraction of its potential proteolytic activity, that can

only be fully exploited upon allosteric activation. However, HTRA1$_{D450R}$ might still be accessible to VDAC-induced activity modulation, since peptides derived from the VDAC C-termini were found to act in a PDZ-independent fashion.

In contrast to the monomer-forming interface mutants the activity of HTRA1$_{G295R}$ could not be enhanced via application of the VDAC-derived peptides (see section 4.4.1). However, the G295R mutant was found to migrate as a dimer in glutaraldehyde crosslinking assays suggesting that a more severe folding defect might underlie its loss of proteolytic activity. In line with this finding, no formation of mixed oligomers could be observed upon incubation of HTRA1$_{G295R}$ with the wildtype enzyme (data not shown) suggesting that the dimer exists as a compact structure, that is held together by stable interactions.

Furthermore, the mutant's inaccessibilty to activity modulation is in line with evidence gained from computational analyses [15]. Mapping of the CARASIL-relevant interface mutations onto the HTRA1 structure shows that glycine 295 is situated within a β-sheet at the trimer center. Substitution of the small, nonpolar amino acid glycine for the charged, bulky arginine residue might thus result in a steric distortion of the β-sheet structure causing severe perturbations in the folding of the catalytic domain. Furthermore, the positively charged arginine side-chain would be pointing towards the inner cavity of the trimer, where it might form an intra-protomer salt bridge with aspartate 320 thereby disrupting its interaction with threonine 293* and 294* in the adjacent protomer. Thus the G295R mutation causes major steric distortions, which affect several features of the catalytic domain. Taken together these characteristics dramatically impede the G295R mutant's potential for activity restoration hence explaining its lack of responsiveness to the VDAC peptides.

In summary, these findings suggest that despite their ability to restore proteolytic function in the monomer-forming CARASIL mutants the VDAC peptides' potential to enhance proteolytic activity is limited when it comes to the restoration of HTRA1 mutants displaying either severe distortions within the active site or those showing a

[15] Computer-based structural analyses were conducted Dr. Kenny Bravo-Rodriguez, Department for Microbiology II, University of Duisburg-Essen.

general insusceptibility to modulating stimuli immediately affecting the proteolytic domain. Yet their activating effects are likely to extend to mutants affecting either the PDZ domain or signal relay across the inter-protomer gap, since they appeared independent of both these processes.

5.3.4 Potential physiological relevance of the HTRA1-VDAC interaction

The strong and robust activity enhancement observed in HTRA1 upon application of the VDAC2 and VDAC3 C-termini might point to a physiologically relevant interaction which triggers an intrinsic regulation mechanism resulting in a profound increase of the enzyme's proteolytic activity. The VDACs (voltage-dependent anion-selective channels) are a family of integral outer mitochondrial membrane (OMM) proteins forming conserved β-barrel structures that are embedded within the lipid bilayer and participate in a variety of exchange- and communication processes between the mitochondria and the surrounding cytosol including the exchange of the energy equivalents ATP and ADP (Bayrhuber *et al.* 2008). Furthermore, it has been proposed that the VDACs function as a platform for numerous protein-protein interactions thus contributing for example to the recruitment of pro-apoptotic proteins to the OMM (Setoguchi *et al.* 2006).

Structural studies of the three mammalian VDAC isoforms (VDAC1, VDAC2 and VDAC3) display a highly conserved topology consisting of a large pore formed by a 19-stranded β-barrel, whose internal diameter lies between two to four nanometers, and a single N-terminal helix protruding into the pore (Schredelseker *et al.* 2014). In line with the long L3 loop extension found in most bacterial porins this N-terminal extension is thought to contribute to the adjustment of pore diameter and metabolite selectivity (Bayrhuber *et al.* 2008). The C-terminus, however, is embedded into the β-barrel structure in close proximity to the mitochondrial inter-membrane space (MIMS) (figure 5.4).

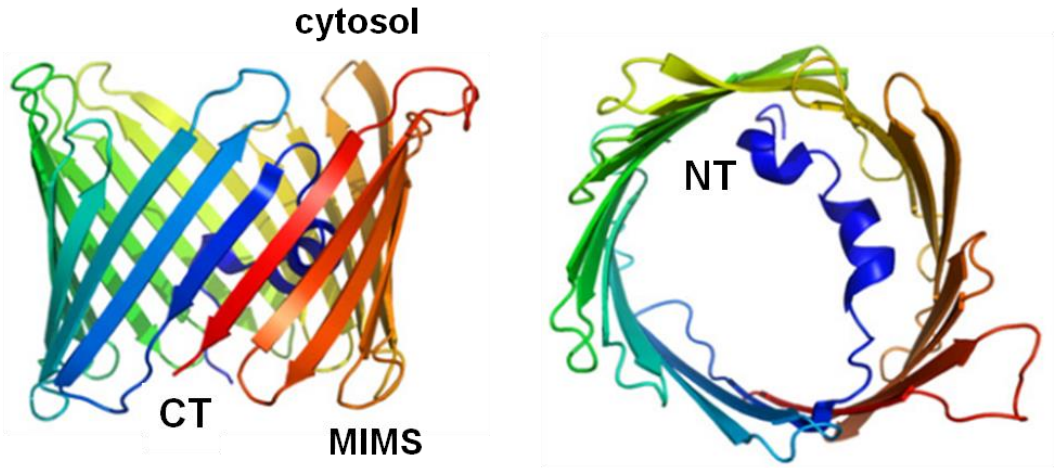

Figure 5.4 Topology of VDAC proteins
The crystal structure of mouse VDAC1 is shown in side- and top-view (ribbon presentation). The structure is rainbow coloured with the N-terminus (NT), which protrudes into the central pore, shown in blue and the C-terminus (CT) pointing towards the mitochondrial inter-membrane space (MIMS) shown in red. Adapted from Zeth (2010).

The origin of mitochondria from gram-negative bacterial ancestors according to the endosymbiotic theory (Zimorski *et al.* 2014) suggests a certain degree of mechanistic conservation regarding the processes governing the insertion of proteins into the mitochondrial membranes as well as the quality control mechanisms, that ensure the proteins' exact topologies. Like most mitochondrial proteins the VDAC precursors are synthesized within the cytosol and subsequently translocated across the OMM by the translocase of the outer mitochondrial membrane (TOM) complex (Becker and Wagner 2018; Rehling *et al.* 2001). From the inter-membrane space the VDACs are inserted into the OMM by the mitochondrial sorting and assembly machinery (SAM). Notably, the core unit of this machinery SAM50 is closely related to BamA, which forms the central moiety of the bacterial β-barrel assembly machinery (BAM) and facilitates the insertion of outer membrane proteins (OMPs) in gram-negative bacteria. Furthermore, the bacterial BAM complex is able to assemble mitochondrial β-barrel proteins and vice versa suggesting a profound mechanistic conservation (Kozjak-Pavlovic *et al.* 2011). Similar to the bacterial BAM complex the SAM machinery recognizes proteins destined for outer membrane insertion via the conserved C-terminal β-signal sequences (polar-X-G-X-X-hydrophobic-X-hydrophobic), which descends from the simpler bacterial YxF-motive and is also present in the three VDAC C-termini investigated in this study (Kutik *et al.* 2008). Whereas the functional conservation of the outer-membrane insertion machineries shared by eukaryotic mitochondria and gram-negative bacteria is well studied, the findings presented in this study might point

to an unprecedented extension of this concept to those factors underlying the quality control mechanisms that govern this process. While in gram-negative bacteria the periplasmic HtrA protease DegS recognizes mislocalized outer membrane proteins via their exposed C-termini (see section 1.1.1), its human homologues HTRA1 and HTRA3 might play a similar role in the cytosol of human cells. However, unlike the bacterial homologue, in which peptide-recognition and allosteric activity enhancement are mediated by the PDZ-domain, HTRA1 appears to integrate the activation signal in a PDZ-independent manner. Since the VDAC C-termini are embedded in the β-barrel structure, they should only be accessible within the un- or mis-assembled protein. However, the C-termini are in close proximity to the mitochondrial inter-membrane space and might thus be accessible to HTRA2 even when the protein is correctly folded and inserted into the outer membrane. This hypothesis would be in line with the finding, that C-terminal sequences derived from VDAC2 and VDAC3 activate the cytosolic HTRAs HTRA1 and HTRA3, but not HTRA2 (see section 4.4.3), as erroneous activation of HTRA2 would be detrimental for the cell.

To gain further insights into the potential physiological relevance of the HTRA1-VDAC interaction additional proteolytic assays using the full length VDAC proteins should be considered. Furthermore, peptide sequences derived from the C-termini of other mitochondrial outer membrane proteins should be tested for their ability to enhance HTRA1 activity.

5.4 Oligomer restoration via compensatory mutations

Whereas the above strategies focus on the restoration of proteolytic activity via supramolecular compounds or small peptidic modulators, an additional approach developed by the group of Martin Dichgans (Institute for Stroke and Dementia Research, University Clinic Munich, unpublished) strives to restore trimer formation in the CARASIL-relevant interface mutants via compensatory mutations within the opposing interface area. Using a computational model based on a simulated structure of $HTRA1_{R274Q}$ and subsequent biochemical characterization the group showed that coexpression of the monomer-forming mutant together with an inactive HTRA1 variant

carrying the compensatory mutation D174R resulted in the formation of mixed trimers displaying considerable proteolytic activity. Thus coexpression with a structurally engineered HTRA construct renders a third promising strategy to alleviate oligomeric assembly defects.

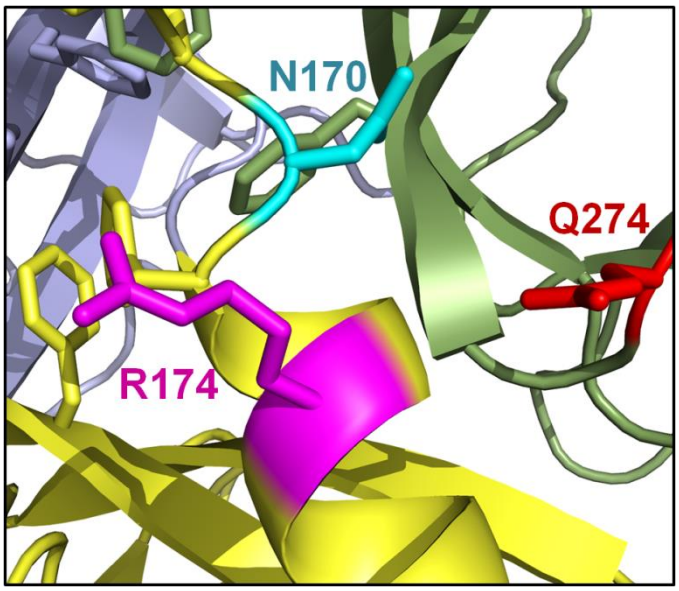

Figure 5.5 Orientation of arginine 174 in HTRA1$_{D174R/R274Q}$
Close-up showing the orientation of arginine 174 (magenta) in HTRA1$_{D174R/R274Q}$. Glutamine 274 is shown in red and asparagine 170 is displayed in cyan.

However, the precise mechanism underlying the restoration of trimer formation and proteolytic activity remained to be determined. In order to gain deeper insights into the structural implications of the rescue effect a crystal structure of HTRA1 comprising both the disease causing and the compensatory mutation was established in the course of this study (see section 4.5)[16]. Comparing the HTRA1$_{D174R/R274Q}$ crystal structure to that of the wildtype protein revealed that trimer restoration was not based on a direct interaction of the newly introduced arginine 174 with the opposing interface area, since its side chain appeared clearly twisted away from the interaction surface. Instead, the subtle rearrangements induced by the compensatory mutation led to a distinct increase in the interaction area between the individual protomers, which might compensate the loss of the inter-molecular salt bridge hence causing trimer restoration. Furthermore, the hydrophilic headgroup of arginine 174 was located within 5.45 Å of asparagine 170, which is situated within the α-helix comprising the ringstacking residues tyrosine 169

[16] Crystallography studies were conducted by the group of Ingrid Vetter, Max-Planck Institute, Dortmund.

and phenylalanine 171 (figure 5.5). However, molecular dynamics simulations suggest that arginine 174 displays a high degree of motional flexibility allowing it to approach the backbone oxygen of asparagine 170 by up to 1,7 Å. This interaction might contribute to preserving the kink in the α-helix thereby stabilizing the hydrophobic cluster at the tip of the trimer. Notably, the pronounced mobility of the newly introduced arginine 174 might also play a role in the exclusion of water molecules from the hydrophobic interaction surface. Whereas the hydrophobic stem region of the arginine side chain is located within the hydrophobic crevice between the trimer tips, its highly flexible, hydrophilic headgroup remains exposed to the solvent thus lowering the desolvation cost for trimer formation. This finding is in accordance with an extensive analysis by Bogan and Thorn (1998) who found that protein-protein interaction hot spots are generally surrounded by a ring of residues serving to eliminate water molecules from the interaction area thus providing an important prerequisite for the highly energetic binding events occuring within the hot spot area.

Testing the effects of the compensatory HTRA1$_{D174R}$ mutant against a panel of other monomer-forming interface mutants revealed that in contrast to the compound-based strategies presented in this study trimer restoration via the compensatory mutation was highly specific for HTRA1$_{R274Q}$[17]. Yet, the mechanistic basis of this allele specificity could not be determined from the HTRA1$_{D174R/R274Q}$ crystal structure indicating that additional studies are needed to further elucidate the mutation's functional implications. Additionally, future investigations should aim to identify further mutations to compensate the loss of trimer formation in the other disease-relevant HTRA1 interface mutants in order to extend the concept of oligomer restoration via protein-based complementation.

Following further refinement, the application of inactive, engineered HTRA1 variants might render a promising protein-repair strategy even in a clinical context, since the inactive protein should harbour less off-target effects compared to the wildtype enzyme. Furthermore, this approach might be widely applicable to other single gene disorders affecting either oligomer assembly or other protein-protein interactions.

[17] Assays were conducted by Nathalie Beaufort, Institute for Stroke and Dementia Research, University Clinic Munich.

6 Outlook

The experimental data presented in this study provide insights into the detrimental mechanistic implications of CARASIL-associated amino acid substitutions within the HTRA1 trimer interface as well as potential avenues towards their functional restoration. These include the reconstitution of trimer stability via the application of supramolecular clamp compounds, the enhancement of proteolytic activity via peptidic modulators and the recovery of oligomer formation via protein-based complementation. Addressing HTRA1 as a therapeutic target in the treatment of CARASIL appears particularly appealing not only due to its immediate involvement in the disease's aetiology, but also since the secreted enzyme should be directly accessible to potential treatment agents administered through the blood stream.

The chemical modulation of protein-protein interactions via supramolecular clamp compounds carrying oxyanion-binding guanidinio carbonyle pyrrole (GCP)-groups at both their termini successfully restores both HTRA1 trimerization and proteolytic activity. However, the compound concentrations required to obtain this effect are far beyond the physiologically feasible concentration range hence suggesting a need for further optimization. As the affinity of a single GCP unit towards an anionic protein surface is relatively low compared to conventional small molecule ligands, future improvements should aim to address additional binding sites across the protomer-protomer interface via multi-armed ligands in order to increase the molecules' total binding affinities. This multivalency-approach might additionally be extended to the attachment of highly affine PDZ-binding peptides via flexible linker moieties, since incorporating different types of molecular recognition processes into a single ligand should not only enhance the compounds' affinities, but also increase their specificity for HTRA1 hence decreasing the chance for off-target effects.

Whereas the application of the molecular clamps might not be feasible as a therapeutic strategy in the treatment of CARASIL due to the above criteria, peptide-induced HTRA1 activation might harbour the potential to be clinically applicable. The data provided in this study as well as computational analyses suggest that peptides derived from the C-termini of the voltage-dependent anion-selective channels (VDACs) 2 and 3 are able to enhance the proteolytic activity of HTRA1 by simultaneously binding to

both the protomer-protomer interaction interface located at the trimer tip and the activation loop LD thus allowing them to circumvent the conserved, trimer-dependent activation cascade by mimicking the L3-LD*-interaction. Yet, to further substantiate this hypothesis site-directed mutagenesis studies directed against the relevant residues should be conducted in order to experimentally verify the computationally calculated binding mode of the VDAC2 peptide and gain deeper insights into the precise mechanisms underlying VDAC2-induced activation. Although the results presented in this thesis indicate that the peptide's effects are restricted to HTRA1 and HTRA3, additional studies should aim to extend our knowledge regarding its specificity in order to exclude potential off-target effects.

The third approach to functionally restore CARASIL-relevant HTRA1 interface mutants is the application of genetically engineered, inactive HTRA1 constructs comprising compensatory mutations. This strategy appears particularly appealing, since the administration of proteolytically inactive variants should harbour the least potential for off-target effects. Structural data derived from an $HTRA1_{D174R/R274Q}$ double mutant suggest that the compensatory mutation D174R restores both trimer formation and proteolytic activity in $HTRA1_{R274Q}$ by increasing the interaction surface between individual protomers. However, the compensatory effect is restricted to this particular interface mutation, whereas the other CARASIL-associated interface mutants remain unaffected. Since the crystallographic data provide no mechanistic explanation for this limitation, additional studies are needed to further elucidate the mutation's functional implications. Furthermore, future investigations should aim to extend the concept of oligomer restoration via protein-based complementation by identifying additional mutations, that compensate the loss of trimer formation in the other disease-relevant HTRA1 interface mutants.

Finally, further investigations into the functional restoration of CARASIL-associated HTRA1 interface mutants might not only yield potential treatment options for this specific disease, but also serve as a proof of principle study to devise general concepts for the restoration of disease-relevant oligomerization defects.

7 Summary

HTRA1, a trimeric serine protease implicated in both cellular signal transduction and protein quality control, belongs to the homo-oligomeric High Temperature Requirement A protease family, whose activation requires a conserved cascade of inter-protomer communication. Among other HTRA1 mutations amino acid substitutions within its trimer interface have been associated with CARASIL (Cerebral Autosomal Recessive Arteriopathy with Subcortical Infarcts and Leucoencephalopathy), a monogenic small vessel disease, that manifests with stroke, dementia, spondylosis deformans and alopecia at an early age of onset. The localization of these mutations as well as the detailed biochemical characterization presented in this study reveal that the associated loss of function phenotype is based on severe oligomerization defects causing a shift of the monomer-trimer equilibrium towards the monomeric state. Based on this finding a portfolio of protein repair strategies allowing for the functional restoration of the mutants' proteolytic activities was developed.

A first approach focuses on the stabilization of inter-protomer contacts via supramolecular guanidinio carbonyle pyrrole (GCP)-clamps, which introduce a synthetic bridge across the inter-protomer gap thus compensating the loss of intrinsic affinity induced by the disease causing mutations. Assessing the compounds' effects via biochemical assays revealed that the GCP-clamps indeed induced a substantial increase in the interface-mutants' proteolytic activities that was associated with a distinct shift of the monomer-trimer equilibrium towards the trimeric form.

A second repair strategy strives to exploit the activating features of regulatory peptides in order to artificially enhance the proteolytic activity of disease-relevant HTRA1 mutants. Testing a collection of peptidic ligands derived from our laboratory portfolio of HTRA1-activating sequences revealed that peptides derived from the C-termini of the mitochondrial channel proteins VDAC2 and VDAC3 were able to increase the proteolytic activity of wildtype HTRA1 as well as the monomeric CARASIL mutants via a novel mechanism that appeared independent of both the PDZ domain and the conserved inter-protomer activation cascade. This unusual mode of activity enhancement not only points to a potential route for therapeutic intervention, but also greatly expands our knowledge regarding HTRA1 activity regulation from PDZ-

dependent modulation via the conserved activation cascade to processes, that are confined to a single protease domain hence abolishing the need for inter-protomer communication.

Whereas the above strategies focus on the chemical modulation of proteolytic activity, an additional biologic approach developed by the group of Martin Dichgans (University Clinic Munich) centers on protein-based complementation of the CARASIL-associated trimer assembly defects via genetically engineered, inactive HTRA1 constructs carrying compensatory mutations. This study reports the determination of a crystal structure for HTRA1 comprising both a disease-relevant and the corresponding compensatory mutation thus shedding light onto the mechanisms underlying this third protein repair strategy.

Taken together, the results presented in this study constitute a diverse repertoire of proof of concept approaches for the functional restoration of disease-relevant HTRA1 interface mutations. On a conceptual level these approaches should be widely applicable to a vast number of biological problems involving the modulation of protein-protein interactions.

Zusammenfassung

HTRA1, eine homo-trimere Serinprotease, die sowohl in der Protein-Qualitätskontrolle, als auch in der Weiterleitung zellulärer Signale eine Rolle spielt, gehört zur High Temperature Requirement A Familie, welche sich durch eine konservierte, Trimer-abhängigige Aktivierungskaskade auszeichnet. Neben anderen HTRA1 Mutationen sind auch Aminosäure-Substitutionen im Trimer-Interface mit der Entstehung von CARASIL (Cerebral Autosomal Recessive Arteriopathy with Subcortical Infarcts and Leucoencephalopathy) assoziiert - einer monogenetischen Erkrankung, die mit frühzeitigen Schlaganfällen, Demenz, Spondylose und Alopezie einhergeht. Sowohl die Lokalisation der Mutationen, als auch ihre detailierte biochemische Analyse zeigen, dass der *Loss-of-Function*-Phänotyp auf schwerwiegenden Oligomerisierungsdefekten basiert, die eine Verschiebung des Monomer-Trimer-Gleichgewichtes hin zur monomeren Form bewirken. Auf Grundlage dieser Ergebnisse konnte ein Portfolio von Protein-Reparatur-Strategien entwickelt werden, die eine funktionelle Wiederherstellung der proteolytischen Aktivität der Mutanten bewirken.

Ein erster Ansatz konzentriert sich auf die Stabilisierung von Inter-Protomer-Kontakten mittels supramolekularer Guanidiniocarbonylpyrrol (GCP)-"Klammern", die eine synthetische Brücke über den Inter-Protomer-Spalt bilden und so den durch die Mutationen hervorgerufenen intrinsischen Affinitätsverlust kompensieren. Biochemische Analysen ergaben, dass die GCP-Liganden eine Erhöhung der Aktivität der Interface-Mutanten bewirkten, die an eine deutliche Verschiebung des Monomer-Trimer-Gleichgewichtes hin zum Trimer gekoppelt war.

Eine zweite Reparatur-Strategie nutzt die aktivierenden Eigenschaften regulatorischer Peptide um die proteolytische Aktivität Krankheits-relevanter HTRA1-Mutanten artifiziell zu verstärken. Biochemische Tests ergaben, dass Peptide, die sich von den C-Termini der mitochondrialen Kanalproteine VDAC2 und VDAC3 ableiten, in der Lage sind sowohl die proteolytische Aktivität von Wildtyp-HTRA1, als auch die der monomeren CARASIL-Mutanten unabhängig von der PDZ-Domäne und der konservierten Inter-Protomer-Aktivierungskaskade zu erhöhen. Dieser ungewöhnliche Mechanismus deutet nicht nur auf eine potentielle therapeutische Interventionsmöglichkeit hin, sondern erweitert auch unser Wissen über die HTRA1-

Aktivitätsregulation von der bereits bekannten PDZ-abhängigen Modulation über die konservierte Aktivierungskaskade hin zu Prozessen, die innerhalb einer einzelnen Protease-Domäne und somit unabhängig von der Inter-Protomer Kommunikationskaskade ablaufen.

Während die oben genannten Strategien sich mit der chemischen Modulation der HTRA1-Aktivität befassen, zielt ein weiterer durch die Arbeitsgruppe von Martin Dichgans (Klinikum der Universität München) entwickelter Ansatz auf die biologische, Protein-basierte Komplementation CARASIL-assoziierter Trimer-Assemblierungsdefekte mittels genetisch modifizierter, inaktiver HTRA1-Konstrukte ab, welche kompensatorische Mutationen tragen. Diese Arbeit zeigt eine HTRA1-Kristallstruktur, die sowohl eine Krankheits-relevante, als auch die entsprechende kompensatorische Mutation beinhaltet, und gibt somit Aufschluss über die Mechanismen, die dieser dritten Reparatur-Strategie zugrundeliegen.

Zusammengefasst erzeugen die in dieser Arbeit präsentierten Daten eine vielfältige Sammlung von Ansätzen zur funktionellen Restaurierung Krankheits-relevanter HTRA1 Interface-Mutationen. Auf konzeptioneller Ebene sollten diese Strategien zudem weitgehend übertragbar auf eine Vielzahl biologischer Fragestellungen sein, die die Modulation von Protein-Protein-Kontakten beinhalten.

8 References

Alamowitch, S.; Plaisier, E.; Favrole, P.; Prost, C.; Chen, Z.; van Agtmael, T. et al. (2009): Cerebrovascular disease related to COL4A1 mutations in HANAC syndrome. In *Neurology* 73 (22), pp. 1873–1882. DOI: 10.1212/WNL.0b013e3181c3fd12.

Albright, R. A.; Mossing, M. C.; Matthews, B. W. (1996): High-resolution structure of an engineered Cro monomer shows changes in conformation relative to the native dimer. In *Biochemistry* 35 (3), pp. 735–742. DOI: 10.1021/bi951958n.

Altieri, Amanda S.; Hinton, Denise P.; Byrd, R. Andrew (1995): Association of Biomolecular Systems via Pulsed Field Gradient NMR Self-Diffusion Measurements. In *J. Am. Chem. Soc.* 117 (28), pp. 7566–7567. DOI: 10.1021/ja00133a039.

An, Eunkyung; Sen, Supti; Park, Sung Kyu; Gordish-Dressman, Heather; Hathout, Yetrib (2010): Identification of novel substrates for the serine protease HTRA1 in the human RPE secretome. In *Investigative ophthalmology & visual science* 51 (7), pp. 3379–3386. DOI: 10.1167/iovs.09-4853.

Arima, Kunimasa; Yanagawa, Sohei; Ito, Nobuo; Ikeda, Shu-ichi (2003): Cerebral arterial pathology of CADASIL and CARASIL (Maeda syndrome). In *Neuropathology : official journal of the Japanese Society of Neuropathology* 23 (4), pp. 327–334.

Artavanis-Tsakonas, S.; Rand, M. D.; Lake, R. J. (1999): Notch signaling: cell fate control and signal integration in development. In *Science (New York, N.Y.)* 284 (5415), pp. 770–776.

Azem, A.; Weiss, C.; Goloubinoff, P. (1998): Structural analysis of GroE chaperonin complexes using chemical cross-linking. In *Methods in enzymology* 290, pp. 253–268.

Bai, Xiao-Chen; Pan, Xi-jiang; Wang, Xiao-jing; Ye, Yun-ying; Chang, Lei-Fu; Leng, Dong et al. (2011): Characterization of the structure and function of Escherichia coli DegQ as a representative of the DegQ-like proteases of bacterial HtrA family proteins. In *Structure (London, England : 1993)* 19 (9), pp. 1328–1337. DOI: 10.1016/j.str.2011.06.013.

Baldi, Alfonso; Luca, Antonio de; Morini, Monica; Battista, Tullio; Felsani, Armando; Baldi, Feliciano et al. (2002): The HtrA1 serine protease is down-regulated during

human melanoma progression and represses growth of metastatic melanoma cells. In *Oncogene* 21 (43), pp. 6684–6688. DOI: 10.1038/sj.onc.1205911.

Bayrakli, Fatih; Balaban, Hatice; Gurelik, Mustafa; Hizmetli, Sami; Topaktas, Suat (2014): Mutation in the HTRA1 gene in a patient with degenerated spine as a component of CARASIL syndrome. In *Turkish neurosurgery* 24 (1), pp. 67–69. DOI: 10.5137/1019-5149.JTN.6226-12.1.

Bayrhuber, Monika; Meins, Thomas; Habeck, Michael; Becker, Stefan; Giller, Karin; Villinger, Saskia et al. (2008): Structure of the human voltage-dependent anion channel. In *Proceedings of the National Academy of Sciences of the United States of America* 105 (40), pp. 15370–15375. DOI: 10.1073/pnas.0808115105.

Beaufort, Nathalie; Scharrer, Eva; Kremmer, Elisabeth; Lux, Vanda; Ehrmann, Michael; Huber, Robert et al. (2014): Cerebral small vessel disease-related protease HtrA1 processes latent TGF-β binding protein 1 and facilitates TGF-β signaling. In *Proceedings of the National Academy of Sciences of the United States of America* 111 (46), pp. 16496–16501. DOI: 10.1073/pnas.1418087111.

Becker, Thomas; Wagner, Richard (2018): Mitochondrial Outer Membrane Channels: Emerging Diversity in Transport Processes. In *BioEssays : news and reviews in molecular, cellular and developmental biology* 40 (7), e1800013. DOI: 10.1002/bies.201800013.

Bejugam, Pruthvi Raj; Kuppili, Raja R.; Singh, Nitu; Gadewal, Nikhil; Chaganti, Lalith K.; Sastry, G. Madhavi; Bose, Kakoli (2013): Allosteric regulation of serine protease HtrA2 through novel non-canonical substrate binding pocket. In *PloS one* 8 (2), e55416. DOI: 10.1371/journal.pone.0055416.

Bianchi, Silvia; Di Palma, Chiara; Gallus, Gian Nicola; Taglia, Ilaria; Poggiani, Antonella; Rosini, Francesca et al. (2014): Two novel HTRA1 mutations in a European CARASIL patient. In *Neurology* 82 (10), pp. 898–900. DOI: 10.1212/WNL.0000000000000202.

Bogan, A. A.; Thorn, K. S. (1998): Anatomy of hot spots in protein interfaces. In *Journal of molecular biology* 280 (1), pp. 1–9. DOI: 10.1006/jmbi.1998.1843.

Bowden, Marissa A.; Di Nezza-Cossens, Lisa A.; Jobling, Tom; Salamonsen, Lois A.; Nie, Guiying (2006): Serine proteases HTRA1 and HTRA3 are down-regulated with

increasing grades of human endometrial cancer. In *Gynecologic oncology* 103 (1), pp. 253–260. DOI: 10.1016/j.ygyno.2006.03.006.

Bradford, Marion M. (1976): A rapid and sensitive method for the quantitation of microgram quantities of protein utilizing the principle of protein-dye binding. In *Analytical Biochemistry* 72 (1-2), pp. 248–254. DOI: 10.1016/0003-2697(76)90527-3.

Bravo-Rodriguez, Kenny; Hagemeier, Birte; Drescher, Lea; Lorenz, Marian; Rey, Juliana; Meltzer, Michael et al. (2018): Utilities for Mass Spectrometry Analysis of Proteins. Fast post processing of mass spectrometry data. In *Rapid communications in mass spectrometry : RCM*. DOI: 10.1002/rcm.8243.

Brooke, Benjamin S.; Habashi, Jennifer P.; Judge, Daniel P.; Patel, Nishant; Loeys, Bart; Dietz, Harry C. (2008): Angiotensin II blockade and aortic-root dilation in Marfan's syndrome. In *The New England journal of medicine* 358 (26), pp. 2787–2795. DOI: 10.1056/NEJMoa0706585.

Cabrera, Alvaro Cortes; Melo, Esther; Roth, Doris; Topp, Andreas; Delobel, Frederic; Stucki, Corinne et al. (2017): HtrA1 activation is driven by an allosteric mechanism of inter-monomer communication. In *Scientific reports* 7 (1), p. 14804. DOI: 10.1038/s41598-017-14208-z.

Cai, Bin; Zeng, Jiabin; Lin, Yi; Lin, Yu; Lin, WenPing; Lin, Wei et al. (2015): A frameshift mutation in HTRA1 expands CARASIL syndrome and peripheral small arterial disease to the Chinese population. In *Neurological sciences : official journal of the Italian Neurological Society and of the Italian Society of Clinical Neurophysiology* 36 (8), pp. 1387–1391. DOI: 10.1007/s10072-015-2121-5.

Campioni, Mara; Severino, Anna; Manente, Lucrezia; Tuduce, Ioana L.; Toldo, Stefano; Caraglia, Michele et al. (2010): The serine protease HtrA1 specifically interacts and degrades the tuberous sclerosis complex 2 protein. In *Molecular cancer research : MCR* 8 (9), pp. 1248–1260. DOI: 10.1158/1541-7786.MCR-09-0473.

Chen, Yan; He, Zhiyi; Meng, Su; Li, Lei; Yang, Hua; Zhang, Xiaotang (2013): A novel mutation of the high-temperature requirement A serine peptidase 1 (HTRA1) gene in a Chinese family with cerebral autosomal recessive arteriopathy with subcortical infarcts and leukoencephalopathy (CARASIL). In *The Journal of international medical research* 41 (5), pp. 1445–1455. DOI: 10.1177/0300060513480926.

Chien, Jeremy; Aletti, Giovanni; Baldi, Alfonso; Catalano, Vincenzo; Muretto, Pietro; Keeney, Gary L. et al. (2006): Serine protease HtrA1 modulates chemotherapy-induced cytotoxicity. In *The Journal of clinical investigation* 116 (7), pp. 1994–2004. DOI: 10.1172/JCI27698.

Chien, Jeremy; Campioni, Mara; Shridhar, Viji; Baldi, Alfonso (2009a): HtrA Serine Proteases as Potential Therapeutic Targets in Cancer. In *Current cancer drug targets* 9 (4), pp. 451–468.

Chien, Jeremy; He, Xiaoping; Shridhar, Viji (2009b): Identification of tubulins as substrates of serine protease HtrA1 by mixture-based oriented peptide library screening. In *Journal of cellular biochemistry* 107 (2), pp. 253–263. DOI: 10.1002/jcb.22121.

Chien, Jeremy; Ota, Takayo; Aletti, Giovanni; Shridhar, Ravi; Boccellino, Mariarosaria; Quagliuolo, Lucio et al. (2009c): Serine protease HtrA1 associates with microtubules and inhibits cell migration. In *Molecular and cellular biology* 29 (15), pp. 4177–4187. DOI: 10.1128/MCB.00035-09.

Chien, Jeremy; Staub, Julie; Hu, Shou-Ih; Erickson-Johnson, Michele R.; Couch, Fergus J.; Smith, David I. et al. (2004): A candidate tumor suppressor HtrA1 is downregulated in ovarian cancer. In *Oncogene* 23 (8), pp. 1636–1644. DOI: 10.1038/sj.onc.1207271.

Choi, Hyeongjoo; Jung, Yongwon (2018): Applying Multivalent Biomolecular Interactions for Biosensor. In *Chemistry (Weinheim an der Bergstrasse, Germany)*. DOI: 10.1002/chem.201801408.

Choi, Minee L.; Gandhi, Sonia (2018): Crucial role of protein oligomerization in the pathogenesis of Alzheimer's and Parkinson's diseases. In *The FEBS journal*. DOI: 10.1111/febs.14587.

Clausen, Tim; Kaiser, Markus; Huber, Robert; Ehrmann, Michael (2011): HTRA proteases: regulated proteolysis in protein quality control. In *Nature reviews. Molecular cell biology* 12 (3), pp. 152–162. DOI: 10.1038/nrm3065.

Clawson, Gary A.; Bui, Vuong; Xin, Ping; Wang, Ning; Pan, Weihua (2008): Intracellular localization of the tumor suppressor HtrA1/Prss11 and its association with HPV16 E6 and E7 proteins. In *Journal of cellular biochemistry* 105 (1), pp. 81–88. DOI: 10.1002/jcb.21804.

Dhulipala, Vamsidhara C.; Welshons, Wade V.; Reddy, Chada S. (2006): Cell cycle proteins in normal and chemically induced abnormal secondary palate development: a review. In *Human & experimental toxicology* 25 (11), pp. 675–682. DOI: 10.1177/0960327106070848.

Di Donato, Ilaria; Bianchi, Silvia; Gallus, Gian Nicola; Cerase, Alfonso; Taglia, Ilaria; Pescini, Francesca et al. (2017): Heterozygous mutations of HTRA1 gene in patients with familial cerebral small vessel disease. In *CNS neuroscience & therapeutics* 23 (9), pp. 759–765. DOI: 10.1111/cns.12722.

Dijke, Peter ten; Arthur, Helen M. (2007): Extracellular control of TGFbeta signalling in vascular development and disease. In *Nature reviews. Molecular cell biology* 8 (11), pp. 857–869. DOI: 10.1038/nrm2262.

Domenga, Valérie; Fardoux, Peggy; Lacombe, Pierre; Monet, Marie; Maciazek, Jacqueline; Krebs, Luke T. et al. (2004): Notch3 is required for arterial identity and maturation of vascular smooth muscle cells. In *Genes & development* 18 (22), pp. 2730–2735. DOI: 10.1101/gad.308904.

Donnan, Geoffrey A.; Fisher, Marc; Macleod, Malcolm; Davis, Stephen M. (2008): Stroke. In *Lancet (London, England)* 371 (9624), pp. 1612–1623. DOI: 10.1016/S0140-6736(08)60694-7.

Douni, Eleni; Rinotas, Vagelis; Makrinou, Eleni; Zwerina, Jochen; Penninger, Josef M.; Eliopoulos, Elias et al. (2012): A RANKL G278R mutation causing osteopetrosis identifies a functional amino acid essential for trimer assembly in RANKL and TNF. In *Human molecular genetics* 21 (4), pp. 784–798. DOI: 10.1093/hmg/ddr510.

Downward, Julian (2004): PI 3-kinase, Akt and cell survival. In *Seminars in cell & developmental biology* 15 (2), pp. 177–182.

Duguay, Amy R.; Silhavy, Thomas J. (2004): Quality control in the bacterial periplasm. In *Biochimica et biophysica acta* 1694 (1-3), pp. 121–134. DOI: 10.1016/j.bbamcr.2004.04.012.

Dynon, Kemperly; Heng, Sophea; Puryer, Michelle; Li, Ying; Walton, Kelly; Endo, Yaeta; Nie, Guiying (2012): HtrA3 as an early marker for preeclampsia: specific monoclonal antibodies and sensitive high-throughput assays for serum screening. In *PloS one* 7 (9), e45956. DOI: 10.1371/journal.pone.0045956.

Eigenbrot, Charles; Ultsch, Mark; Lipari, Michael T.; Moran, Paul; Lin, S. Jack; Ganesan, Rajkumar et al. (2012): Structural and functional analysis of HtrA1 and its subdomains. In *Structure (London, England : 1993)* 20 (6), pp. 1040–1050. DOI: 10.1016/j.str.2012.03.021.

Fukutake, T.; Hirayama, K. (1995): Familial young-adult-onset arteriosclerotic leukoencephalopathy with alopecia and lumbago without arterial hypertension. In *European neurology* 35 (2), pp. 69–79. DOI: 10.1159/000117096.

Fukutake, Toshio (2011): Cerebral autosomal recessive arteriopathy with subcortical infarcts and leukoencephalopathy (CARASIL): from discovery to gene identification. In *Journal of stroke and cerebrovascular diseases : the official journal of National Stroke Association* 20 (2), pp. 85–93. DOI: 10.1016/j.jstrokecerebrovasdis.2010.11.008.

Goodsell, D. S.; Olson, A. J. (2000): Structural symmetry and protein function. In *Annual review of biophysics and biomolecular structure* 29, pp. 105–153. DOI: 10.1146/annurev.biophys.29.1.105.

Gould, Douglas B.; Phalan, F. Campbell; van Mil, Saskia E.; Sundberg, John P.; Vahedi, Katayoun; Massin, Pascale et al. (2006): Role of COL4A1 in small-vessel disease and hemorrhagic stroke. In *The New England journal of medicine* 354 (14), pp. 1489–1496. DOI: 10.1056/NEJMoa053727.

Graham, Julie R.; Chamberland, Angela; Lin, Qingcong; Li, X. Jian; Dai, David; Zeng, Weilan et al. (2013): Serine protease HTRA1 antagonizes transforming growth factor-β signaling by cleaving its receptors and loss of HTRA1 in vivo enhances bone formation. In *PloS one* 8 (9), e74094. DOI: 10.1371/journal.pone.0074094.

Grau, Sandra; Baldi, Alfonso; Bussani, Rossana; Tian, Xiaodan; Stefanescu, Raluca; Przybylski, Michael et al. (2005): Implications of the serine protease HtrA1 in amyloid precursor protein processing. In *Proceedings of the National Academy of Sciences of the United States of America* 102 (17), pp. 6021–6026. DOI: 10.1073/pnas.0501823102.

Grau, Sandra; Richards, Peter J.; Kerr, Briedgeen; Hughes, Clare; Caterson, Bruce; Williams, Anwen S. et al. (2006): The role of human HtrA1 in arthritic disease. In *The Journal of biological chemistry* 281 (10), pp. 6124–6129. DOI: 10.1074/jbc.M500361200.

Gray, C. W.; Ward, R. V.; Karran, E.; Turconi, S.; Rowles, A.; Viglienghi, D. et al. (2000): Characterization of human HtrA2, a novel serine protease involved in the mammalian cellular stress response. In *European journal of biochemistry* 267 (18), pp. 5699–5710.

Grundke-Iqbal, I.; Vorbrodt, A. W.; Iqbal, K.; Tung, Y. C.; Wang, G. P.; Wisniewski, H. M. (1988): Microtubule-associated polypeptides tau are altered in Alzheimer paired helical filaments. In *Brain research* 464 (1), pp. 43–52.

Gunda, Bence; Mine, Manuele; Kovács, Tibor; Hornyák, Csilla; Bereczki, Dániel; Várallyay, György et al. (2014): COL4A2 mutation causing adult onset recurrent intracerebral hemorrhage and leukoencephalopathy. In *Journal of neurology* 261 (3), pp. 500–503. DOI: 10.1007/s00415-013-7224-4.

Hagestedt, T.; Lichtenberg, B.; Wille, H.; Mandelkow, E. M.; Mandelkow, E. (1989): Tau protein becomes long and stiff upon phosphorylation: correlation between paracrystalline structure and degree of phosphorylation. In *The Journal of cell biology* 109 (4 Pt 1), pp. 1643–1651.

Hansen, Guido; Hilgenfeld, Rolf (2013): Architecture and regulation of HtrA-family proteins involved in protein quality control and stress response. In *Cellular and molecular life sciences : CMLS* 70 (5), pp. 761–775. DOI: 10.1007/s00018-012-1076-4.

Hara, Kenju; Shiga, Atsushi; Fukutake, Toshio; Nozaki, Hiroaki; Miyashita, Akinori; Yokoseki, Akio et al. (2009): Association of HTRA1 mutations and familial ischemic cerebral small-vessel disease. In *The New England journal of medicine* 360 (17), pp. 1729–1739. DOI: 10.1056/NEJMoa0801560.

Harbury, P. B.; Zhang, T.; Kim, P. S.; Alber, T. (1993): A switch between two-, three-, and four-stranded coiled coils in GCN4 leucine zipper mutants. In *Science (New York, N.Y.)* 262 (5138), pp. 1401–1407.

Hasenbein, Sonja; Meltzer, Michael; Hauske, Patrick; Kaiser, Markus; Huber, Robert; Clausen, Tim; Ehrmann, Michael (2010): Conversion of a regulatory into a degradative protease. In *Journal of molecular biology* 397 (4), pp. 957–966. DOI: 10.1016/j.jmb.2010.02.027.

Hasselblatt, Hanna; Kurzbauer, Robert; Wilken, Corinna; Krojer, Tobias; Sawa, Justyna; Kurt, Juliane et al. (2007): Regulation of the sigmaE stress response by DegS:

how the PDZ domain keeps the protease inactive in the resting state and allows integration of different OMP-derived stress signals upon folding stress. In *Genes & development* 21 (20), pp. 2659–2670. DOI: 10.1101/gad.445307.

Hegde, Ramesh; Srinivasula, Srinivasa M.; Zhang, ZhiJia; Wassell, Richard; Mukattash, Rula; Cilenti, Lucia et al. (2002): Identification of Omi/HtrA2 as a mitochondrial apoptotic serine protease that disrupts inhibitor of apoptosis protein-caspase interaction. In *The Journal of biological chemistry* 277 (1), pp. 432–438. DOI: 10.1074/jbc.M109721200.

Hosseini-Farahabadi, Sara; Geetha-Loganathan, Poongodi; Fu, Katherine; Nimmagadda, Suresh; Yang, Hoe Joong; Richman, Joy M. (2013): Dual functions for WNT5A during cartilage development and in disease. In *Matrix biology : journal of the International Society for Matrix Biology* 32 (5), pp. 252–264. DOI: 10.1016/j.matbio.2013.02.005.

Hynes, Richard O. (2009): The extracellular matrix. Not just pretty fibrils. In *Science (New York, N.Y.)* 326 (5957), pp. 1216–1219. DOI: 10.1126/science.1176009.

Ibrahimi, Muhammad; Nozaki, Hiroaki; Lee, Angelica; Onodera, Osamu; Reichwein, Raymond; Wicklund, Matthew; El-Ghanem, Mohammad (2017): A CARASIL Patient from Americas with Novel Mutation and Atypical Features: Case Presentation and Literature Review. In *Cerebrovascular diseases (Basel, Switzerland)* 44 (3-4), pp. 135–140. DOI: 10.1159/000477358.

Inagaki, A.; Nishizawa, H.; Ota, S.; Suzuki, M.; Inuzuka, H.; Miyamura, H. et al. (2012): Upregulation of HtrA4 in the placentas of patients with severe pre-eclampsia. In *Placenta* 33 (11), pp. 919–926. DOI: 10.1016/j.placenta.2012.08.003.

Ito, Shinji; Takao, Masaki; Fukutake, Toshio; Hatsuta, Hiroyuki; Funabe, Sayaka; Ito, Nobuo et al. (2016): Histopathologic Analysis of Cerebral Autosomal Recessive Arteriopathy with Subcortical Infarcts and Leukoencephalopathy (CARASIL): A Report of a New Genetically Confirmed Case and Comparison to 2 Previous Cases. In *Journal of neuropathology and experimental neurology*. DOI: 10.1093/jnen/nlw078.

Jiang, Qian-Qian; Bartsch, Lina; Sicking, Wilhelm; Wich, Peter R.; Heider, Dominik; Hoffmann, Daniel; Schmuck, Carsten (2013): A new approach to inhibit human β-tryptase by protein surface binding of four-armed peptide ligands with two different sets

of arms. In *Organic & biomolecular chemistry* 11 (10), pp. 1631–1639. DOI: 10.1039/c3ob27302d.

Joutel, A.; Andreux, F.; Gaulis, S.; Domenga, V.; Cecillon, M.; Battail, N. et al. (2000): The ectodomain of the Notch3 receptor accumulates within the cerebrovasculature of CADASIL patients. In *The Journal of clinical investigation* 105 (5), pp. 597–605. DOI: 10.1172/JCI8047.

Jubb, Harry; Blundell, Tom L.; Ascher, David B. (2015): Flexibility and small pockets at protein-protein interfaces: New insights into druggability. In *Progress in biophysics and molecular biology* 119 (1), pp. 2–9. DOI: 10.1016/j.pbiomolbio.2015.01.009.

Kalluri, Raghu; Neilson, Eric G. (2003): Epithelial-mesenchymal transition and its implications for fibrosis. In *The Journal of clinical investigation* 112 (12), pp. 1776–1784. DOI: 10.1172/JCI20530.

Kast, Jessica; Hanecker, Patrizia; Beaufort, Nathalie; Giese, Armin; Joutel, Anne; Dichgans, Martin et al. (2014): Sequestration of latent TGF-β binding protein 1 into CADASIL-related Notch3-ECD deposits. In *Acta neuropathologica communications* 2, p. 96. DOI: 10.1186/s40478-014-0096-8.

Kavanagh, David; Spitzer, Dirk; Kothari, Parul H.; Shaikh, Aisha; Liszewski, M. Kathryn; Richards, Anna; Atkinson, John P. (2008): New roles for the major human 3'-5' exonuclease TREX1 in human disease. In *Cell cycle (Georgetown, Tex.)* 7 (12), pp. 1718–1725. DOI: 10.4161/cc.7.12.6162.

Khaleeli, Zhaleh; Jaunmuktane, Zane; Beaufort, Nathalie; Houlden, Henry; Haffner, Christof; Brandner, Sebastian et al. (2015): A novel HTRA1 exon 2 mutation causes loss of protease activity in a Pakistani CARASIL patient. In *Journal of neurology* 262 (5), pp. 1369–1372. DOI: 10.1007/s00415-015-7769-5.

Kitamoto, Takeo; Takahashi, Keikichi; Takimoto, Hiroaki; Tomizuka, Kazuma; Hayasaka, Michiko; Tabira, Takeshi; Hanaoka, Kazunori (2005): Functional redundancy of the Notch gene family during mouse embryogenesis: analysis of Notch gene expression in Notch3-deficient mice. In *Biochemical and biophysical research communications* 331 (4), pp. 1154–1162. DOI: 10.1016/j.bbrc.2005.03.241.

Klose, Ralph; Adam, M. Gordian; Weis, Eva-Maria; Moll, Iris; Wüstehube-Lausch, Joycelyn; Tetzlaff, Fabian et al. (2018): Inactivation of the serine protease HTRA1

inhibits tumor growth by deregulating angiogenesis. In *Oncogene* 37 (31), pp. 4260–4272. DOI: 10.1038/s41388-018-0258-4.

Kono, Yu; Nishioka, Kenya; Li, Yuanzhe; Komatuzaki, Yo; Ito, Yuta; Yoshino, Hiroyo et al. (2018): Heterozygous HTRA1 mutations with mimicking symptoms of CARASIL in two families. In *Clinical neurology and neurosurgery* 172, pp. 174–176. DOI: 10.1016/j.clineuro.2018.07.009.

Kotorii, Satoshi; Goto, Hirofumi; Kondo, Takayuki; Matsuo, Hidenori; Takahashi, Keikichi; Shibuya, Noritoshi (2006): Case of CADASIL showing spontaneous subcortical hemorrhage with a novel mutation of Notch3 gene. In *Rinsho shinkeigaku = Clinical neurology* 46 (9), pp. 644–648.

Kozjak-Pavlovic, Vera; Ott, Christine; Götz, Monika; Rudel, Thomas (2011): Neisserial Omp85 protein is selectively recognized and assembled into functional complexes in the outer membrane of human mitochondria. In *The Journal of biological chemistry* 286 (30), pp. 27019–27026. DOI: 10.1074/jbc.M111.232249.

Krojer, Tobias; Garrido-Franco, Marta; Huber, Robert; Ehrmann, Michael; Clausen, Tim (2002): Crystal structure of DegP (HtrA) reveals a new protease-chaperone machine. In *Nature* 416 (6879), pp. 455–459. DOI: 10.1038/416455a.

Krojer, Tobias; Sawa, Justyna; Huber, Robert; Clausen, Tim (2010): HtrA proteases have a conserved activation mechanism that can be triggered by distinct molecular cues. In *Nature structural & molecular biology* 17 (7), pp. 844–852. DOI: 10.1038/nsmb.1840.

Krojer, Tobias; Sawa, Justyna; Schäfer, Eva; Saibil, Helen R.; Ehrmann, Michael; Clausen, Tim (2008): Structural basis for the regulated protease and chaperone function of DegP. In *Nature* 453 (7197), pp. 885–890. DOI: 10.1038/nature07004.

Kutik, Stephan; Stojanovski, Diana; Becker, Lars; Becker, Thomas; Meinecke, Michael; Krüger, Vivien et al. (2008): Dissecting membrane insertion of mitochondrial beta-barrel proteins. In *Cell* 132 (6), pp. 1011–1024. DOI: 10.1016/j.cell.2008.01.028.

Lanfranconi, Silvia; Markus, Hugh S. (2010): COL4A1 mutations as a monogenic cause of cerebral small vessel disease: a systematic review. In *Stroke* 41 (8), e513-8. DOI: 10.1161/STROKEAHA.110.581918.

Launay, S.; Maubert, E.; Lebeurrier, N.; Tennstaedt, A.; Campioni, M.; Docagne, F. et al. (2008): HtrA1-dependent proteolysis of TGF-beta controls both neuronal maturation and developmental survival. In *Cell death and differentiation* 15 (9), pp. 1408–1416. DOI: 10.1038/cdd.2008.82.

Lee, Ho-Jin; Zheng, Jie J. (2010): PDZ domains and their binding partners: structure, specificity, and modification. In *Cell communication and signaling : CCS* 8, p. 8. DOI: 10.1186/1478-811X-8-8.

Letunic, Ivica; Doerks, Tobias; Bork, Peer (2012): SMART 7: recent updates to the protein domain annotation resource. In *Nucleic acids research* 40 (Database issue), D302-5. DOI: 10.1093/nar/gkr931.

Leyhe, T.; Wiendl, H.; Buchkremer, G.; Wormstall, H. (2005): CADASIL: underdiagnosed in psychiatric patients? In *Acta psychiatrica Scandinavica* 111 (5), 392-6; discussion 396-7. DOI: 10.1111/j.1600-0447.2004.00452.x.

Li, Wenyu; Srinivasula, Srinivasa M.; Chai, Jijie; Li, Pingwei; Wu, Jia-Wei; Zhang, ZhiJia et al. (2002): Structural insights into the pro-apoptotic function of mitochondrial serine protease HtrA2/Omi. In *Nature structural biology* 9 (6), pp. 436–441. DOI: 10.1038/nsb795.

Li, Ying; Puryer, Michelle; Lin, Eliane; Hale, Kathryn; Salamonsen, Lois A.; Manuelpillai, Ursula et al. (2011): Placental HtrA3 is regulated by oxygen tension and serum levels are altered during early pregnancy in women destined to develop preeclampsia. In *The Journal of clinical endocrinology and metabolism* 96 (2), pp. 403–411. DOI: 10.1210/jc.2010-1405.

Li, Yuxin; Takeshita, Kyosuke; Liu, Ping-Yen; Satoh, Minoru; Oyama, Naotsugu; Mukai, Yasushi et al. (2009): Smooth muscle Notch1 mediates neointimal formation after vascular injury. In *Circulation* 119 (20), pp. 2686–2692. DOI: 10.1161/CIRCULATIONAHA.108.790485.

Liese, Susanne; Netz, Roland R. (2018): Quantitative Prediction of Multivalent Ligand-Receptor Binding Affinities for Influenza, Cholera, and Anthrax Inhibition. In *ACS nano* 12 (5), pp. 4140–4147. DOI: 10.1021/acsnano.7b08479.

Liu, X.; Alexander, V.; Vijayachandra, K.; Bhogte, E.; Diamond, I.; Glick, A. (2001): Conditional epidermal expression of TGFbeta 1 blocks neonatal lethality but causes a reversible hyperplasia and alopecia. In *Proceedings of the National Academy of*

Sciences of the United States of America 98 (16), pp. 9139–9144. DOI: 10.1073/pnas.161016098.

Loeys, Bart L.; Schwarze, Ulrike; Holm, Tammy; Callewaert, Bert L.; Thomas, George H.; Pannu, Hariyadarshi et al. (2006): Aneurysm syndromes caused by mutations in the TGF-beta receptor. In *The New England journal of medicine* 355 (8), pp. 788–798. DOI: 10.1056/NEJMoa055695.

MacBeath, G.; Kast, P.; Hilvert, D. (1998): Probing enzyme quaternary structure by combinatorial mutagenesis and selection. In *Protein science : a publication of the Protein Society* 7 (8), pp. 1757–1767. DOI: 10.1002/pro.5560070810.

Maeda, S.; Nemoto, K.; Suwa, N.; Yamagata, J.; Nagashima, Y. (1965): Clinico-pathological conference on a case of encephalomalacia (A question of Binswanger's disease). In *Saishin igaku. Modern medicine* 20, pp. 933–940.

Malet, Hélène; Canellas, Flavia; Sawa, Justyna; Yan, Jun; Thalassinos, Konstantinos; Ehrmann, Michael et al. (2012): Newly folded substrates inside the molecular cage of the HtrA chaperone DegQ. In *Nature structural & molecular biology* 19 (2), pp. 152–157. DOI: 10.1038/nsmb.2210.

Maric, Hans Michael; Kasaragod, Vikram Babu; Schindelin, Hermann (2014): Modulation of gephyrin-glycine receptor affinity by multivalency. In *ACS chemical biology* 9 (11), pp. 2554–2562. DOI: 10.1021/cb500303a.

Martins, L. Miguel; Iaccarino, Ingram; Tenev, Tencho; Gschmeissner, Stephen; Totty, Nicholas F.; Lemoine, Nicholas R. et al. (2002): The serine protease Omi/HtrA2 regulates apoptosis by binding XIAP through a reaper-like motif. In *The Journal of biological chemistry* 277 (1), pp. 439–444. DOI: 10.1074/jbc.M109784200.

Meltzer, Michael; Hasenbein, Sonja; Mamant, Nicolette; Merdanovic, Melisa; Poepsel, Simon; Hauske, Patrick et al. (2009): Structure, function and regulation of the conserved serine proteases DegP and DegS of Escherichia coli. In *Research in microbiology* 160 (9), pp. 660–666. DOI: 10.1016/j.resmic.2009.07.012.

Mendioroz, M.; Fernández-Cadenas, I.; Del Río-Espinola, A.; Rovira, A.; Solé, E.; Fernández-Figueras, M. T. et al. (2010): A missense HTRA1 mutation expands CARASIL syndrome to the Caucasian population. In *Neurology* 75 (22), pp. 2033–2035. DOI: 10.1212/WNL.0b013e3181ff96ac.

Menezes Cordeiro, Inês; Nzwalo, Hipólito; Sá, Francisca; Ferreira, Rita Bastos; Alonso, Isabel; Afonso, Luís; Basílio, Carlos (2015): Shifting the CARASIL paradigm: report of a non-Asian family and literature review. In *Stroke* 46 (4), pp. 1110–1112. DOI: 10.1161/STROKEAHA.114.006735.

Merdanovic, Melisa; Mamant, Nicolette; Meltzer, Michael; Poepsel, Simon; Auckenthaler, Alexandra; Melgaard, Rie et al. (2010): Determinants of structural and functional plasticity of a widely conserved protease chaperone complex. In *Nature structural & molecular biology* 17 (7), pp. 837–843. DOI: 10.1038/nsmb.1839.

Merril, C. R.; Goldman, D.; Sedman, S. A.; Ebert, M. H. (1981): Ultrasensitive stain for proteins in polyacrylamide gels shows regional variation in cerebrospinal fluid proteins. In *Science (New York, N.Y.)* 211 (4489), pp. 1437–1438.

Monet-Leprêtre, Marie; Haddad, Iman; Baron-Menguy, Céline; Fouillot-Panchal, Maï; Riani, Meriem; Domenga-Denier, Valérie et al. (2013): Abnormal recruitment of extracellular matrix proteins by excess Notch3 ECD: a new pathomechanism in CADASIL. In *Brain : a journal of neurology* 136 (Pt 6), pp. 1830–1845. DOI: 10.1093/brain/awt092.

Nam, Min-Kyung; Seong, Young-Mo; Park, Hyo-Jin; Choi, Ju-Youn; Kang, Seongman; Rhim, Hyangshuk (2006): The homotrimeric structure of HtrA2 is indispensable for executing its serine protease activity. In *Experimental & molecular medicine* 38 (1), pp. 36–43. DOI: 10.1038/emm.2006.5.

Narkiewicz, Joanna; Klasa-Mazurkiewicz, Dagmara; Zurawa-Janicka, Dorota; Skorko-Glonek, Joanna; Emerich, Janusz; Lipinska, Barbara (2008): Changes in mRNA and protein levels of human HtrA1, HtrA2 and HtrA3 in ovarian cancer. In *Clinical biochemistry* 41 (7-8), pp. 561–569. DOI: 10.1016/j.clinbiochem.2008.01.004.

Narkiewicz, Joanna; Lapinska-Szumczyk, Sylwia; Zurawa-Janicka, Dorota; Skorko-Glonek, Joanna; Emerich, Janusz; Lipinska, Barbara (2009): Expression of human HtrA1, HtrA2, HtrA3 and TGF-beta1 genes in primary endometrial cancer. In *Oncology reports* 21 (6), pp. 1529–1537.

Nie, Gui-Ying; Hampton, Anne; Li, Ying; Findlay, Jock K.; Salamonsen, Lois A. (2003a): Identification and cloning of two isoforms of human high-temperature requirement factor A3 (HtrA3), characterization of its genomic structure and

comparison of its tissue distribution with HtrA1 and HtrA2. In *The Biochemical journal* 371 (Pt 1), pp. 39–48. DOI: 10.1042/BJ20021569.

Nie, Gui-Ying; Li, Ying; Minoura, Hiroyuki; Batten, Leigh; Ooi, Guck T.; Findlay, Jock K.; Salamonsen, Lois A. (2003b): A novel serine protease of the mammalian HtrA family is up-regulated in mouse uterus coinciding with placentation. In *Molecular human reproduction* 9 (5), pp. 279–290.

Nishimoto, Y.; Shibata, M.; Nihonmatsu, M.; Nozaki, H.; Shiga, A.; Shirata, A. et al. (2011): A novel mutation in the HTRA1 gene causes CARASIL without alopecia. In *Neurology* 76 (15), pp. 1353–1355. DOI: 10.1212/WNL.0b013e318215281d.

Nooren, Irene M. A.; Thornton, Janet M. (2003): Structural characterisation and functional significance of transient protein-protein interactions. In *Journal of molecular biology* 325 (5), pp. 991–1018.

Nozaki, Hiroaki; Kato, Taisuke; Nihonmatsu, Megumi; Saito, Yohei; Mizuta, Ikuko; Noda, Tomoko et al. (2016): Distinct molecular mechanisms of HTRA1 mutants in manifesting heterozygotes with CARASIL. In *Neurology* 86 (21), pp. 1964–1974. DOI: 10.1212/WNL.0000000000002694.

Oka, Chio; Tsujimoto, Rumi; Kajikawa, Miwa; Koshiba-Takeuchi, Kazuko; Ina, Junko; Yano, Masato et al. (2004): HtrA1 serine protease inhibits signaling mediated by Tgfbeta family proteins. In *Development (Cambridge, England)* 131 (5), pp. 1041–1053. DOI: 10.1242/dev.00999.

Page, Michael J.; Di Cera, Enrico (2008): Evolution of peptidase diversity. In *The Journal of biological chemistry* 283 (44), pp. 30010–30014. DOI: 10.1074/jbc.M804650200.

Pallen, M. J.; Ponting, C. P. (1997): PDZ domains in bacterial proteins. In *Molecular microbiology* 26 (2), pp. 411–413.

Pantoni, Leonardo (2010): Cerebral small vessel disease: from pathogenesis and clinical characteristics to therapeutic challenges. In *The Lancet. Neurology* 9 (7), pp. 689–701. DOI: 10.1016/S1474-4422(10)70104-6.

Park, Kinam (2014): Ligand affinity: multivalency counterbalances PEGylation. In *Journal of controlled release : official journal of the Controlled Release Society* 194, p. 351. DOI: 10.1016/j.jconrel.2014.10.014.

Pei, X. Y.; Holliger, P.; Murzin, A. G.; Williams, R. L. (1997): The 2.0-A resolution crystal structure of a trimeric antibody fragment with noncognate VH-VL domain pairs shows a rearrangement of VH CDR3. In *Proceedings of the National Academy of Sciences of the United States of America* 94 (18), pp. 9637–9642.

Poepsel, Simon; Sprengel, Andreas; Sacca, Barbara; Kaschani, Farnusch; Kaiser, Markus; Gatsogiannis, Christos et al. (2015): Determinants of amyloid fibril degradation by the PDZ protease HTRA1. In *Nature chemical biology* 11 (11), pp. 862–869. DOI: 10.1038/nchembio.1931.

Ponnalagu, Devasena; Singh, Harpreet (2017): Anion Channels of Mitochondria. In *Handbook of experimental pharmacology* 240, pp. 71–101. DOI: 10.1007/164_2016_39.

Preethish-Kumar, Veeramani; Nozaki, Hiroaki; Tiwari, Sarbesh; Vengalil, Seena; Bhat, Maya; Prasad, Chandrajit et al. (2017): CARASIL families from India with 3 novel null mutations in the HTRA1 gene. In *Neurology* 89 (23), pp. 2392–2394. DOI: 10.1212/WNL.0000000000004710.

Rannikmäe, Kristiina; Davies, Gail; Thomson, Pippa A.; Bevan, Steve; Devan, William J.; Falcone, Guido J. et al. (2015): Common variation in COL4A1/COL4A2 is associated with sporadic cerebral small vessel disease. In *Neurology* 84 (9), pp. 918–926. DOI: 10.1212/WNL.0000000000001309.

Razvi, S. S. M.; Davidson, R.; Bone, I.; Muir, K. W. (2005): The prevalence of cerebral autosomal dominant arteriopathy with subcortical infarcts and leucoencephalopathy (CADASIL) in the west of Scotland. In *Journal of neurology, neurosurgery, and psychiatry* 76 (5), pp. 739–741. DOI: 10.1136/jnnp.2004.051847.

Rehling, P.; Wiedemann, N.; Pfanner, N.; Truscott, K. N. (2001): The mitochondrial import machinery for preproteins. In *Critical reviews in biochemistry and molecular biology* 36 (3), pp. 291–336. DOI: 10.1080/20014091074200.

Rey, Juliana (2018): (Allosterische) Aktivitätsregulation der humanen Serinprotease HTRA1. PhD thesis. University Duisburg-Essen, Essen. Department of Microbiology II.

Richards, Anna; van den Maagdenberg, Arn M. J. M.; Jen, Joanna C.; Kavanagh, David; Bertram, Paula; Spitzer, Dirk et al. (2007): C-terminal truncations in human 3'-5' DNA exonuclease TREX1 cause autosomal dominant retinal vasculopathy with

cerebral leukodystrophy. In *Nature genetics* 39 (9), pp. 1068–1070. DOI: 10.1038/ng2082.

Riebe, Steffen; Vallet, Cecilia; van der Vight, Felix; Gonzalez-Abradelo, Dario; Wölper, Christoph; Strassert, Cristian A. et al. (2017): Aromatic Thioethers as Novel Luminophores with Aggregation-Induced Fluorescence and Phosphorescence. In *Chemistry (Weinheim an der Bergstrasse, Germany)* 23 (55), pp. 13660–13668. DOI: 10.1002/chem.201701867.

Robinson, P. N.; Arteaga-Solis, E.; Baldock, C.; Collod-Béroud, G.; Booms, P.; Paepe, A. de et al. (2006): The molecular genetics of Marfan syndrome and related disorders. In *Journal of medical genetics* 43 (10), pp. 769–787. DOI: 10.1136/jmg.2005.039669.

Ruchoux, Marie Magdeleine; Domenga, Valérie; Brulin, Peggy; Maciazek, Jacqueline; Limol, Sylvie; Tournier-Lasserve, Elisabeth; Joutel, Anne (2003): Transgenic mice expressing mutant Notch3 develop vascular alterations characteristic of cerebral autosomal dominant arteriopathy with subcortical infarcts and leukoencephalopathy. In *The American journal of pathology* 162 (1), pp. 329–342. DOI: 10.1016/S0002-9440(10)63824-2.

Scharpfenecker, Marion; van Dinther, Maarten; Liu, Zhen; van Bezooijen, Rutger L.; Zhao, Qinghai; Pukac, Laurie et al. (2007): BMP-9 signals via ALK1 and inhibits bFGF-induced endothelial cell proliferation and VEGF-stimulated angiogenesis. In *Journal of cell science* 120 (Pt 6), pp. 964–972. DOI: 10.1242/jcs.002949.

Schillinger, Jasmin; Severin, Katharina; Kaschani, Farnusch; Kaiser, Markus; Ehrmann, Michael (2018): HTRA1-Dependent Cell Cycle Proteomics. In *Journal of proteome research* 17 (8), pp. 2679–2694. DOI: 10.1021/acs.jproteome.8b00129.

Schindelin, Johannes; Arganda-Carreras, Ignacio; Frise, Erwin; Kaynig, Verena; Longair, Mark; Pietzsch, Tobias et al. (2012): Fiji: an open-source platform for biological-image analysis. In *Nature methods* 9 (7), pp. 676–682. DOI: 10.1038/nmeth.2019.

Schmidt, Helena; Zeginigg, Marion; Wiltgen, Marco; Freudenberger, Paul; Petrovic, Katja; Cavalieri, Margherita et al. (2011): Genetic variants of the NOTCH3 gene in the elderly and magnetic resonance imaging correlates of age-related cerebral small vessel disease. In *Brain : a journal of neurology* 134 (Pt 11), pp. 3384–3397. DOI: 10.1093/brain/awr252.

Schredelseker, Johann; Paz, Aviv; López, Carlos J.; Altenbach, Christian; Leung, Calvin S.; Drexler, Maria K. et al. (2014): High resolution structure and double electron-electron resonance of the zebrafish voltage-dependent anion channel 2 reveal an oligomeric population. In *The Journal of biological chemistry* 289 (18), pp. 12566–12577. DOI: 10.1074/jbc.M113.497438.

Setoguchi, Kiyoko; Otera, Hidenori; Mihara, Katsuyoshi (2006): Cytosolic factor- and TOM-independent import of C-tail-anchored mitochondrial outer membrane proteins. In *The EMBO journal* 25 (24), pp. 5635–5647. DOI: 10.1038/sj.emboj.7601438.

Shawber, Carrie J.; Kitajewski, Jan (2004): Notch function in the vasculature: insights from zebrafish, mouse and man. In *BioEssays : news and reviews in molecular, cellular and developmental biology* 26 (3), pp. 225–234. DOI: 10.1002/bies.20004.

Shen, Qing-Tao; Bai, Xiao-Chen; Chang, Lei-Fu; Wu, Yi; Wang, Hong-Wei; Sui, Sen-Fang (2009): Bowl-shaped oligomeric structures on membranes as DegP's new functional forms in protein quality control. In *Proceedings of the National Academy of Sciences of the United States of America* 106 (12), pp. 4858–4863. DOI: 10.1073/pnas.0811780106.

Shiga, Atsushi; Nozaki, Hiroaki; Yokoseki, Akio; Nihonmatsu, Megumi; Kawata, Hirotoshi; Kato, Taisuke et al. (2011): Cerebral small-vessel disease protein HTRA1 controls the amount of TGF-β1 via cleavage of proTGF-β1. In *Human molecular genetics* 20 (9), pp. 1800–1810. DOI: 10.1093/hmg/ddr063.

Shridhar, Viji; Sen, Ami; Chien, Jeremy; Staub, Julie; Avula, Rajeswari; Kovats, Steve et al. (2002): Identification of underexpressed genes in early- and late-stage primary ovarian tumors by suppression subtraction hybridization. In *Cancer research* 62 (1), pp. 262–270.

Singh, Harmeet; Li, Ying; Fuller, Peter J.; Harrison, Craig; Rao, Jyothsna; Stephens, Andrew N.; Nie, Guiying (2013): HtrA3 Is Downregulated in Cancer Cell Lines and Significantly Reduced in Primary Serous and Granulosa Cell Ovarian Tumors. In *Journal of Cancer* 4 (2), pp. 152–164. DOI: 10.7150/jca.5702.

Singh, Harmeet; Zhao, Min; Chen, Qi; Wang, Yao; Li, Ying; Kaitu'u-Lino, Tu'uhevaha J. et al. (2015): Human HtrA4 Expression Is Restricted to the Placenta, Is Significantly Up-Regulated in Early-Onset Preeclampsia, and High Levels of HtrA4 Cause

Endothelial Dysfunction. In *The Journal of clinical endocrinology and metabolism* 100 (7), E936-45. DOI: 10.1210/jc.2014-3969.

Singh, Nitu; D'Souza, Areetha; Cholleti, Anuradha; Sastry, G. Madhavi; Bose, Kakoli (2014): Dual regulatory switch confers tighter control on HtrA2 proteolytic activity. In *The FEBS journal* 281 (10), pp. 2456–2470. DOI: 10.1111/febs.12799.

Sörös, Peter; Hachinski, Vladimir (2012): Cardiovascular and neurological causes of sudden death after ischaemic stroke. In *The Lancet. Neurology* 11 (2), pp. 179–188. DOI: 10.1016/S1474-4422(11)70291-5.

Srinivasula, Srinivasa M.; Gupta, Sanjeev; Datta, Pinaki; Zhang, ZhiJia; Hegde, Ramesh; Cheong, NaEun et al. (2003): Inhibitor of apoptosis proteins are substrates for the mitochondrial serine protease Omi/HtrA2. In *The Journal of biological chemistry* 278 (34), pp. 31469–31472. DOI: 10.1074/jbc.C300240200.

Stejskal, E. O.; Tanner, J. E. (1965): Spin Diffusion Measurements. Spin Echoes in the Presence of a Time-Dependent Field Gradient. In *The Journal of Chemical Physics* 42 (1), pp. 288–292. DOI: 10.1063/1.1695690.

Sweeney, Catherine; Morrow, David; Birney, Yvonne A.; Coyle, Seamus; Hennessy, Colm; Scheller, Agnieszka et al. (2004): Notch 1 and 3 receptor signaling modulates vascular smooth muscle cell growth, apoptosis, and migration via a CBF-1/RBP-Jk dependent pathway. In *FASEB journal : official publication of the Federation of American Societies for Experimental Biology* 18 (12), pp. 1421–1423. DOI: 10.1096/fj.04-1700fje.

Tateoka, Toru; Onda, Hideaki; Hirota, Kengo; Kasuya, Hidetoshi; Shinohara, Toyoaki; Kinouchi, Hiroyuki; Akagawa, Hiroyuki (2016): Unusual case of cerebral small vessel disease with a heterozygous nonsense mutation in HTRA1. In *Journal of the neurological sciences* 362, pp. 144–146. DOI: 10.1016/j.jns.2016.01.037.

Tennstaedt, Annette; Pöpsel, Simon; Truebestein, Linda; Hauske, Patrick; Brockmann, Anke; Schmidt, Nina et al. (2012): Human high temperature requirement serine protease A1 (HTRA1) degrades tau protein aggregates. In *The Journal of biological chemistry* 287 (25), pp. 20931–20941. DOI: 10.1074/jbc.M111.316232.

Thaler, Franziska S.; Catak, Cihan; Einhäupl, Maximilian; Müller, Susanna; Seelos, Klaus; Wollenweber, Frank A.; Kümpfel, Tania (2018): Cerebral small vessel disease

caused by a novel heterozygous mutation in HTRA1. In *Journal of the neurological sciences* 388, pp. 19–21. DOI: 10.1016/j.jns.2018.02.043.

Thompson, Charlie S.; Hakim, Antoine M. (2009): Living beyond our physiological means. Small vessel disease of the brain is an expression of a systemic failure in arteriolar function: a unifying hypothesis. In *Stroke* 40 (5), e322-30. DOI: 10.1161/STROKEAHA.108.542266.

Tocharus, Jiraporn; Tsuchiya, Akiho; Kajikawa, Miwa; Ueta, Yoshifumi; Oka, Chio; Kawaichi, Masashi (2004): Developmentally regulated expression of mouse HtrA3 and its role as an inhibitor of TGF-beta signaling. In *Development, growth & differentiation* 46 (3), pp. 257–274. DOI: 10.1111/j.1440-169X.2004.00743.x.

Truebestein, Linda; Tennstaedt, Annette; Mönig, Timon; Krojer, Tobias; Canellas, Flavia; Kaiser, Markus et al. (2011): Substrate-induced remodeling of the active site regulates human HTRA1 activity. In *Nature structural & molecular biology* 18 (3), pp. 386–388. DOI: 10.1038/nsmb.2013.

Verdura, Edgard; Hervé, Dominique; Scharrer, Eva; Amador, Maria Del Mar; Guyant-Maréchal, Lucie; Philippi, Anne et al. (2015): Heterozygous HTRA1 mutations are associated with autosomal dominant cerebral small vessel disease. In *Brain : a journal of neurology* 138 (Pt 8), pp. 2347–2358. DOI: 10.1093/brain/awv155.

Wang, Liang-Jie; Cheong, Mei-Leng; Lee, Yun-Shien; Lee, Ming-Ting; Chen, Hungwen (2012): High-temperature requirement protein A4 (HtrA4) suppresses the fusogenic activity of syncytin-1 and promotes trophoblast invasion. In *Molecular and cellular biology* 32 (18), pp. 3707–3717. DOI: 10.1128/MCB.00223-12.

Wang, Tao; Holt, Cathy M.; Xu, Chiheng; Ridley, Caroline; P O Jones, Richard; Baron, Martin; Trump, Dorothy (2007): Notch3 activation modulates cell growth behaviour and cross-talk to Wnt/TCF signalling pathway. In *Cellular signalling* 19 (12), pp. 2458–2467. DOI: 10.1016/j.cellsig.2007.07.019.

Wang, Wenli; Prince, Chengyu Z.; Hu, Xing; Pollman, Matthew J. (2003): HRT1 modulates vascular smooth muscle cell proliferation and apoptosis. In *Biochemical and biophysical research communications* 308 (3), pp. 596–601.

Wilken, Corinna; Kitzing, Karina; Kurzbauer, Robert; Ehrmann, Michael; Clausen, Tim (2004): Crystal structure of the DegS stress sensor: How a PDZ domain recognizes misfolded protein and activates a protease. In *Cell* 117 (4), pp. 483–494.

Wilson, Andrew J. (2009): Inhibition of protein-protein interactions using designed molecules. In *Chemical Society reviews* 38 (12), pp. 3289–3300. DOI: 10.1039/b807197g.

Wong, C.; Sridhara, S.; Bardwell, J. C.; Jakob, U. (2000): Heating greatly speeds Coomassie blue staining and destaining. In *BioTechniques* 28 (3), 426-8, 430, 432.

Wrase, Robert; Scott, Hannah; Hilgenfeld, Rolf; Hansen, Guido (2011): The Legionella HtrA homologue DegQ is a self-compartmentizing protease that forms large 12-meric assemblies. In *Proceedings of the National Academy of Sciences of the United States of America* 108 (26), pp. 10490–10495. DOI: 10.1073/pnas.1101084108.

Xie, Fei; Zhang, Li-San (2018): A Chinese CARASIL Patient Caused by Novel Compound Heterozygous Mutations in HTRA1. In *Journal of stroke and cerebrovascular diseases : the official journal of National Stroke Association* 27 (10), pp. 2840–2842. DOI: 10.1016/j.jstrokecerebrovasdis.2018.06.017.

Yamamoto, Masahiro; Xin, Bing; Watanabe, Kenji; Ooshio, Takako; Fujii, Kiyonaga; Chen, Xi et al. (2017): Oncogenic Determination of a Broad Spectrum of Phenotypes of Hepatocyte-Derived Mouse Liver Tumors. In *The American journal of pathology* 187 (12), pp. 2711–2725. DOI: 10.1016/j.ajpath.2017.07.022.

Yamamoto, Y.; Craggs, L.; Baumann, M.; Kalimo, H.; Kalaria, R. N. (2011): Review: molecular genetics and pathology of hereditary small vessel diseases of the brain. In *Neuropathology and applied neurobiology* 37 (1), pp. 94–113. DOI: 10.1111/j.1365-2990.2010.01147.x.

Yan, Lijing L.; Li, Chaoyun; Chen, Jie; Luo, Rong; Bettger, Janet; Zhu, Yishan et al. (2017): Cardiovascular, Respiratory, and Related Disorders. Stroke. 3rd. Edited by Dorairaj Prabhakaran, Shuchi Anand, Thomas A. Gaziano, Jean-Claude Mbanya, Yangfeng Wu, Rachel Nugent. Washington (DC).

Yang, Qi-Heng; Church-Hajduk, Robin; Ren, Jinyu; Newton, Michelle L.; Du, Chunying (2003): Omi/HtrA2 catalytic cleavage of inhibitor of apoptosis (IAP) irreversibly inactivates IAPs and facilitates caspase activity in apoptosis. In *Genes & development* 17 (12), pp. 1487–1496. DOI: 10.1101/gad.1097903.

Zeth, Kornelius (2010): Structure and evolution of mitochondrial outer membrane proteins of beta-barrel topology. In *Biochimica et biophysica acta* 1797 (6-7), pp. 1292–1299. DOI: 10.1016/j.bbabio.2010.04.019.

Zhou, Yong; Jiang, Qiujie; Takahagi, Shunsuke; Shao, Changxia; Uitto, Jouni (2013): Premature termination codon read-through in the ABCC6 gene. Potential treatment for pseudoxanthoma elasticum. In *The Journal of investigative dermatology* 133 (12), pp. 2672–2677. DOI: 10.1038/jid.2013.234.

Zimorski, Verena; Ku, Chuan; Martin, William F.; Gould, Sven B. (2014): Endosymbiotic theory for organelle origins. In *Current opinion in microbiology* 22, pp. 38–48. DOI: 10.1016/j.mib.2014.09.008.

Zurawa-Janicka, Dorota; Wenta, Tomasz; Jarzab, Miroslaw; Skorko-Glonek, Joanna; Glaza, Przemyslaw; Gieldon, Artur et al. (2017): Structural insights into the activation mechanisms of human HtrA serine proteases. In *Archives of biochemistry and biophysics* 621, pp. 6–23. DOI: 10.1016/j.abb.2017.04.004.

9 Danksagung

Die Danksagung ist in der Online-Version aus Gründen des Datenschutzes nicht enthalten.

10 Lebenslauf

Der Lebenslauf ist in der Online-Version aus Gründen des Datenschutzes nicht enthalten.

Erklärung:

Hiermit erkläre ich, gem. § 7Abs. (2) d) + f)der Promotionsordnung der Fakultät für Biologie zur Erlangung des Dr. rer. nat., dass ich die vorliegende Dissertation selbständig verfasst und mich keiner anderen als der angegebenen Hilfsmittel bedient,bei der Abfassung der Dissertation nur die angegeben Hilfsmittel benutzt und alle wörtlich oder inhaltlich übernommenen Stellen als solche gekennzeichnet habe.

Essen, den _____ _____

Unterschrift des/r Doktoranden/in

Erklärung:

Hiermit erkläre ich, gem. § 7Abs. (2) e) + g) der Promotionsordnung der Fakultät für Biologie zur Erlangung des Dr. rer. nat., dass ich keine anderen Promotionen bzw. Promotionsversuche in der Vergangenheit durchgeführt habe und dass diese Arbeit von keiner anderen Fakultät/Fachbereich abgelehnt worden ist.

Essen, den _____ _____

Unterschrift des/r Doktoranden/in

Erklärung:

Hiermit erkläre ich, gem. § 6 Abs. (2) g) der Promotionsordnung der Fakultät für Biologie zur Erlangung der Dr. rer. nat., dass ich das Arbeitsgebiet, dem das Thema „Protein Repair Strategies for the Functional Restoration of CARASIL-relevant HTRA1 Mutants“ zuzuordnen ist, in Forschung und Lehre vertrete und den Antrag von Linda Ingendahl befürworte und die Betreuung auch im Falle eines Weggangs, wenn nicht wichtige Gründe dem entgegenstehen, weiterführen werde.

_____

Name des Mitglieds der Universität Duisburg-Essen in Druckbuchstaben

Essen, den _____ _____

Unterschrift eines Mitglieds der Universität Duisburg-Essen